

Electronic Thesis and Dissertation Repository

---

9-21-2017 10:30 AM

## A study on chemical stabilization of Oil Sands Mature Fine Tailings

Yixuan Wang, *The University of Western Ontario*

Supervisor: Julie Shang, *The University of Western Ontario*

A thesis submitted in partial fulfillment of the requirements for the Master of Engineering Science degree in Civil and Environmental Engineering

© Yixuan Wang 2017

Follow this and additional works at: <https://ir.lib.uwo.ca/etd>

---

### Recommended Citation

Wang, Yixuan, "A study on chemical stabilization of Oil Sands Mature Fine Tailings" (2017). *Electronic Thesis and Dissertation Repository*. 4937.

<https://ir.lib.uwo.ca/etd/4937>

This Dissertation/Thesis is brought to you for free and open access by Scholarship@Western. It has been accepted for inclusion in Electronic Thesis and Dissertation Repository by an authorized administrator of Scholarship@Western. For more information, please contact [wlsadmin@uwo.ca](mailto:wlsadmin@uwo.ca).

## ABSTRACT

Oil Sands Mature Fine Tailings (MFT) are generated from extraction of bitumen from oil sands. Fine tailings contain significant fraction of clay minerals, which makes dewatering and consolidation difficult and time-consuming. In this thesis, chemical stabilization of MFT is investigated in an experimental program. Portland cement (PC) and two liquid-based silicate grouts (NS and AAAS) are used for stabilization of MFT. The effectiveness of these stabilizers at different dosages and curing durations is assessed by conducting a series of laboratory tests in terms of the undrained shear strength ( $S_u$ ) and solid content (S%), plasticity and pore fluid chemistry. The gel time and gel syneresis of silicate grouts are studied. Scanning electron microscopy (SEM) observations and X-ray diffraction (XRD) analyses are conducted to understand the microstructural changes in MFT after chemical stabilization.

The results indicate that the inclusion of Portland cement or silicate grouts increases the solid contents and Atterberg limits of MFT. The undrained shear strength of MFT after chemical treatment increases up to 7.65 kPa with 10% PC, 15.5 kPa with 15% PC, 7.55 kPa with 15% NS and 5.5 kPa with 8% AAAS after 28 days of curing period. The pH of MFT paste increases after chemical treatments. Furthermore, SEM analyses indicate that after chemical treatment by Portland cement, fibrous cement hydrates (C-S-H gel) formed during stabilization process bind the MFT particles together, while after the treatment of silicate grouts, gelling products with undulating and irregular shapes serve as cementation agent. The XRD analysis of MFT shows that clay minerals' peak intensities in XRD patterns reduce after chemical stabilization. The results also indicate the additional C-S-H peaks in cement-MFT mixtures but show no new secondary mineral formations in silicate-MFT mixtures.

*Keywords:* chemical additives, stabilization, PC, NS, AAAS, setting agent, Mature Fine Tailings, undrained shear strength, solid content, plasticity, SEM, XRD

## **ACKNOWLEDGEMENTS**

I would like to express my sincere appreciation to my supervisor Professor Julie Q. Shang, for her constant guidance, patience and encouragement throughout my MEdSc study at the University of Western Ontario.

My thanks also extend to the faculty and technical staff in Civil and Environmental Engineering Department at Western, especially to Ms. Melodie Richards and Ms. Caitlin Marshall, for their laboratory supports. Special thanks to Dr. Grace Li and Dr. Brian Hart, for their kind advice in sample preparation (freeze drying), laser diffraction particle size and SEM/EDS analysis. Sincere thanks to Prof. Naggar, Prof. Yanful and Prof. Hart for serving as my thesis examination committee members. I am also grateful to Sharon Lackie at the University of Windsor for the help in ESEM imaging.

Thanks to Xianglian Li, Tim Evans and Mike MacDonald from National Silicates Ltd, who provided the silicate products and shared knowledge about the silicate chemistry.

My gratitude is also extended to my friends and fellow students. Special thanks to Dr. Yu Guo for his inspiration, technical and timely help during my study.

Finally, and especially, I would like to express my profound gratitude to my beloved parents and relatives, for their unceasing love and generous support.

# DEDICATION

*Dedicated to*  
*The Memory of My Grandmother*

# TABLE OF CONTENTS

<b>ABSTRACT</b> .....	<b>i</b>
<b>ACKNOWLEDGEMENTS</b> .....	<b>ii</b>
<b>DEDICATION</b> .....	<b>iii</b>
<b>TABLE OF CONTENTS</b> .....	<b>iv</b>
<b>LIST OF TABLES</b> .....	<b>ix</b>
<b>LIST OF FIGURES</b> .....	<b>xi</b>
<b>NOMENCLATURE</b> .....	<b>xvii</b>
<b>CHAPTER 1 INTRODUCTION</b> .....	<b>1</b>
1.1 Background.....	1
1.2 Research objectives .....	2
1.3 Organizations of thesis .....	3
1.4 Contributions of the thesis .....	4
References.....	5
<b>CHAPTER 2 LIERATURE REVIEW</b> .....	<b>7</b>
2.1 Introduction.....	7
2.2 Oil Sand Mature Fine Tailings (MFT) .....	7
2.2.1 Production of MFT .....	7
2.2.2 Property and behavior of MFT .....	8

2.2.3 Issues in oil sand MFT management.....	9
2.2.4 Treatment technologies of MFT .....	10
2.3 Clay microstructure .....	11
2.3.1 Clay minerals.....	11
2.3.2 Diffuse double layer and zeta potential.....	12
2.3.3 Clay particle associations .....	13
2.3.4 Microscopic analysis .....	13
2.4 Chemical stabilization .....	15
2.4.1 Introduction .....	15
2.4.2 Ground improvement by Portland cement .....	16
2.4.3 Ground improvement by Silicates.....	19
2.5. Case study .....	23
2.5.1 Cement stabilization .....	23
2.5.2 Sodium silicate grouts stabilization.....	25
2.5.3 Comments on the case study .....	26
References.....	37
<b>CHAPTER 3 MATERIALS AND METHODOLOGY.....</b>	<b>47</b>
3.1 General.....	47
3.2 Materials .....	47

3.2.1 MFT samples .....	47
3.2.2 Chemical stabilizers .....	48
3.3 Test method .....	49
3.3.1 Water content and solid content .....	49
3.3.2 Atterberg limit and plasticity .....	50
3.3.3 Undrained shear strength.....	50
3.3.4 Oedometer test.....	52
3.3.5 Specific gravity.....	53
3.3.6 Grain size distribution .....	53
3.3.7 Water chemistry and zeta potential of solid particles .....	53
3.3.8 SEM and XRD analyses .....	54
3.4 Summary .....	55
References.....	64
<b>CHAPTER 4 STABILIZATION OF OIL SANDS MATURE FINE TAILINGS (MFT) BY PORTLAND CEMENT.....</b>	<b>66</b>
4.1 Introduction.....	66
4.2 Sample Preparation.....	67
4.3 Results and discussion .....	67
4.3.1 Water content and Solid content .....	67

4.3.2 Index properties .....	68
4.3.3 Undrained shear strength.....	70
4.3.4 Consolidation tests .....	71
4.3.5 X-ray diffraction analysis.....	72
4.3.6 Scanning electron microscope analysis.....	74
4.4. Summary .....	75
References.....	90
<b>CHAPTER 5 STABILIZATION OF OIL SANDS MATURE FINE TAILINGS (MFT) BY SILICATE GROUTS.....</b>	<b>94</b>
5.1 Introduction.....	94
5.2 Experimental set up .....	95
5.2.1 Design consideration for testing program .....	95
5.2.2 Sample preparation.....	96
5.3 Results and discussion.....	96
5.3.1 Gel time .....	96
5.3.2 Water content and Solid content .....	97
5.3.3 Strength properties .....	98
5.3.4 Index Properties.....	100
5.3.5 Water chemistry.....	102



5.3.6 Zeta potential .....	103
5.3.7 XRD analysis (Mineralogy) .....	103
5.3.8 SEM imaging (Morphology) .....	104
5.4 Practical implications .....	106
5.5 Summary .....	106
References.....	130
<b>CHAPTER 6 CONCLUSION AND RECOMMENDATION .....</b>	<b>132</b>
6.1 Summary .....	132
6.2 Conclusion .....	132
6.3 Recommendations.....	134
<b>APPENDIX A .....</b>	<b>135</b>
<b>APPENDIX B .....</b>	<b>136</b>
<b>APPENDIX C .....</b>	<b>139</b>
<b>CURRICULUM VITAE.....</b>	<b>143</b>

# LIST OF TABLES

## CHAPTER 2

Table 2.1 Summary of literature on the physical and geotechnical properties of raw oil sand MFT .....28

Table 2.2 Summary of literature on the clay mineralogy of raw oil sand MFT.....28

Table 2.3 Summary of literature on treatment technology of raw oil sand MFT.....29

## CHAPTER 3

Table 3.1 Characteristics of MFT used in this study .....56

Table 3.2 Oxide compositions of Portland cement used in the study. ....57

Table 3.3 Specification of silicate products used in the study.....57

Table 3.4 Typical values of K for Eq.3.4. ....57

## CHAPTER 4

Table 4.1 Overall test plan for this study. ....77

Table 4.2 Compressibility index ( $C_c$ ) of MFT samples treated by Portland cement. ....77

## CHAPTER 5

Table 5.1 Grouting formula for TYPE N sodium silicate (NS).....109

Table 5.2 Grouting formula for Aqueous Alkaline Aluminosilicate (AAAS)

.....	110
Table 5.3 Overall test plan for this study. ....	111
Table 5.4 Mixing ratio for N sodium silicate (NS).....	112
Table 5.5 Mixing ratio for Aqueous Alkaline Aluminosilicate (AAAS)	112
Table 5.6 Summary of Sensitivity of silicate-treated MFT samples. ....	113
Table 5.7 Index properties of silicate-treated MFT samples. ....	114
Table 5.8 Aquatic chemistry of decanted liquids from NS-treated MFT samples.....	115

## LIST OF FIGURES

### CHAPTER 2

Fig. 2.1 local distribution of oil sands in northern Alberta (Government of Alberta,2007) .....	30
Fig. 2.2 Typical arrangement of oil sand particles (ARC Tailings, 1977)	30
Fig. 2.3 Hot water extraction in oil sand processing (modified from Masliyah et al., 2004) .....	31
Fig. 2.4 Management of Tailing Ponds (ERCB, 2011).....	31
Fig. 2.5 Structure of the main clay minerals: (a) Kaolinite, (b) Illite, (C)Montmorillonite. (Modified from M. van der Perk, 2013) .....	32
Fig. 2.6a Distribution of cations and anions away from the clay surface (Mitchell and Soga, 2005) .....	32
Fig. 2.6b Stern-Gouy Double layer (modified from Shang et al., 1994)..	32
Fig. 2.6c The corresponding potential profile (Shang, J.Q. 1997) .....	32
Fig. 2.7 Structure of the main clay minerals: (a) Dispersed and deflocculated, (b) Aggregated (FF) but deflocculated, (c) Flocculated (EF) but dispersed, (d) Flocculated (EE) but dispersed, (e) Flocculated (EF) and aggregated, (f) Flocculated (EE) and aggregated, (g) Flocculated (EF and EE) and aggregated; (c) and (d): Card-house structure; (e), (f) and (g): Book-house structure. (van Olphen, 1963).....	34

Fig. 2.8 SEM images show effect of evaporation on MFT microstructure at 5 cm height after 10 days. (Roshani et al., 2017) .....34

Fig. 2.9 Soil stabilization by Portland cement: (a) Hydration reaction (b) Cation exchange (c) Pozzolanic reaction (compiled and modified from Prusinski and Bhattacharja, 1999) .....35

Fig. 2.10 Schematic diagram elucidating soil-cement hydration stages and pozzolanic reaction. (after Chew et al., 2004; Xing et al., 2009) .....36

### **CHAPTER 3**

Fig 3.1 Grain size distribution of original MFT .....58

Fig 3.2 X-ray Diffraction (XRD) on original MFT sample.....58

Fig 3.3 SEM imaging on freeze-dried original MFT (Mag=1,000X) .....59

Fig 3.4 EDS analysis on freeze-dried original MFT .....59

Fig 3.5 SEM micrograph for as-received cement (3,000x) .....60

Fig 3.6 XRD pattern of silicate powders .....61

Fig 3.7 Silicate viscosity VS silicate dilution ratios .....61

Fig 3.8 Close-up view of the colloidal Silicate gel.....62

Fig 3.9 ESEM imaging on the colloidal Silicate gel .....62

Fig 3.10 Freeze-drying of MFT samples .....63

Fig 3.11 Device for the sample preparation of SEM observation .....63

### **CHAPTER 4**

Fig. 4.1 Laboratory mixing device used in the study .....78

Fig. 4.2 Cylindrical plastic mold for curing, left: 50mm*100mm; Right: 100mm*200mm .....	78
Fig. 4.3 Daily quality of cement-treated MFT samples in 2” mold (50mm*100mm) versus curing time.....	79
Fig. 4.4 Water content and solid content of cement-treated MFT samples .....	79
Fig. 4.5 Atterberg limits of cement-treated MFT samples.....	80
Fig. 4.6 Casagrande plasticity chart.....	80
Fig. 4.7 Effect of curing time on particle size distribution curves of 10%- PC-MFT sample (measured from laser BT-9300S).....	81
Fig. 4.8 Correlation between falling cone, pocket penetrometer and laboratory shear vane tests .....	82
Fig. 4.9 Undrained shear strength of cement-treated Oil sands MFT .....	82
Fig. 4.10 1-D consolidation curves of cement-treated MFT after 28 days .....	83
Fig. 4.11 1-D consolidation curves of cement-treated MFT after 14, 28 days .....	83
Fig. 4.12 XRD patterns of original and cement-treated MFT samples after 28 days .....	84
Fig. 4.13 pH of cement-treated MFT samples at various curing periods.	85
Fig. 4. 14 SEM photos of 10% PC-stabilized MFT sample after 28-day curing, .....	86

Fig. 4.15 SEM photos of 10% PC-stabilized MFT sample after 28-day curing, (the black rectangular in figure (a) and (c) mark the zoomed-in areas in figure (b) and (d); the white arrows label the fibrous C-S-H morphology).....87

Fig. 4.16 SEM photos of 15% PC-stabilized MFT sample after 28-day curing, (4,000x; the white circle in figure mark the MFT-cement cluster) .....88

Fig. 4.17 SEM photos of 15% PC-stabilized MFT sample after 7-day curing (the black rectangular in figure (a) and (c) mark the zoomed-in areas in figure (b) and (d); the white circle in figure (b) mark Quartz mineral); .....89

**CHAPTER 5**

Fig. 5.1 (a) Mixing device and impeller blade; (b) Flow pattern during mixing (modified from Yao, 2016) ..... 115

Fig. 5.2 (a) Gel time determination of NS grout system; (b) Effects of setting agent and silicate concentration on the gel time of NS grout ..... 116

Fig. 5.3 (a) Gel time determination of AAAS grout system; (b) Effects of setting agent and silicate concentration on the gel time of AAAS grout 116

Fig. 5.4 (a) Water content of NS treated MFT; (b) Solid content of NS treated MFT ..... 117

Fig. 5.5 (a) Water content of AAAS treated MFT; (b) Solid content of AAAS treated MFT ..... 117

Fig. 5.6 Effects of silicate type and concentrations on the undrained shear strength gain of MFT samples .....	118
Fig. 5.7 Effects of curing period on the undrained shear strength gain of silicate- treated MFT samples.....	118
Fig. 5.8 Remolded undrained shear strength of NS treated MFT samples .....	119
Fig. 5.9 Remolded undrained shear strength of AAAS treated MFT samples .....	119
Fig. 5.10 Sensitivity of NS treated MFT samples .....	120
Fig. 5.11 Sensitivity of AAAS treated MFT samples .....	120
Fig. 5.12 Atterberg limits of NS treated samples .....	121
Fig. 5.13 Atterberg limits of AAAS treated samples .....	121
Fig. 5.14 Liquid limit test of MFT samples treated by high amount of silicates.....	122
Fig. 5.15 Plastic limit test of MFT samples treated by high amount of silicates.....	122
Fig. 5.16 Casagrande plasticity chart.....	123
Fig. 5.17 (a) Electrical conductivity of NS-treated MFT; (b) Electrical conductivity of AAAS-treated MFT; .....	124
Fig. 5.18 (a) pH of NS-treated MFT; (b) pH of AAAS-treated MFT;....	124
Fig. 5.19 The volume of decanted liquid of NS-treated MFT samples ..	125
Fig. 5.20 Zeta potential of the solid particles in silicate-treated MFT	



samples.....	125
Fig. 5.21 XRD pattern of NS-treated MFT samples.....	126
Fig. 5.22 XRD pattern of AAAS-treated MFT samples .....	126
Fig. 5.23 XRD pattern of initial MFT sample and 5% silicates treated MFT samples.....	127
Fig. 5.24 SEM photos after 28-day curing (Mag=2000x). (a) 5% NS-MFT; (b) 5% AAAS-MFT; (c) 10% NS-MFT; (d) 10% NS-MFT; (e) 40% NS-MFT; (f) 40% AAAS-MFT;.....	128
Fig. 5.25 SEM photos for 10% silicate-treated MFT samples consolidated up to a stress level of 5 kPa after 28-day curing (Mag=2000x): (a) NS; (b) AAAS.....	129

## **NOMENCLATURE**

MFT: Mature fine tailings

USCS: unified soil classification system

ICP: Inductively coupled plasma

SEM: Scanning electron microscopy

EDS: Energy-dispersive X-ray spectroscopy

XRD: X-ray diffraction

ASTM: American Society for Testing and Materials

PC: Portland cement

NS: Type N sodium silicate

AAAS: Aqueous alkaline aluminosilicate

$S_u$  ( $C_u$ ): Undisturbed undrained shear strength (kPa)

$S_{ur}$ : Remolded undrained shear strength (kPa)

$S_t$ : Sensitivity

G<sub>s</sub>: Specific gravity

W%: Water content

S%: Solid content

e: void ratio

e-log  $\sigma'$ : compression curves

$P_c'$ : preconsolidation pressure

cP(s): centipoise, unit of viscosity

LL: Liquid limit

PL( $I_p$ ): plastic limit

PI: plasticity index

LI: Liquidity index

ZP: Zeta potential (mV)

$\mu\text{S/cm}$ : micro Siemens/centimeter, electrical conductivity unit

$\text{mS/cm}$ : milli Siemens/meter, electrical conductivity unit

C-S-H: Calcium silicate hydrates

rpm: revolution(s) per minute

NTU: Nephelometric turbidity unit

# CHAPTER 1 INTRODUCTION

## 1.1 Background

Extraction of Bitumen from the surface-mined oil sands ores in northern Alberta generates large volumes of tailings with high water content, which are mixtures of clay, silt, sand, residual bitumen and other hydrocarbons (Beier and Segó, 2008; Jeeravipoolvarn et al., 2009). The tailing suspension gradually settle to achieve approximate 30% (w/w) solid content, known as mature fine tailings (MFT) during the deposition (Siddique et al., 2014; Thompson et al., 2017). The accumulation of MFT and tailing storage ponds exerts significant impacts on the indigenous economics and environment, and compels the oil sand industry to take measures to meet the regulations set forth by the government (Farkish and Fall, 2013; Wang et al., 2014). Therefore, minimizing the volume, increasing the density and strength of MFT are likely to be the most important goals for the ongoing treatment (Salam et al., 2016).

Chemical treatment or stabilization is one of soil improvement techniques in geotechnical applications. The process involves the incorporation of chemical additives to the soil matrix, leaving to improvement of physical and engineering properties of soft soil through chemical reactions between the soil particles, pore fluid and stabilizers (e.g. Bell, 1988; Sherwood 1993; Latifi et al., 2016a). The stabilizers can be divided into two broad categories: traditional agent (e.g. cement, lime, fly ash) and nontraditional agent (e.g. ionic, polymer, enzyme) (Rauch et al., 2003; Tingle et al., 2007). The latter one is being actively marketed and supplied as concentrated liquids (Latifi et al., 2016b). However, these liquid-based products have their proprietary properties and it is difficult to predict their performance on their practical use in a specific project because little information is readily available (Latifi et al., 2017).

This research investigates the influence of a sodium silicate product (NS) and a novel aluminosilicate product (AAAS)- an ionic and alkaline aqueous stabilizer on the

treatment of MFT. In the case of silicate solutions, they are used with inorganic setting agents (e.g. calcium chloride, lime, etc.) in chemical grouting on sandy soils but limited studies are conducted on fine-grained soils. In addition, the mechanisms of stabilization by silicates and organic setting agents (e.g. organic acids, esters) were poorly documented. Portland cement was used in this study to compare with liquid-based silicate grouts. Though extensive research has been conducted on the application of Portland cement as a cementitious binder for soil improvement, effects of Portland cement on the improvement of MFT have not yet been reported in the literature.

This study provides much needed information on utilizing cement and silicates to deal with MFT. The results also provide insights for other fine-grained geo-materials with high water content and compressibility, such as waste sludge and dredged mud, on the treatability of cement and silicates.

## **1.2 Research objectives**

The objective of this research was to characterize and examine the effect of traditional and nontraditional chemical stabilizers in improving MFT. The entire experimental conducted to develop an overall understanding of the stabilization process. The specific objectives are listed as follows:

- To determine the basic properties of untreated MFT and chemical binders for the subsequent analysis.
- To design and carry out an assessment on the binder dosages and curing time required to obtain desired parameters from the geotechnical point of view.
- To evaluate and compare the effectiveness of traditional solid stabilizer (PC) with non-traditional liquid based additives (silicate grouts) on the treatment of MFT.
- To interpret and understand the mineralogical and microstructural changes of MFT after chemical treatment by microscopic and spectroscopic studies.

### **1.3 Organizations of thesis**

The thesis is divided into six chapters.

Chapter 1: This chapter shows the outline of the thesis, including the research objective and original contributions.

Chapter 2: The chapter provides a comprehensive review, including a description of MFT, production of MFT, properties of MFT, related issues and management perspectives. In addition, the background of clay structures and properties, as well as the principles responsible for the stabilization process using Portland cement and silicate grouts are reviewed in detail.

Chapter 3: This chapter presents the information pertaining to the testing methods and the stabilizers (Portland cement and liquid silicates) used in this study.

Chapter 4: This chapter discusses the laboratory test results of the cement-treated MFT samples and explain the results in light of both macroscopy and microscopy. The results of undrained shear strength, solid content, Atterberg limits and compressibility are reported to evaluate the effects of binder dosages and curing time on MFT treatment.

Chapter 5: This chapter contains an experimental program developed to fortify the oil sands tailings using liquid-based silicate grouts. The results of undrained shear strength, sensitivity, solid content, Atterberg limits, gel time, pore water chemistry and Zeta potential are reported. The underlying mechanisms are discussed on the basis of microstructural observations.

Chapter 6: This chapter summarizes the study, and makes comparison and evaluation between two chemical agents in relation to the MFT treatment. The key findings are highlighted based on the results obtained in this study. The recommendations for future studies are also proposed.

## **1.4 Contributions of the thesis**

The contribution of the work is outlined as follows:

- Evaluation and interpretation of the effect of Portland cement treatment on oil sands MFT.
- Optimization of the treatment efficacy of different silicate products with organic setting agents.
- Establishment of the correlation between inherent silicate properties, such as gel time and gel syneresis, with the engineering properties of the MFT samples.
- Paired micro-level analysis on cement and silicate amended MFT, for understanding mechanisms of stabilization process of the MFT.

## References

**Beier, N., and Segoo, D. (2008)** The oil sands tailings research facility. *Geotech. News*, 2008: 72–77

**Bell, FG (1988).** “Stabilisation and Treatment of Clay Soils with Lime, Part 1 – Basic Principles,” *Ground Eng*, 21, 10–15.

**Farkish A, Fall M. (2013)** Rapid dewatering of oil sand mature fine tailings using super absorbent polymer (SAP). *J Minerals Eng*;50(51):38–47.

**Jeeravipoolvarn, S., Scott, J.D., Chalaturnyk, R.J. (2009)** 10 m standpipe tests on oil sands tailings: long term experimental results and prediction. *Canadian Geotechnical Journal*, 46:875-888

**Latifi N, Meehan CL, Abd Majid MZ, Horpibulsuk S (2016a)** Strengthening montmorillonitic and kaolinitic clays using a calcium-based non-traditional additive: a micro-level study. *Appl Clay Sci* 132:182–193.

**Latifi N, Rashid ASA, Siddiqua S, Abd Majid MZ (2016b)** Strength measurement and textural characteristics of tropical residual soil stabilised with liquid polymer. *Measurement* 91:46–54.

**Latifi N, Eisazadeh A, Marto A, Meehan C.L, (2017)** Tropical residual soil stabilization: A powder form material for increasing soil strength. *Constr Build Mater* 147 827-836

**Rauch A. F., Katz L. E., and Liljestrang H. M., (2003)** An Analysis of the Mechanisms and Efficacy of Three Liquid Chemical Soil Stabilizers, Center for Transportation Research, The University of Texas at Austin

**Salam, A.M., Örmeci, B., Simms, P.H., (2016)** Determination of the optimum polymer dose for dewatering of oil sands tailings using UV–vis spectrophotometry. *J. Petrol. Sci. Eng.* 147, 68–76.



**Sherwood, T.P. (1993)** Soil stabilization with cement and lime: state of the art review. HMSO Books, London.

**Siddique, T., Kuznetsov, P., Kuznetsova, A., Li, C., Young, R., Arocena, J.M., Foght, J.M., (2014b)** Microbially-accelerated consolidation of oil sands tailings. Pathway II: solidphase biogeochemistry. *Front. Microbiol.* 5 (Article 107).

**Thompson, D.K., Motta F.L., Soares J.B.P., (2017)** Investigation on the flocculation of oil sands mature fine tailings with alkoxy silanes. *Miner.Eng.*111. 90-99.

**Tingle JS, Newman JK, Larson SL, Weiss CA, Rushing JF (2007)** Stabilization mechanisms of nontraditional additives. *Transp Res Rec: J Transp Res Board* 1989(1):59–67

**Wang, C., Harbottle, D., Liu, Q., Xu, Z., (2014)** Current state of fine mineral tailings treatment: a critical review on theory and practice. *Miner. Eng.* 58, 113–131.

# CHAPTER 2 LIERATURE REVIEW

## 2.1 Introduction

The chapter begins with the introduction of Canadian Oil Sands. A brief description of tailings production, fine tailing properties and related issues, as well as the disposal technologies are presented. Next, the concepts of clay fabrics and microscopic analysis are reviewed to better understand the soil behavior during the chemical stabilization. The commonly used chemical additives (i.e. Portland cement and silicate-based materials) for the soft soil improvements are also reviewed in detail, followed by a brief discussion on their applications. At the end of this chapter, several up-to-date cases relevant to the present study are discussed.

## 2.2 Oil Sand Mature Fine Tailings (MFT)

### 2.2.1 Production of MFT

Canada holds one of the largest oil sand deposits. The oil sands deposits nearly cover the entire area of the northern Alberta, as shown in **Fig. 2.1**. There are three main geographical oil sand regions: Athabasca, Peace River and Cold lake. Of these, Athabasca is the only one currently subjecting to commercial exploitation by Canadian companies, and it possesses the largest deposit of bitumen (over  $1.4 \times 10^{11} m^3$ ) in the world allowing for large-scale surface mining (CCA, 2009).

Oil sands are mainly composed of oil, bitumen, sands, fines and water. **Fig. 2.2** depicts the general arrangement of these components, showing that the sand grains are being surrounded by a water film and a bitumen film (ARC Tailings, 1977). The production of bitumen from oil sands relies on the open-pit mining and hot water extraction process (Beier et al., 2013). At shallow depth to the earth oil sands are excavated and then transported to the plant using pipelines, followed by agitation with a mixture of hot water, steam and process aids (e.g. caustic soda) for the bitumen recovery. **Fig 2.3**

depicts the procedures of the extraction process in detail. Nearly 90% of the bitumen can be recovered during this process, but byproduct is also generated, i.e oil sand tailing stream (termed as ‘whole tailings’), along with the crude oil. The whole tailings are typically composed of the same substances as bulk oil sands but with much less bitumen. The whole tailings are transferred to tailing storage facilities where tailings particles gradually settle and segregate (see **Fig. 2.4**). The sand-sized particles and fines entrapped within large particles settle quickly to form dykes and beaches while leftover fines, bitumen accumulate in the center of tailings ponds to form so-called Fluid fine tailings (FFT) with the solid content in the order of 8% (OSRIN Report, 2010). After several years, the FFT settles and reaches the solid content to 30%-35%. At this solid content, FFT may stay in slurry-like state for up to 150 years without any treatment (Kasperski, 1992). These dispersed and suspended particle groups trap a large amount of water and show no further self-weight consolidation, hence they are known as Mature fine tailings (MFT).

The long-term storage of MFT in the tailing ponds is a major challenge for the oil sand industry and raises significant public concerns in terms of environmental protection and land use. In this regard, many ongoing efforts are undertaking, e.g., dewatering and strengthening of MFT for water recycle and land reclamation.

### **2.2.2 Property and behavior of MFT**

The properties of MFT measured in the laboratory tests by many researchers are summarized in **Table 2.1**. The results show that there is no significant difference regarding the basic properties of Alberta oil sand tailings. However, the large fraction of dispersed clay particles (i.e. 30%-50%), as well as the presence of bitumen in the MFT exerts a great influence on geotechnical properties of the tailings. For example, high fine contents in MFT are responsible for the low settling rate of solids, and low hydraulic conductivity (i.e. typically  $10^{-6}$ - $10^{-9}$  m/s), which is also affected by the bitumen content, impedes the water flow within and through the MFT (Scott et al.,

1985). It was also reported that the undrained shear strength of the initial MFT is extremely low, typically much less than 1 kPa, and the viscosity of MFT suspensions generally increases with time and solid content (OSRIN Report, 2010; Yao, 2016). All these properties indicate that dewatering of MFT is difficult and time-consuming.

The chemistry and composition of the tailings pore water, which are greatly affected by the water or chemicals used during the extraction process, may also have a considerable influence on the MFT structure (Allen, 2008). The tailing water is basic in nature with a typical pH range of 7.6-8.4, carrying suspended solids and toxic compounds (Allen, 2008), such as heavy metals (Liang et al. 2011). In general, bicarbonate ( $\text{HCO}_3^-$ ) is the dominant anion in MFT with lesser concentration of chloride ( $\text{Cl}^-$ ), phosphate ( $\text{PO}_4^{3-}$ ) etc., sodium ion ( $\text{Na}^+$ ) is the dominant metal cation with lesser concentration of potassium ( $\text{K}^+$ ), calcium ( $\text{Ca}^{2+}$ ) and magnesium ( $\text{Mg}^{2+}$ ) etc. (Proskin et al., 2012). It is also reported that MFT contained high concentrations of sulfate ( $\text{SO}_4^{2-}$ ) (Wolter and Naeth, 2014).

### **2.2.3 Issues in oil sand MFT management**

There are two major issues associated with the MFT: i.e. the water quality, supply and reuse, and land use of tailings ponds and reclamation. It is important to recycle water from the extraction process to reduce the freshwater usage. However, it was reported that reinforcing use of recycled water may contribute to a decline in quality of facilities (Gosselin, 2010). In addition to this, the expansion of tailings ponds due to the increasing production of MFT has emerged to be a concern, as more than 220 km<sup>2</sup> of Alberta's total lands have been devoted to the tailings ponds (Government of Alberta, 2013) which increases the risk of groundwater contamination.

In light of these problems, effective disposal strategies are imperative for MFT management. Dewatering and solidification of the tailings are necessary so that MFT slurry become trafficable for reclamation. To this end, some requirements (e.g. Directive 074 (2009), Directive 085 (2016)) have been set out which compel the

industry to meet the goals through multiple technologies.

#### **2.2.4 Treatment technologies of MFT**

Over the years, some promising approaches for the MFT treatment have been introduced and applied. OSRIN Report (2010) presented a review of these treatment technologies, which can be categorized in five types:

- Physical/Mechanical Processes
- Mixtures/Co-disposal
- Permanent Storage
- Natural Processes
- Chemical/Biological Amendments

Physical/Mechanical processes are used to separate water from the solids by various means such as centrifugation, surcharge loading, electrical treatment or filtration; Mixtures/Co-disposal techniques involve mixing tailings with soil materials (e.g. coarse sand) and other available wastes to densify the tailings; Permanent Storage of MFT can be achieved by using water capping. A layer of water is placed over the tailing deposits which avoid liberation of blowing dust from the tailings (Kirk et al., 2014), and also allows the formation of lakes habitable for animals and plants (MacKinnon et al., 2017); Natural Processes involve using environmental or geophysical processes to remove water from solids, such as freeze-thaw and evaporation (OSRIN Report, 2010); Chemical amendments are aimed to remove water by changing the properties of the tailings. Thickened tailings (TT) technology is one of the chemical treatment method, during which the chemical additives called flocculants are added to coagulate the fine fractions in the tailings and make them settle down.

The anticipated effectiveness of MFT treatment can be achieved by combining more than one techniques (Farkish, 2013). It is noted that some technologies are still in the laboratory research stage due to lack of either the technical or economic feasibility,

whereas some of them have been implemented in the field successfully.

**Table 2.3** summarizes the state-of-the-art approaches on MFT treatment from available references (as of the year 2017). It is noted that chemical amendments for MFT treatment have gained interests over time, and some promising results are obtained. As an example, Zhu et al., (2017) reported that after adding the dual polymer flocculants to the MFT, the solid content of MFT increased significantly from 35.6% to maximum 64.1%. It is also reported that the polymers changed the pore sizes and porosity of the MFT, hence dewaterability of tailings was improved.

## **2.3 Clay microstructure**

As indicated previously, MFTs contain significant fraction of clay minerals. Applications of chemical additives to the MFT may change the clay structural characteristics and mineral compositions. Thus, it is necessary to understand the properties of clay minerals and their effects on soil behaviors.

### **2.3.1 Clay minerals**

Clays are distinguished from other soil particles by their small sizes (less than 2 microns), net negative electrical charges as well as the plasticity when mixed with water (Mitchell and Soga, 2005). The main groups of crystalline materials in clays are Kaolinite, Illite and Montmorillonite, as depicted in **Fig. 2.5**. Kaolinite consists of one silica sheet and one alumina sheet bonded together into a layer, and the layers are held by strong hydrogen bonds; Illite and Montmorillonite have quite similar structures that consist of repeated layers of one alumina sheet and two silica sheets, but Illite layers are held by potassium ions whereas Montmorillonite layers are held by weak molecule forces (Budhu, 2007). Therefore, as for the Montmorillonite, it is possible for water to penetrate and separate the interlayers. This is the main reason why Montmorillonite has a greater ability to adsorb water and a higher swelling potential compared to Kaolinite and Illite.

### 2.3.2 Diffuse double layer and zeta potential

It is known that the surface charges on clay minerals are negative because of the isomorphous substitution (Mitchell and Soga, 2005). The negative charges attract counterions and positive hydrogen side of water molecules, forming a region known as ‘electrical double layer’ on the mineral surface. This region is divided into two parts: the inner region (Stern layer) where the cations are strongly bonded and an outer region (Gouy diffuse layer) where the cations are less firmly bonded (**Fig. 2.6a**). Therefore, the largest concentration of cations occurs near the clay surface and decreases with distance till the surface charge of particle is balanced (**Fig. 2.6b**). Note that the water film which is firmly adsorbed on the mineral surface, called as ‘adsorbed water’, is very thin and cannot be mechanically removed (Mitchell and Soga, 2005).

Within the Gouy diffuse layer there is an imaginary boundary inside which the ions and particles form a stable entity, and these ions are considered to be part of the solid phase (Somasundaran and Zhang, 2006). Beyond this boundary (known as ‘shear plane’) the ions are supposed to move freely, and the electrical potential at this boundary is called zeta potential (**Fig. 2.6c**). However, the location of the zeta potential cannot be quantitatively determined by the existing theories (Shang, 1997), as the position of the shear plane is not constant in the diffuse layer owing to the variation of pore fluid chemistry. Hence, in order to characterize the electrical properties of the clay particles, zeta potential can only be experimentally measured as a substitute for the surface potential or Stern potential which cannot be obtained from the tests (Lu, 2016).

The magnitude of zeta potential changes with the double layer thickness (Moayedi et al., 2012). In general, the thicker the double layer, the higher the zeta potential and therefore higher surface potential of charged clay particles. However, changes in double layer thickness can alter the engineering performances of clays. For example, a thicker double layer contributes to a smaller effective pore space, which in turn reduces the hydraulic conductivity of soils. (Schmitz, 2006).

### 2.3.3 Clay particle associations

In general, the interactions between interparticle forces, i.e., attractive forces (London Van der Waals forces) and repulsive forces (Double layer forces) occurs when two clay particles approach each other, which greatly influences the modes of particle association in clay suspensions. Based on the different geometries, the associations of clay particles can be simply defined as four types (Mitchell and Soga, 2005):

- Dispersed (No face-to-face (FF) association of clay particles),
- Aggregated (Face-to-face (FF) association of several clay particles),
- Flocculated (Edge-to-edge (EE) or edge-to-face (EF) association of clay particles)
- Deflocculated (No EE or EF association of clay particles).

**Fig. 2.7.** depicts the common arrangement of soil particles. In particular, the clay structure with flocculated but dispersed particle arrangement is referred to as ‘card-house structure’ (**Fig. 2.7 (c) and (d)**), while the clay structure with flocculated and aggregated particle arrangement is termed as ‘book-house structure’ (**Fig. 2.7 (f), (e) and (g)**) (Mitchell and Soga, 2005).

### 2.3.4 Microscopic analysis

#### 2.3.4.1 Surface Imaging by Scanning electron microscope (SEM)

The scanning electron microscope (SEM) can provide visual information on clay particles and material surface directly, such as the structural arrangement of particles and distribution of the pore spaces between the aggregates (Mitchell and Soga, 2005).

There are two commonly used SEM techniques: Regular SEM and Environmental SEM (ESEM). Regular SEM observation technique requires high vacuum so that only dehydrated and electrically conductive samples can be observed, while ESEM allows moisture inside the samples under various pressures and temperatures. In SEM or ESEM, when a beam of the electrons hit the sample, the specimen surface releases the



electrons that can be detected and scanned, generating the images. In general, SEM is equipped with an energy-dispersive spectrometry (EDS) detector. When imaging the clayey soils, EDS is usually performed to find the elemental information on the clay particles and potential composition of products in stabilized soils or geo-materials (e.g. Jeeravipoolvarn, 2010).

It is noted that some investigations on MFT fabrics has been done by SEM. Tang et al., (1997) captured the microstructure of the raw MFT, suggesting that MFT had typically ‘card-house’ structure with large pore spaces entrapping bulk of water; Fard (2011) investigated the raw MFT using ESEM technique, and indicated that the clay particles existed not only in the water film, but also at the surface of the sand grains; Liang et al (2015) used SEM to track the fabric changes of MFT induced by the microbial-based treatments and found that the tailing particles united into the large particles after treatment, rendering a higher undrained shear strength; Roshani et al., (2017) performed SEM analysis on the MFT samples being dried in a column with 10m height, and reported that the ‘card-house’ structure (**Fig. 2.8**) was more prominent at the bottom of the column since evaporation had no influence at that location. This observation was in agreement with a study conducted earlier by Jeeravipoolvarn (2005), who also reported that the samples appeared more compressed with flocculated but dispersed associations at the bottom of the 10m stand pipe.

#### **2.3.4.2 Identification of minerals by X-Ray Diffraction (XRD) analysis**

XRD identifies mineralogy of crystalline compounds based on their unique crystal structure. In geotechnical engineering, X-ray powder diffraction is widely used to characterize the nature of clay minerals and nonclay minerals occurring in soils (Mitchell and Soga, 2005). In general, the pulverized solid powders are slightly pressed into the sample holders without rubbing at the smooth surface so that the dry particles are well distributed and randomly oriented. When the target materials (clay particles) are bombarded with a beam of electrons, X-rays are generated. During this process, the locations (angles) and intensities of the diffracted X-rays are collected. The minerals

can be identified by matching the peaks in the patterns with the data available in the references or typical standard files.

Although the amounts and types of the clay minerals found in the tailing ponds vary enormously, it is reported that kaolinite and illite are the main clay minerals in MFT, as summarized in **Table 2.2**, while the non-clay fraction of MFT is mainly composed of Quartz ( $\text{SiO}_2$ ).

## **2.4 Chemical stabilization**

### **2.4.1 Introduction**

Soil stabilization by chemical admixtures was developed in Japan during 1970-1980, and now it has been one of the effective methods used to deal with the soft ground (Kazemian and Huat, 2010). Chemical stabilization can be simply defined as a process of improving the weak properties (e.g. shear strength, compressibility, hydraulic conductivity etc.) of the soft soils by introduction of the chemical agents (Makusa, 2013). These chemical admixtures can be either in slurry format (wet method) or powder format (dry method), and they can be categorized into three groups (Little and Nair, 2009):

- **Traditional stabilizers:** lime, Portland cement, fly ash, granulated slag, etc.
- **Non-traditional stabilizers:** enzymes, polymers/biopolymers, electrolytes, etc
- **By-product stabilizers:** cement kiln dust (CKD), lime kiln dust (LKD) etc.

Among them, the traditional stabilizers such as Portland cement are still the most popular options because they are quite compatible with other stabilizers and easy to obtain (Hausmann, 1990). However, the production of these traditional stabilizers is usually accompanied by the generation of some industrial byproducts (e.g. CKD, LKD) which can also be used in the soil stabilization as a stabilizer with the same mechanisms (Latifi et al., 2014).

Moayed et al., (2013) reported that the non-traditional stabilizers such as polymers have also gained much popularity among engineers because of their shorter curing. Several investigations indicate that these novel stabilizers work through diversified mechanisms including encapsulation of clay minerals, exchange of interlayer cations, breakdown of clay mineral with expulsion of water from the double layer, or interlayer expansion with subsequent moisture entrapment (Katz et al., 2001; Tingle and Santoni, 2003; Eisazadeh et al., 2010).

It should be stressed that the selection of the stabilizers, however, depends heavily upon the soil type and project goals. For example, Portland cement is assumed to be appropriate to treat the calcium clays with low plasticity index (less than about 25), whereas the expansive sodium bentonites and hydrogen clays respond better to lime stabilization (Das, 2012).

## **2.4.2 Ground improvement by Portland cement**

### **2.4.2.1 Introduction**

Portland cement (PC), as one of the most common traditional stabilizers, has been used for many years in strengthening the soft soils such as silty, clayey peat and organic soils (Makusa, 2013). The typical Portland cement consists of four main components: Tricalcium silicate ( $C_3S$ ), dicalcium silicate ( $C_2S$ ), tricalcium aluminate ( $C_3A$ ) and tetracalcium aluminoferrites ( $C_4AF$ ), as indicated by Prusinski, et al (1999). When placed into the soils, these main components of Portland cement react with the soil water and directly lead to the artificial cementation, irrespective of what the soil minerals are (EuroSoilStab, 2002). This may be the chief reason why cement can be used to enhance a broad range of soils.

In engineering applications, the designed strength of a cement-treated soil is usually determined based on its strength at 28 days to predict long-term strength gain. Reportedly, after a few years cement-treated soils have strengths that are 2–6 times higher than their 28-day strength gain (Nakarai and Yoshida, 2015).

For deep excavation projects, cement stabilization work is normally performed before the excavation commences (Tan, et al., 2002). The work can be achieved by mixing cement with the soft in-situ soil at great depth to produce soil-cement columns. Accordingly, these methods are termed as deep cement mixing (DCM) and cement jet grouting. In regions where lime is not available at reasonable costs, cement may be a preferred alternative due to the fast strength development (Chew et al., 2004).

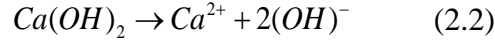
Portland cement's success in soil improvement is documented by many researchers. For instance, Bergado et al., (1996) reported that cement stabilization not only caused a reduction in soil water content, but also an increase in the plastic limit. In addition, the soil behavior changed from normally consolidated ductile behavior to over-consolidated brittle behavior; Yin (2001) found that after cement treatment, the strength and stiffness of the Hong Kong marine clay increased with the increase in the cement/soil ratio, and the cohesion of the cement-treated clay increased as the initial soil moisture decreased. Quang and Chai (2015) measured the hydraulic conductivity of cement-treated clays and reported that the treated clays exhibited a higher permeability, due to the high concentration of  $Ca^{2+}$  which depressed the double layer of the clays.

#### **2.4.2.2 Mechanism**

Hydration of Portland cement is the key chemical reaction responsible for the short-term strength gain of the soil-cement mixture. When cement is in contact with water, the hydration reaction (see **Fig. 2.9a**) is initiated immediately, generating cementitious products such as hydrated gels. These products serve as the “glues” since they fill the voids, enwrap the clay particles as well as link the surrounding cement grains and form a hardened framework (Prusinski and Bhattacharja,1999; Saeed et al., 2014). Due to this artificial cementation effect, the soil particles become agglomerated and therefore the whole matrix is strengthened. The reaction is given as follows (Kamruzzaman, 2002):



In addition, the hydration of cement supplies calcium ions ( $Ca^{2+}$ ) exchangeable with the monovalent ions existed on clay particle surfaces such as sodium and potassium which are less electronegative. The reaction is given as follows (Kamruzzaman, 2002):



The exchange reaction (see **Fig. 2.9b**) reduces the thickness of double layer of clay particles and results in an increase of interparticle attractive forces so that the clay particles get closer and become more flocculated (Al-Rawas et al., 2005; Xing et al., 2009).

Besides, cement raises the pH of the soil-cement mix. The higher the pH level, the greater likelihood of the reactive silica and alumina from the clay lattice dissolving into the pore fluid (Eades and Grim, 1966). These hydrous silica and alumina react with the available calcium ions in the soil water, forming the secondary bridging gels which further crystallize and bond the soil particles (clusters) in a similar way to those gels created by the cement hydration (Maaitah, 2012). This process is known as “pozzolanic reaction” (see **Fig. 2.9c**). Generally, it takes a longer time in comparison to the hydration reaction, basically over months or years depending on temperature, soil chemistry and mineralogy (Wild et al., 1993). In short, the pozzolanic reaction gives rise to a further improvement of the strength and stiffness of the soil after long-term curing. These reactions are given as follows (Kamruzzaman, 2002):

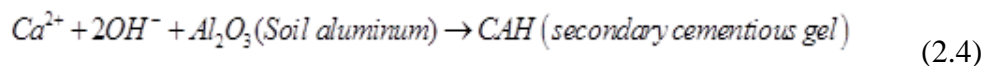


**Fig. 2.10** is a pictorial summary in terms of the aforementioned mechanisms and the resulting cementitious products. As indicated in figure, after adding Portland cement into soils, Ettringite crystals or calcium sulfates (Gypsums) may form during curing if there is abundant soluble sulfate in the soil. The formation of the Ettringite crystals in the soil body is usually accompanied by volumetric swelling which could cause damages to the soil structure and lead to a loss of strength during curing. The major

issue associated with the sulfate attack in the cement-stabilized soils is that it impedes the generation of the cementitious products such as C-S-H and C-A-H gel (Sasanian, 2011). To fix this problem, the sulphate-resistance Portland cement characterized by high iron content and low  $C_3A$  content was well developed and used although it was more expensive than the normal cement (Tariq and Yanful, 2013).

Moreover, several works on the cement-stabilized soils reported that the carbonation is another reason behind the strength gain of the soil. That is, the cement hydrates (e.g. poorly-crystalized C-S-H, C-A-H gel) in the soil react with the carbon dioxide ( $CO_2$ ), producing the calcium carbonates ( $CaCO_3$ ) within the soil matrix. For example, Nakarai and Yoshida (2015) investigated the effect of carbonation on the cement-treated sands and indicated that the formation of calcium carbonate ( $CaCO_3$ ) significantly promoted the long-term strength gain of sands under the natural conditions, as the porous sand allowed for deeper penetration of  $CO_2$  relative to clay. In addition, carbonation was also found to be effective in improving the short-term strength of cement-stabilized sediment (Chen et al., 2009).

### **2.4.3 Ground improvement by Silicates**

#### **2.4.3.1 Introduction**

Sodium silicate (waterglass, chemical formula:  $(Na_2SiO_2)_nO$ ) is an industry chemical produced by fusing sand ( $SiO_2$ ) with soda ash ( $Na_2CO_3$ ) at high temperature. Concentrated liquid is the most popular marketed form of the sodium silicates. As a member of the silicate family, sodium silicate is typically inorganic, glassy and colorless which has been considered as the most convenient and cost-effective source of the soluble silicates (Power, 2007). It is also claimed by the silicate manufactures that sodium silicate products are environmental-friendly (nontoxic), noncorrosive, and easy to use. It is worth mentioning that sodium silicate has been successfully used as a raw material in a wide range of applications such as water shut off in the oil field and sealing concrete in the structures. In geotechnical applications, sodium silicates are

extensively used for chemical grouting in excavation and tunneling projects (PQ Corporation, 2003).

#### **2.4.3.2 Property of silicates and silicate-based grouts**

Sodium silicate has two important properties that controlling its performance in use, i.e. molar ratio and viscosity (Littlejohn et al., 1997; PQ Corporation Bulletin):

- Molar (weight) ratio is referred to the ratio of  $\text{SiO}_2:\text{Na}_2\text{O}$ , which determines the reactivity and mechanical properties of the silicate solution.
- Viscosity is the property of a fluid to resist flow under forces. For silicate solutions, the viscosity is a function of the molar ratio, temperature and total solid content ( $\text{SiO}_2\% + \text{Na}_2\text{O}\%$ ). Silicate viscosity can be reduced by dilution.

As a soil stabilizer, sodium silicate is generally used with a setting agent (reactant). Examples of setting agents are pozzolans, acidic salts, organic acids or esters (PQ Corporation, 2003). For most grouting applications, the silicate solutions are diluted by water first and then mixed with a setting agent to form a resulting grout, prior to the injection. By doing so, the grout can penetrate the soil without the need of mixing. It should be noted that the solutions (i.e. diluted silicates and aqueous setting agents) can also be injected into soil separately.

The engineering properties of silicate-based grouts or mixtures have a profound influence on the soil performance. The properties include:

- Grout viscosity: For a given temperature, the initial grout viscosity is a function of the silicate/water ratio, type of the silicate used (solid content %, molar ratio), and amount of the setting agent used. After a certain period of time, the grout viscosity begins to build up sharply, indicating that the gel formation commences.
- Gel time/set time. Gel time is the interval between initial mixing of the chemicals and formation of the gel (US Army Corps of Engineers, 1995). For a specific project, gel time needs to be flexible but the decision of the gel time depends heavily on the situations and practical purposes. Karol (2003) indicated that at longer gel time, the

colloid silicate-based grouts placed in the treated area may be flushed away by groundwater flow as they are not yet able to form a rigid gel. If the gel time is short, the treated area may not be adequately covered by the grouts, and what's worse, the pipeline may be blocked in the transportation of grouts (Lin, 2006).

- Cure time. The gel continues to gain strength after gelation. The time interval until the desired properties are attained is termed as cure time (US Army Corps of Engineers, 1995).

- Syneresis. The gel shrinks and squeezes the liquid out of it when the system approach an equilibrium after gelation, and this phenomenon is called 'syneresis' (Al-Dhafeeri et al., 2008). It was found that the more rapidly the gel sets, the higher the syneresis rate becomes and more volume of liquid expelled (Ferguson and Applebey, 1930). Furthermore, it was reported that the syneresis of the gels may cause an increase in the hydraulic conductivity of those silicate-treated soils (Powers, 2007).

The strength that a silicate gel imparts to a stabilized soil is primarily a function of the silicate content and curing conditions (Karol, 2003). The silicate content used in grouting may vary from 10 to 70% by volume, depending on the result desired (US Army Corps of Engineers, 1995).

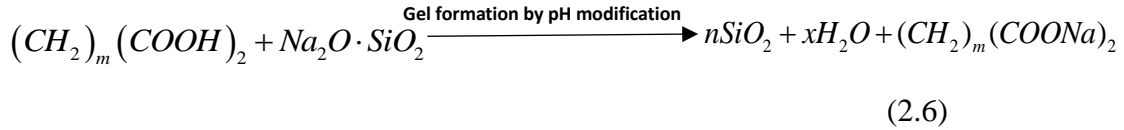
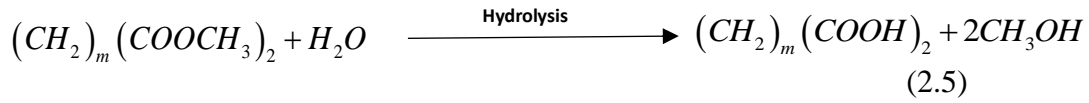
### **2.4.3.3 Mechanism**

Similar to the stabilization by using Portland cement, the soils are densified and fortified by the chemical products (e.g. silica gels) derived from the silicates. The working mechanisms for the silicates are listed as follows (McDonald et al, 2009):

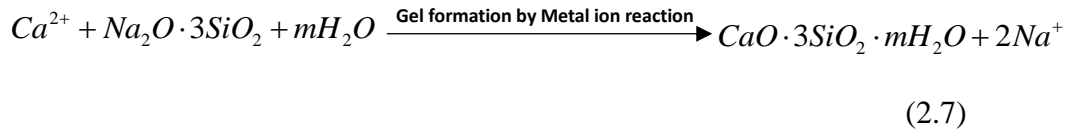
- Gelation (Polymerization). The formation of the gel occurs when pH of a silicate solution drops lower than 10.7. After neutralization, the silica is no longer soluble. The silicate species begin to form particles and line up to form a network, finally thickening to the silica gel (Iler, 1979). It should be noted that water molecules are captured and locked in the network of silicate molecules in the gels (Pham and Hatzignatiou, 2016). The organic reagent does not appear to be a significant chemical constituent of the final



gel (Malone et al., 1995). The reactions are given as follows (PQ Corporation<sup>1</sup>):



- Metal ion reaction (Precipitation). Polyvalent metal ions react with silicate solution to produce gelatinous products, such as insoluble calcium silicates (Ma et al., 2002):



- Hydration (Dehydration). The silicate solution gradually forms dried film coating when heated. This physical bond has a high level of water resistance.

- Surface charge modification. Silicates contributes an ionic charge of 2 to other particles, modifying their surface property which causes the particles to repel with each other.

It should be noted that each reaction listed above could coexist with another one at same time. When sodium silicate is used in conjunction with a setting agent, the resulting silica gel is formed by consumption of the base (Eq. 2.6) or precipitation of metal ions (Eq. 2.7). The gel binds the soil grains together, imparting a cohesive property to the overall soil-silicates matrix, thereby increasing the soil strength (Malone et al., 1995). However, the magnitude of the strength improvement depends largely on the ability of these gels to coat the particles. It is also reported that there is little change in the friction resistance of the soil deposits (Malone et al., 1995). The process that the precipitates (e.g. insoluble silicates) sheaths around the soil particles is generally accompanied by

---

<sup>1</sup> The reaction equations were obtained through personal communications with PQ Corporation.

cementation effects (Wooltorton, 1955). However, the detailed mechanism such as the nature of the bonding action of hydrated precipitates has not been fully understood to date.

## **2.5. Case study**

### **2.5.1 Cement stabilization**

**Chew et al., (2004)** investigated the engineering properties and microstructural evolution of Singapore marine clay, a highly plastic and inorganic soil, after stabilization with cement. The predominant clay mineral was Illite. The authors indicated that the introduction of cement made structured soil. Some indicative results could be obtained:

- The majority of decrease in water content took place within the first 7 days, the reduction became more significant as more cement was added.
- Unconfined compressive strength (UCS) test results showed that the treated specimen became much more brittle after adding large amount of cement, and the soil behavior was similar to sensitive clays.
- The 7-day strength of the soil was contributed largely by the cement hydration which relied on the cement content, while 28-day strength of the soil was contributed largely by the pozzolanic reaction which relied on the availability of clay minerals.
- The optimal cement dosage was found to be 10%.
- Stabilization of the clay slurry using Portland cement increased the porosity and pore sizes of the soils. The pore sizes decreased gradually as more cementitious products formed during the curing process.

**Bahmani et al., (2016)** reported a study on the strength development of cement-treated residual soil using nano silica as supplementary material. Some interesting results could

be summarized as follows:

- A more significant decrease in the water content was observed in samples with nano silica within the first 7 days of curing, compared to that of samples with cement only. This could be attributed to the accelerating effect of nano-silica on the cement hydration.
- Addition of nano silica increased the compressive strength and plasticity index of the cement-treated soil.
- The specimens containing nano-silica were denser and more homogeneous than the samples with cement only. This was because of a better distribution of C-S-H gels in the soil-cement matrix with the aid of nano-silica.
- Additional formation of C-S-H gels in the cement-treated soil occurred when more nano-silica was added, as nano-silica with high amount of  $\text{SiO}_2$  could react with hydration product ( $\text{Ca(OH)}_2$ ) and therefore enhanced the rate of pozzolanic reaction.
- The inclusion of nano silica could reduce cement consumption in soil and accelerated the improvement process.

**Ho et al., (2017)** investigated the effects of carbonation, water content, and pozzolanic reaction under the constant temperature ( $20^\circ\text{C}$ ) and humidity (60%) on the strength development of cement-treated soils. The results were:

- The hydration reaction and pozzonlanic reaction were the main mechanisms for the strength development of the cement-treated soil when the specimens were cured under the sealed condition.
- The carbonation and suction (changes in the water content) were the main mechanisms for the strength development of the cement-treated soil when the specimens were cured at the unsealed condition.
- Soils with a higher clay content might have a higher ability of retaining water and a slower water evaporation rate.

- Carbonation of cementitious products caused a strength development in the clay-sand-cement mixture, especially at the early stage. After 28 days, the effect of carbonation to the strength gain turned to be smaller. This was mainly because of the carbonation of C-S-H gel, instead of the carbonation of Ca (OH)<sub>2</sub>.

### **2.5.2 Sodium silicate grouts stabilization**

**Moayedi et al., (2012)** evaluated the effect of sodium silicate together with two different activators (i.e. calcium chloride and aluminum sulfate) on the strength development of organic soil with high initial moisture content (158%) by conducting the unconfined compression (UCS) test. The aim of the study was to design and optimize the sodium silicate grouts for stabilizing the Kaolinite-dominant organic soils. Some conclusions can be drawn based on their experimental results:

- The soil strength increased as the silicate concentration increased.
- Aluminum sulfate was a better setting agent than calcium chloride in terms of the strength development with the same concentrations of sodium silicates.
- After 14-day curing, the soils added with 3mol/L sodium silicate solution and 0.1mol/L Aluminum sulfate exhibited the highest strength gain among other combinations listed in paper, which was over 2.7 times greater than that of the original soils.

**Latifi et al., (2014)** conducted an experimental study on tropical laterite soil stabilized by sodium silicate-based binder (TX-85). The purpose of the study was to explore the microstructure and engineering properties such as the strength behavior of the soil stabilized with the liquid additive, and to identify the exact mechanism that responsible for the stabilization process. The study involved Unconfined compressive strength (UCS) test and compaction tests, as well as spectroscopic analyses such as SEM and XRD. The main findings of this research are summarized as follows:

- The dry density of the laterite soil was reduced by adding TX-85.
- Significant increase in the strength properties of the soil (as high as 984 kPa) was observed after 7-day curing. It was reported that most of soil-silicate reactions took place during the first 7 days.
- The optimal concentration for TX-85 was found to be 9%, and a higher concentration caused adverse effect on the strength improvement of soil.
- Microscopic analysis (SEM and XRD) showed that the main reason for the strength increase was due to the formation of gel-form compound: Sodium aluminosilicate hydrate (N-A-S-H).

**Stempkowska et al., (2017)** studied the effects of silicate modulus (weight ratio of  $\text{SiO}_2$ :  $\text{Na}_2\text{O}$ ) on the stabilization of Kaolin clay slurry. It is noted that the ‘stabilization’ here referred to the fluidization rather than the solidification of the slurry. There was no setting agent being used in their study. They performed the rheological measurements using the rotary viscometer. The research concluded that:

- The addition of silicates to the slurry resulted in a suspension with low viscosity and high density, and 0.3 wt % concentration of sodium silicate with the silicate modulus in the range of 2.0-2.5 could be the best choice for the Kaolin slurry stabilization.
- The silicates with a higher  $\text{SiO}_2$ :  $\text{Na}_2\text{O}$  ratio (e.g. greater than 2.5) dispersed the Kaolin grains in the slurry while the silicates with lower  $\text{SiO}_2$ :  $\text{Na}_2\text{O}$  ratio (e.g. smaller than 2.0) contributed more free silica in suspension and increased the pH of the slurry.
- Ion exchange was found to be the main mechanism for the stabilization of clay slurry using silicates.

### **2.5.3 Comments on the case study**

Over the past a few decades, researches mainly focused on the studies of the

fundamental mechanisms (e.g. hydration, pozzolanic reaction) in the cement stabilization process, as well as the improved mechanical properties (e.g. compressive strength) of the treated domestic soils. As time progresses and technology develops, more interests are directed to the investigation of physicochemical properties of cement-treated soils, as well as the mechanisms responsible for the long-term strength gain in addition to pozzolanic reaction. Recently, in order to address the environmental concerns with cement such as higher energy consumption and CO<sub>2</sub> emissions (Chang, et al. 2016), the use of supplementary additives and partial replacements for cement is investigated. It is reported that a small amount of additional materials, such as nano-silica (Ghasabkolaei et al., 2016), waste phosphorus slag (Li and Poon, 2015) and metakaolin (Wu et al., 2016) may enhance the strength of cement-treated soils.

In the case of the silicate-based stabilization, studies are focused on the strength characteristics and microstructural evolutions related to the soil mixed with silicates. Recently, more attention has been paid to the influence of silicate properties (ingredients, solid content, molar ratio etc.) on the soil performance. Also, the role of setting agent and clay type on the clay-water-silicate interaction has been the subject of substantial studies.

## **2.6 Summary**

A review of properties and treatment technologies of MFT are presented in this chapter. The backgrounds of the clay structures, as well as the mechanisms of soil stabilization using chemical additives (Portland cement and silicate grouts) are discussed. By using these stabilizers, promising results are obtained in terms of the soil improvements. The review inspired the current study.

**Table 2.1 Summary of literature on the physical and geotechnical properties of oil sand MFT from Alberta, Canada**

	Reference								
	Jeeravipoolvarn 2005	Owolagba, 2013	Guo and Shang 2014	Gholami 2014	Bajwa 2015	Yao 2016	Roshani et al 2017	Bourges-Gastaud et al 2017	Alam, et al 2017
Water content, %	233.3	240	171.3	181.7	140	212.5	121.7	123.7	158.4
Solid content, %	30	29	36.9	35.5	42	32	45	44.7	38.70
Bitumen content, %	3	-	-	-	-	1.3	18.37	7.4	-
Bulk density (g/cm <sup>3</sup> )	1.28	-	-	-	1.22-1.30	1.21	1.31	-	-
Initial void ratio, e	-	6.1	4.39	-	-	-	3.44	-	-
Specific gravity, Gs	2.28	2.34	2.51	2.2	2.22	2.3	2.37	-	2.58
Liquid limit, %	44-53	48	51.6	45	45	55	51.2	68	54.42
Plastic limit, %	21	21	29.1	19	19	28	37.2	31	36.04
Plasticity index	23-32	27	22.5	26	26	27	14.0	37	28.38
Fines, %	93	96	100	93	98	91	95	72	100
Clays, %	48	52	20	46	40	48	18	~34.5	19

**Table 2.2 Summary of literature on the clay mineralogy of raw oil sand MFT.**

Reference	Detected clay minerals in OST	Tailing source
Omotoso et al., 2002	Kaolinite, Illite and mixed layer clays (Illite-smectite/kaolinite-smectite)	MFT from Syncrude and Suncor pond
Rima, 2013	Kaolinite, Illite and Muscovite (28%, 11% and 2% of entire minerals, respectively)	MFT from North Alberta
Islam, 2014	Kaolinite, Illite	MFT from Syncrude and Imperial Oil
Nursi, 2015	Kaolinite and Illite (30.7% and 36.0% of solid fraction respectively,	MFT from Syncrude Canada Ltc.
Zhu et al., 2017	Kaolinite and Illite (36.7% and 30.7% of entire minerals, respectively)	MFT provided by Syncrude
Bourges-Gastaud et al., 2017	Kaolinite and Illite (14% and 3% of solid fraction respectively, without bentonite)	MFT provided by Shell

**Table 2.3 Summary of literature on treatment technology of raw oil sand MFT.**

Technology	Type	Reported effectiveness in geotechnical investigation	Source*
In-line thickening (mix tailings with flocculant and coagulant)	Chemical amendment	Undrained shear strength was the highest (exceeded 5kPa) for ILTT-MFT followed by sheared ILTT-MFT.	Jeeravipoolvarn, 2010
Freeze-thaw	Natural process	Compressibility was reduced to 1/2 the original one; Hydraulic conductivity was increased to 6 times of the original one.	Zhang, 2012
Centrifuge	Physical/mechanical process	Solid content increased from 29% to 61%.	Owolagba, 2013
Microbial induced calcium carbonate precipitation	Chemical/biological amendment	The undrained shear strength of MFT sample significantly increased.	Liang, 2015
Surface geo-polymerization technique	Chemical amendment	-	Nusri, 2016
Gypsum amendment	Chemical amendment	Enhanced sedimentation and settling rate because of the production of the gas channel within MFT.	Liu et al., 2016
Polymer (Tubifex) treatment	Chemical/biological amendment	solid content (initially diluted to 5.8 %) increased up to 41% (maximum);	Yang et al., 2016
Polymer treatment	Chemical amendment	-	Yao, 2016
Dual Polymer Flocculants treatment	Chemical amendment	Solid content increased from 35.6% to 46.2%-64.1%;	Zhu et al, 2017
Electrokinetic treatment	Physical/mechanical process	Solid content increased from 45% to 64%-70%; Shear strength increased from 0kPa to 25kPa	Bourges-Gastaud et al., 2017
Super-absorbent polymer treatment and dry under atmospheric conditions	Combined chemical amendment with natural process	the highest strength increase (7.3 kPa) after 30 days.	Roshani et al., 2017

\*References are listed in chronological order till the year of 2017.



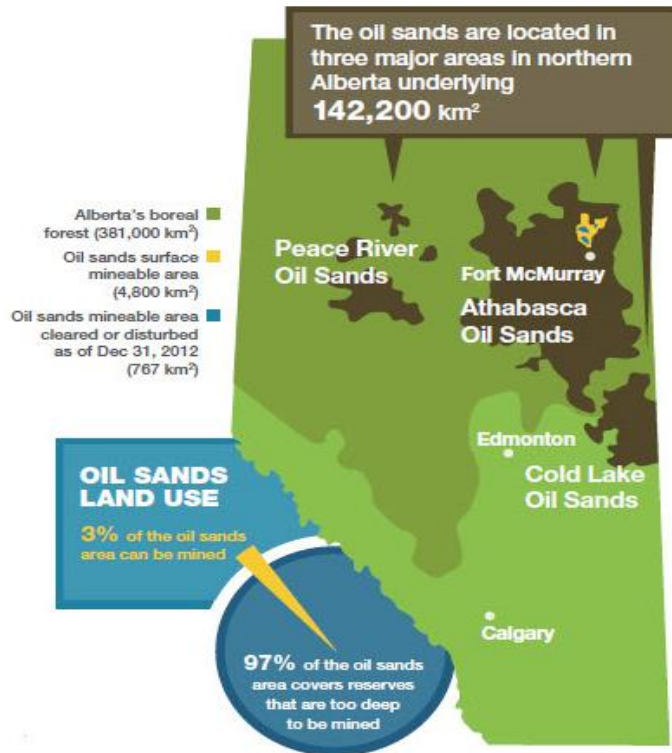


Fig. 2.1 local distribution of oil sands in northern Alberta (Government of Alberta,2007)

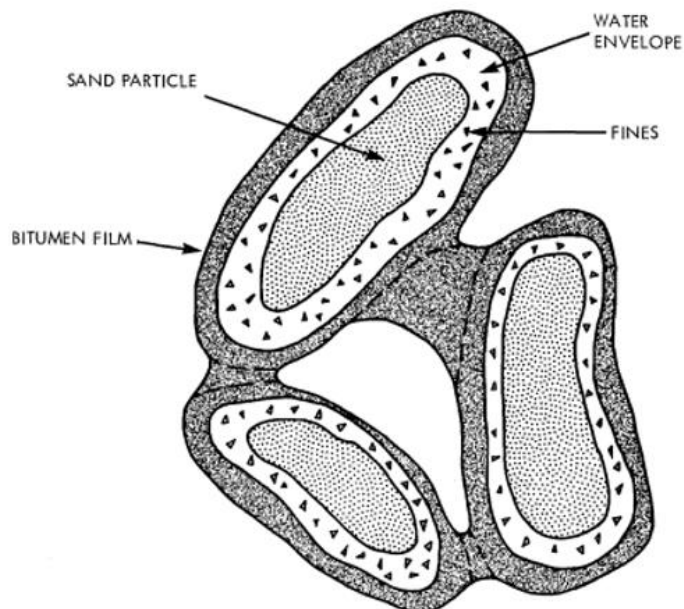


Fig. 2.2 Typical arrangement of oil sand particles (ARC Tailings, 1977)

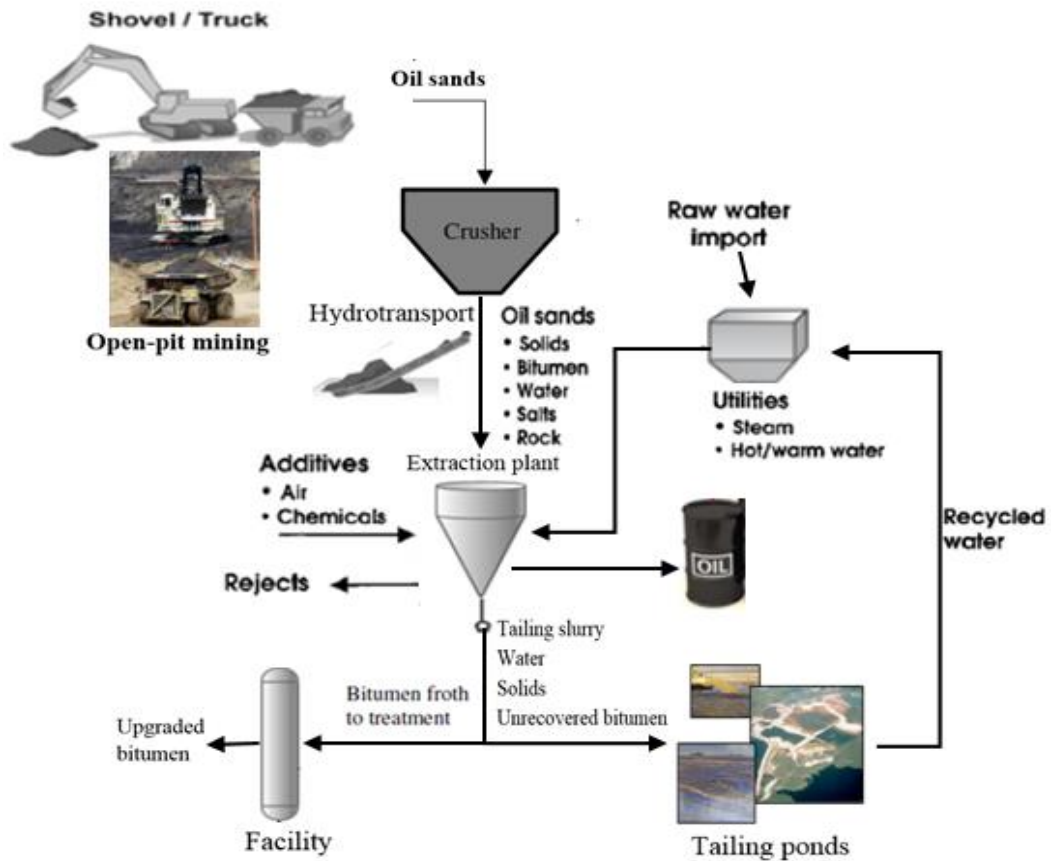
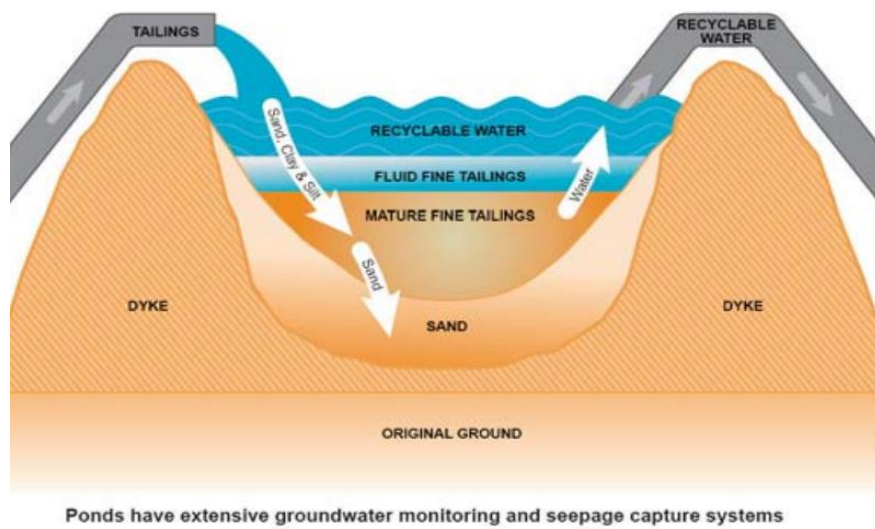
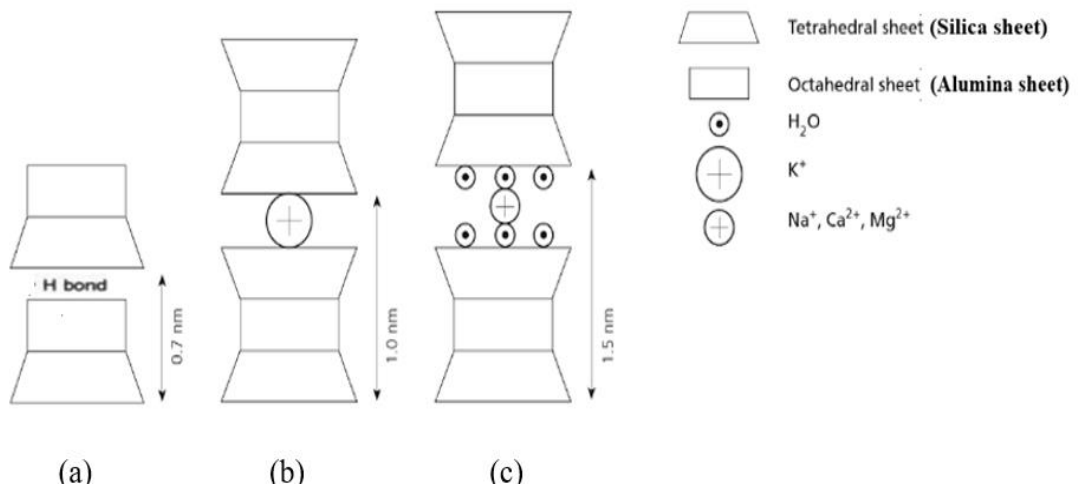


Fig. 2.3 Hot water extraction in oil sand processing (modified from Masliyah et al., 2004)



Ponds have extensive groundwater monitoring and seepage capture systems

Fig. 2.4 Management of Tailing Ponds (ERCB, 2011)



**Fig. 2.5 Structure of the main clay minerals: (a) Kaolinite, (b) Illite, (c) Montmorillonite. (Modified from M. van der Perk, 2013)**

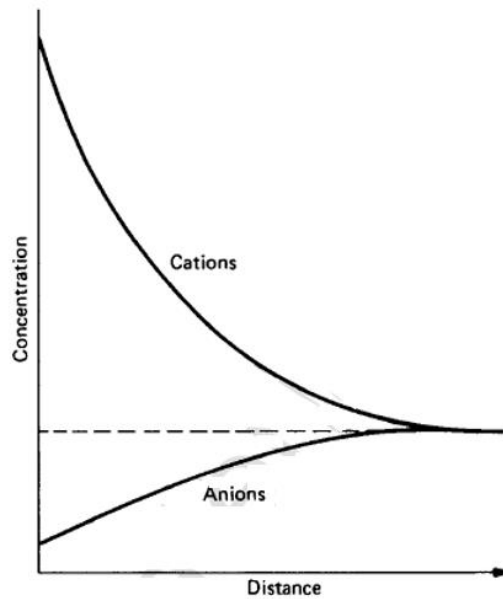


**Fig. 2.6a Distribution of cations and anions away from the clay surface (Mitchell and Soga, 2005)**

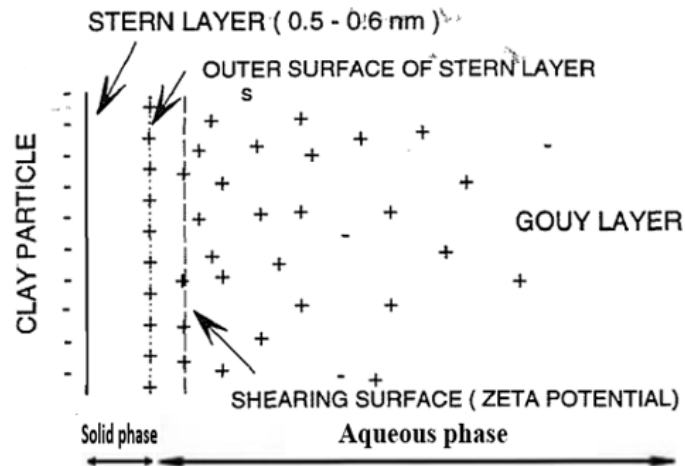


Fig. 2.6b Stern-Gouy Double Layer (modified from Shang et al., 1994)

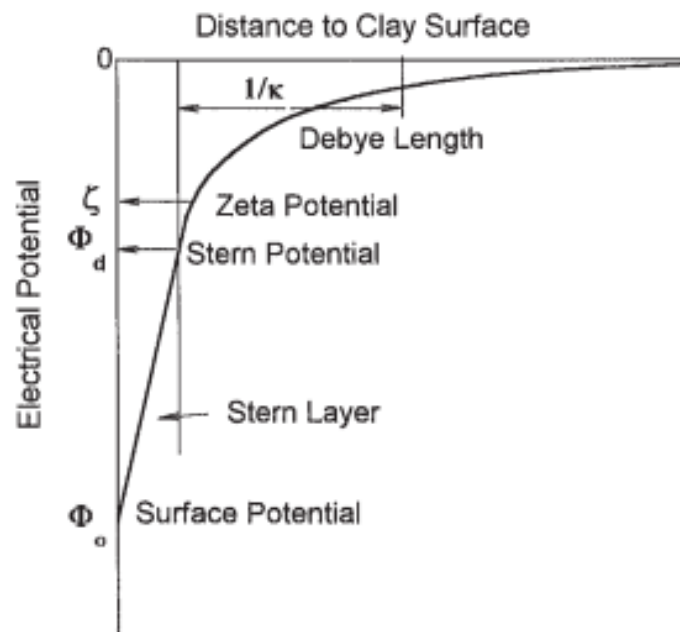
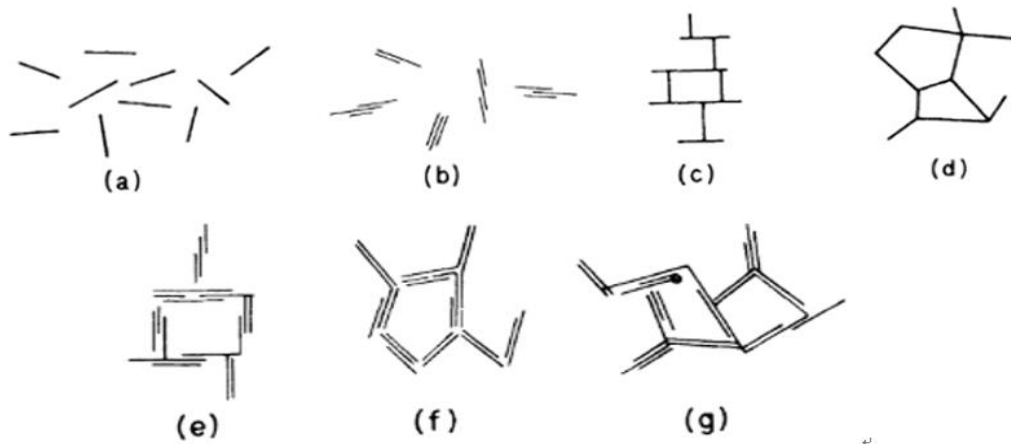
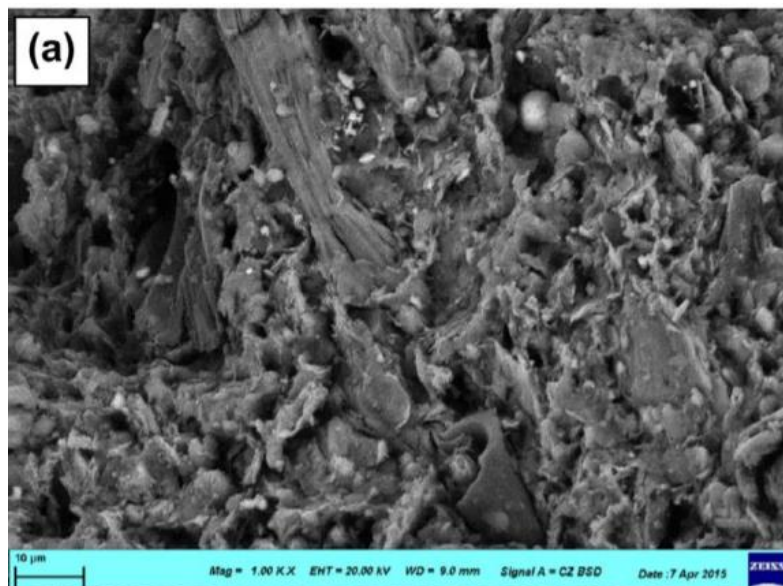


Fig. 2.6c The corresponding potential profile (Shang, J.Q. 1997).



**Fig. 2.7** Structure of the main clay minerals: (a) Dispersed and deflocculated, (b) Aggregated (FF) but deflocculated, (c) Flocculated (EF) but dispersed, (d) Flocculated (EE) but dispersed, (e) Flocculated (EF) and aggregated, (f) Flocculated (EE) and aggregated, (g) Flocculated (EF and EE) and aggregated; (c) and (d): Card-house structure; (e), (f) and (g): Book-house structure. (van Olphen, 1963)



**Fig. 2.8** SEM images show effect of evaporation on MFT microstructure at 5 cm height after 10 days. (Roshani et al., 2017)

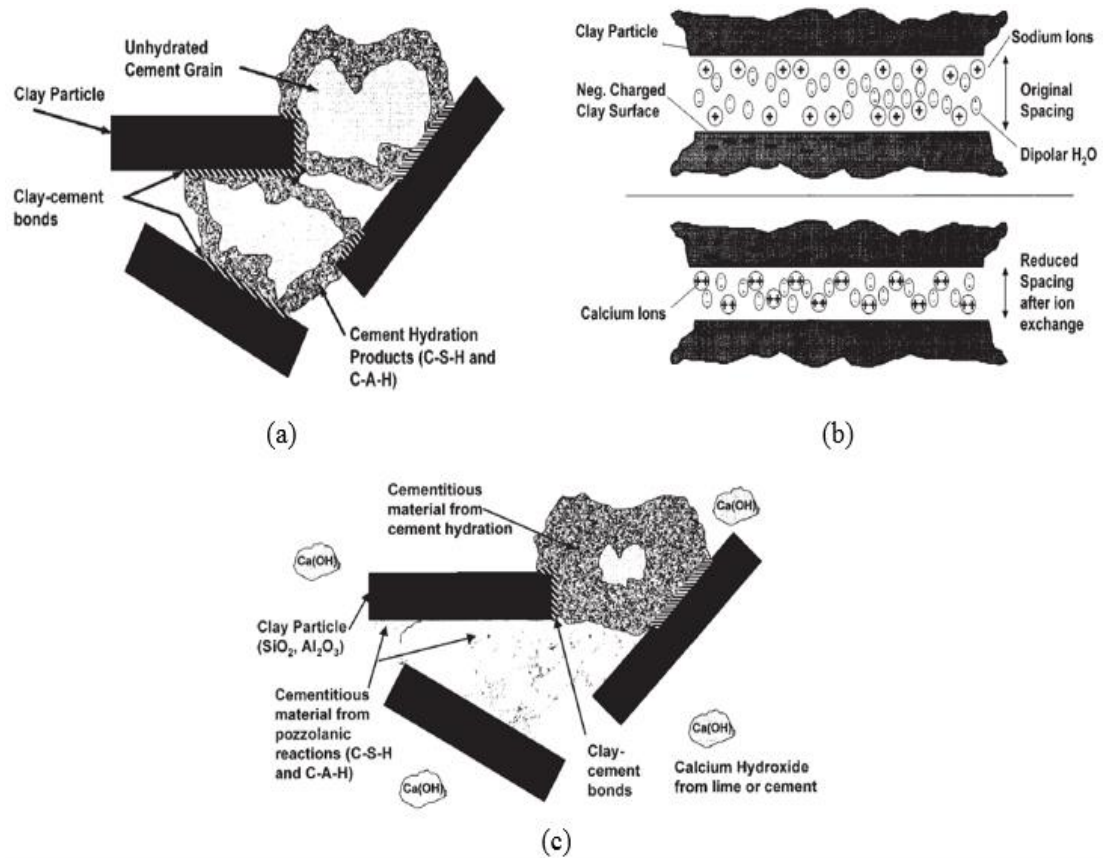


**Fig. 2.9 Soil stabilization by Portland cement: (a) Hydration reaction (b) Cation exchange (c) Pozzolanic reaction (compiled and modified from Prusinski and Bhattacharja, 1999)**

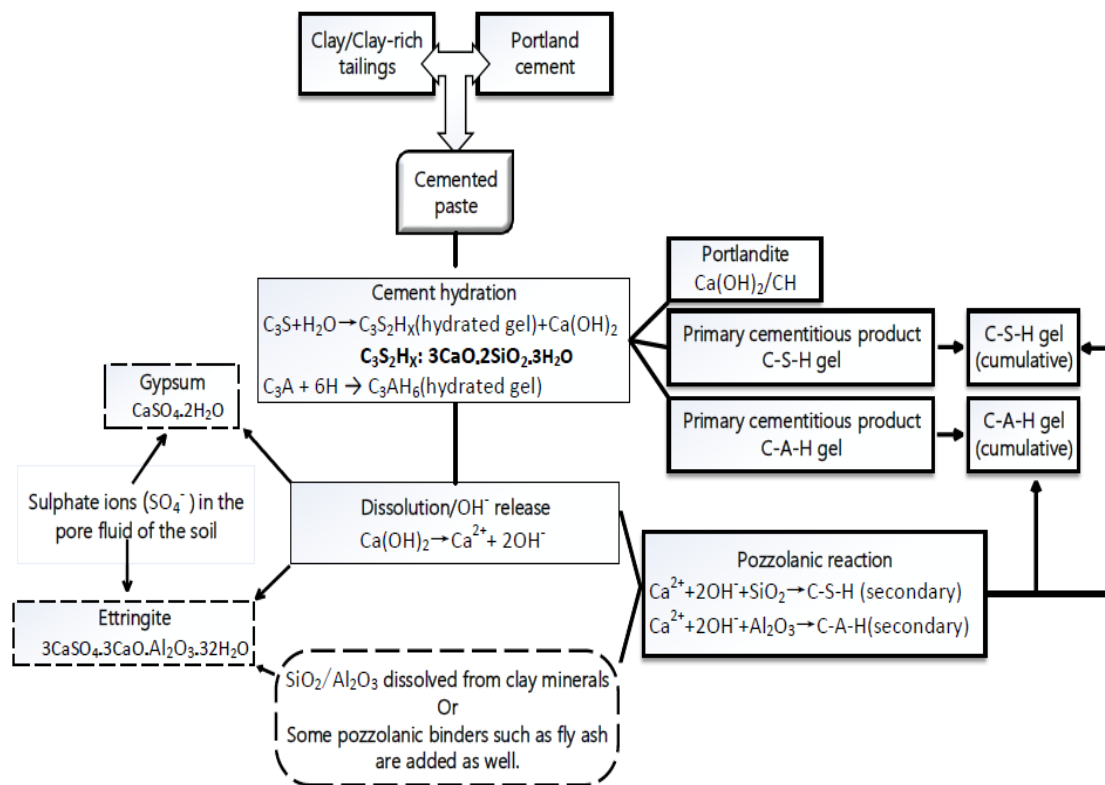


**Fig. 2.10 Schematic diagram elucidating soil-cement hydration stages and pozzolanic reaction. (after Chew et al., 2004; Xing et al., 2009)**

## References

**Alam, R., Shang, J. Q., & Islam, S. (2017).** Electrophoresis and its applications in oil sand tailings management. *International Journal of Mineral Processing*, 161, 41–49

**Al-Dhafeeri, A.M.; Nasr-El-Din, H.A.; Al-Harith, A.M.** Evaluation of Rigless Water Shutoff Treatments to be used in Arab-C Carbonate Reservoir in Saudi Arabia. In *Proceedings of the CIPC/SPE Gas Technology Symposium Joint Conference*, Calgary, AB, Canada, 16–19 June 2008.

**Allen, E. W. (2008).** Process water treatment in Canada's oil sands industry: I. Target pollutants and treatment objectives. *Journal of Environmental Engineering and Science*, 7(2), 123-138.

**Al-Rawas, A.A., Hagoa, A.W. and Al-Sarmib, H. 2005.** Effect of Lime, Cement and Sarooj (Artificial Pozzolan) Undrained Shear... Mohammed Shukri Al-Zoubi - 62 - on the Swelling Potential of an Expansive Soil from Oman. *Building and Environment*, 40: 681-687.

**ARC, CTFAOIL SANDS, 1977.** CLAY TAILINGS FROM ALBERTA OIL SANDS AND OTHER SOURCES. A REVIEW Prepared by The Alberta Research Council 11315 -87 Avenue, Edmonton.

**Bahmani, S.H., Farzadnia, N., Asadi, A., Huat, B.B.K., 2016.** The effect of size and replacement content of nanosilica on strength development of cement treated residual soil. *Constr. Build. Mater.* 118:294–306.

**Bajwa.T.M (2015).** Microstructure and macroscopic behaviour of polymer amended oil sands mature fine tailings. Ph.D. Thesis, Carleton University, Canada

**Beier, N., Wilson, W., Dunmola, A., Sego, D., 2013.** Impact of flocculation-based dewatering on the shear strength of oil sands fine tailings. *Can. Geotech. J.* 50 (9), 1001–1007

**Bergado, D.T., Anderson, L.R., Miura, N., Balasubramaniam, A.S., 1996.** Soft



Ground Improvement in Lowland and Other Environments. ASCE Press, NY, U.S.A.

**Bourgès-Gastaud S, Dolez P, Blond E. Touze-Foltz N. (2017).** “Dewatering of oil sands tailings with an electrokinetic geocomposite.” Minerals Engineering 100 (2017) 177–186

**Budhu. M. (2007)** Soil mechanics and foundations, John Wiley & Sons, Hoboken, NY.

**Chang, I., Im, J. and Chun, C.G. (2016)** Introduction of Microbial Biopolymers in Soil Treatment for Future Environmentally-Friendly and Sustainable Geotechnical Engineering. Sustainability, 8, 251.

**Chen Q, Ke Y, Zhang L, Tyrer M, Hills CD, Xue G. (2009).** Application of accelerated carbonation with a combination of  $\text{Na}_2\text{CO}_3$  and  $\text{CO}_2$  in cement-based solidification/stabilization of heavy metal-bearing sediment. J Hazard Mater 166:421–427

**Chew SH, Kamruzzaman HM, Lee FH (2004).** Physicochemical and engineering behaviour of cement treated clays. J Geotech Geoenviron Eng 130(7):696–706

**Council of Canadian Academies (CCA). 2009.** The Sustainable Management of Groundwater in Canada. Ottawa.

**Das, Braja M (2012).** Fundamentals of Geotechnical Engineering 4th (fourth) Edition, Cengage Learning, Technology & Engineering.

**Directive 074 (2009).** Tailings performance criteria and requirements for oil sands mining schemes, Energy Resources Conservation Board (ERCB), Alberta

**Directive 085 (2016).** Fluid Tailings Management for Oil Sands Mining Projects, Alberta Energy Regulator (AER), Alberta

**ERCB. 2011.** Regulatory Action in Alberta’s Oil Sand. Energy Resources Conservation Board-Washington, D.C.

**Eades JL, Grim RE. 1966.** A quick test to determine requirements for lime stabilization. Highway Research Board Bulletin; 139: 61e72.

**Eisazadeh A, Kassim KA, and Nur H 2010.** Molecular characteristics of phosphoric acid treated soils. World Academy of Science, Engineering and Technology Journal. Vol. 63, 1-3.

**EuroSoilStab. (2002).** Development of Design and Construction Methods to Stabilize Soft Organic Soils: Design Guide for soft soil stabilization. CT97-0351, European Commission, Industrial and Materials Technologies Programme (Rite-EuRam III) Bryssel.

**Fard, M. A.H. 2011.** Characterization of clay minerals in the Athabasca oil sands in water extraction and nonaqueous solvent extraction processes Ph.D. thesis. Department of Chemical and Materials Engineering, The University of Alberta, Edmonton, Alberta.

**Farkish A (2013).** SAP Based Rapid Dewatering of Oil Sands Mature Fine Tailings. Master Thesis, University of Ottawa, Canada.

**Ferguson, J.; Applebey, M.P.** The syneresis of silica gel. Trans. Faraday Soc. 1930, 26, 642-655.

**Ghasabkolaei, N., Janalizadeh, A., Jahanshahi, M., Roshan, N., and Ghasemi, S.E. (2016).** “Physical and geotechnical properties of cement-treated clayey soil using silica nanoparticles: An experimental study.” Eur. Phys. J. Plus, 131(5), 1–11.

**Gholami. M (2014).** Shear Behaviour of Oil Sand Fine Tailings in simple shear and triaxial devices. Master Thesis, Carleton University, Canada

**Gosselin P., Naeth M.A., Plourde A., Van Der Kraak G., Xu Z., 2010** Environmental and Health Impacts of Canada’s Oil Sands Industry, Royal Society of Canada Ottawa, Ontario, Canada

**Government of Alberta.** “About Oil Sands” Facts and Statistics, Alberta Energy. Available at <http://www.energy.alberta.ca/OilSands/791.asp>

**Guo, Y. and Shang, J.Q. (2014)** A study on electrokinetic dewatering of oil sands tailings. Environmental Geotechnics, 1, No.2, 121-134.

**Hausmann, M. R. (1990).** Engineering Principles of Ground Modification, McGraw

Hill, NY.

**Ho L S, Nakarai K, Ogawa Y, Sasaki T, Morioka M. (2017)** Strength development of cement-treated soils: Effects of water content, carbonation, and pozzolanic reaction under drying curing condition *Constr. Build. Mater.* 134; 703–712

**Liu H, Tan S.Y, Yu T, Liu Y. (2016)** Sulfate reducing bacterial community and in situ activity in mature fine tailings analyzed by real time qPCR and microsensor. *JOURNAL OF ENVIRONMENTAL SCIENCES* 44; 141 – 147

**Iler R.K.** *The Chemistry of Silica, Solubility, Polymerization, Colloid and Surface Properties, and Biochemistry* [Book]: Wiley-Interscience, 1979.

**Islam, S. (2014).** Thickening of Mature Fine Oil Sands Tailings, M.Esc.Thesis, Western University, London, Canada

**Jeeravipoolvarn, S. (2005).** Compression behaviour of thixotropic oil sands tailings. M.A.Sc. thesis, Department of Civil and Environmental Engineering, The University of Alberta, Edmonton, Alberta.

**Jeeravipoolvarn, S. (2010).** Doctoral dissertation: Geotechnical behavior of in-line thickened oil sands tailings. University of Alberta, Edmonton, Alberta, Canada

**Kamruzzaman, A.H.M,** “Physio-Chemical & Engineering Behaviour of Cement Treated Singapore Marine Clay,” Ph.D. dissertation, National University of Singapore, Singapore, 2002.

**Karol R.H. (2003)** *Chemical Grouting And Soil Stabilization, Revised And Expanded* CRC Press, 3rd ed. Technology & Engineering

**Kasperski, K.L. (1992).** “A review of properties and treatment of oil sands tailings.” *AOSTRA Journal of Research*, 8, 11-53.

**Katz, L. E., Rauch, A. F., Liljestrand, H. M., Harmon, J. S., Shaw, K. S., & Albers, H. (2001).** Mechanisms of soil stabilization with liquid ionic stabilizer. *Transportation Research Record: Journal of the Transportation Research Board*, 1757(1), 50-57.

**Kazemian S and Huat BBK (2010)** *Assessment of Stabilization Methods for Soft*

Soils by Admixtures. International conference on science and social research, Kuala Lumpur, Malaysia

**Kirk JL, Muir DC, Gleason A, Wang X, Lawson G, Frank RA, Lehnerr I, Wrona F. (2014).** Atmospheric deposition of mercury and methylmercury to landscapes and waterbodies of the Athabasca oil sands region. *Environ Sci Technol* 48: 7374–7383.

**Latifi, N., Eisazadeh, A., and Marto, A. (2014).** “Strength behavior and microstructural characteristics of tropical laterite soil treated with sodium silicate-based liquid stabilizer.” *Environ. Earth Sci.*, 72(1), 91–98.

**Liang J, Guo Z, Deng L, Liu Y (2015).** Mature fine tailings consolidation through microbial induced calcium carbonate precipitation. *Can J Civ Eng* 42:1–4

**Liang, X., X. Zhu and E.C. Butler, 2011.** Comparison of four advanced oxidation processes for the removal of naphthenic acids from model oil sands process water. *Journal of Hazardous Materials* 190(1-3): 168-176.

**Li, J., Poon, C.S., 2017.** Innovative solidification/stabilization of lead contaminated soil using incineration sewage sludge ash. *Chemosphere* 173, 143-152

**Lin Y. (2006)** “Colloidal Silica Transport Mechanisms for Passive Site Stabilization of Liquefiable Soils.” Ph.D. dissertation, Drexel University, Philadelphia, PA.

**Little, D.N. and Nair S., (2009)** Recommended practice for stabilization of sulphate Rich Subgrade Soils [R]. College station, Texas: Texas Transportation Institute.

**Littlejohn, G. S., Concannon, M., and Wright, R. H. (1997)** “Engineering properties of silicate-R100 ester chemical grout”, *Ground Engineering*, pp.36-40.

**Lu, Qiuyi. (2016)** Understanding Two-step Polymer Flocculation of Oil Sands Tailings. Ph.D. Thesis University of Alberta, Edmonton, Alberta.

**Ma, C., Qin, Z. H., Zhuang, Y. C., Chen, L. Z., and Chen, B. (2015).** “Influence of sodium silicate and promoters on unconfined compressive strength of Portland cement-stabilized clay.” *Soils and Foundations*, Vol. 55, No. 5, pp. 1222-1232.

**Maaitah Omer Nawaf, 2012.** Soil Stabilization by Chemical Agent, *Geotech Geol Eng*

(2012) 30:1345–1356

**Mackinnon, M, H Boerger, W Zubot, 2017.** Water capping of tailings, Canadian Patent CA2901710 A1

**M. van der Perk,** Soil and Water Contamination: CRC Press, The Netherlands, 2013.

**Masliyah, J. Zhou, Z. Xu, Z. Czarnecki, J. Hamza, H. (2004)** “Understanding Water-Based Bitumen Extraction from Athabasca Oil Sands,” Can. J. Chem. Eng. 82, 628.

**Makusa, G. P. (2013).** Soil stabilization methods and materials in engineering practice: State of the art review. Lulea°, Sweden: Lulea° University of Technology.

**McDonald M, Hamilton J. (2009).** Institute for Briquetting and Agglomeration in biennial conference-institute of briquetting and agglomeration; 31;29-40; Institute for Briquetting and Agglomeration by Institute for Briquetting and Agglomeration, San Antonio.

**Mitchell J.K. and K. Soga,** Fundamentals of soil behavior. 3rd ed. (2005), NY: Wiley.

**Moayed F, Mashaghi A, Tans SJ (2013)** A Polypeptide-DNA Hybrid with Selective Linking Capability Applied to Single Molecule Nano-Mechanical Measurements Using Optical Tweezers. PLOS ONE 8(1): e54440.

**Malone, J.M., Barlaz, M.A., and R.H.Borden.** “Leachability of organic compounds from sodium silicate grouts containing organic reagents”. Hazardous and Industrial Waste Proceedings, 27th Mid-Atlantic Conference, Jul. 6, 1995.

**Moayedi, H., Huat, B.B.K., Kazemian, S., and Daneshmand, S., 2012.** Stabilization of organic soil using sodium silicate system grout. International Journal of Physical Sciences, Vol. 7, No. 9: pp. 1395-1402.

**Nakarai K., Yoshida T., (2015)** Effect of carbonation on strength development of cement-treated Toyoura silica sand, Soils Found. 55 (4) 857–865.

**Nusri S, 2015** “Using Surface Geopolymerisation Reactions to Strengthen Athabasca Oil Sands Mature Fine Tailings,” University of Alberta,

**Omotoso, O. E., Munoz, V. A., and Mikula, R. J. (2002).** "Mechanisms of crude oil-

mineral interactions." *Spill Science & Technology Bulletin*, 8(1), 45-54.

**OSRIN Report. (2010).** "Oil Sands Tailings Technology Review." BGC Engineering Inc., Oil sands research and information network, University of Alberta, School of Energy and the Environment, Edmonton, Alberta, Canada.

**Owolagba, J. O. (2013).** Doctoral dissertation: Dewatering Behavior of Centrifuged Oil Sand Fine Tailings for Surface Deposition. University of Regina, Regina, Canada

**Pham, L. T. and Hatzignatiou, D.G. 2016.** Rheological Evaluation of a sodium silicate gel system for water management in mature, naturally-fracture oilfields. *Journal of Petroleum Science and Engineering*, 138, 218-233, February.

**Powers, J.P.; Herridge, C.J.; Corwin, A.B.; Schmell, P.C. (2007)** Construction Dewatering and Groundwater Control: New Methods and Applications. John Wiley and Sons: New York; 638 pp.

**PQ Corporation, 2003.** Soluble silicate in geotechnical grouting applications. *Bulletin* 52–53, USA.

**PQ Corporation Bulletin**, Sodium Silicate a Binder for the 21st Century

**Proskin, S., Segó, D. and Alostaz, M. 2012.** Oil sands MFT properties and freeze-thaw effects. *Journal of Cold Regions Engineering*, 26 (2): 29-54.

**Prusinski, J. R. and Bhattacharya, S. (1999).** "Effectiveness of portland cement and lime in stabilizing clay soils." *Transportation Research Record* 1652, TRB, National Research Council, Washington, D.C., pp. 215-227

**Quang, N.D., Chai, J.C., 2015.** Permeability of lime- and cement-treated clayey soils. *Can. Geotech. J.* 52, 1221–1227

**Rima US (2013)** Characterization and centrifuge dewatering of oil sands fine tailings. Master of Applied Science Thesis, University of Regina, Canada

**Roshani, A., Fall, M., and Kennedy, K. (2017).** "Drying Behavior of Mature Fine Tailings Pre-Dewatered with Super-Absorbent Polymer (SAP): Column Experiments," *Geotechnical Testing Journal*, Vol. 40, No. 2, 2017, pp. 210-220.

**Saeed K A, Kassim k A, Nur H.** “Physicochemical characterization of cement treated kaolin clay.” *GRAĐEVINAR* 66 (2014) 6, 513-521

**Sasanian S., Newson T.A., 2011.** “Basic Parameters Governing the behaviour of Cementtreated Clays,” *The Japanese Geotechnical Society, Soils and Foundations* 54 (2014); 209-224.

**Schmitz, R.M., (2006).** Can the diffuse double layer theory describe changes in hydraulic conductivity of compacted clay? *Geotechnical and Geological Engineering* 24. 1835–1844

**Scott, J. D., Dusseault, M.B. and Carrier III, W.D. 1985.** Behaviour of the clay/bitumen/water sludge system from oil sands extraction plants, *Journal of Applied Clay Science*, 1: 207-218

**Shang, J.Q, Lo, K. Y., and Quigley, R. M. (1994).** Quantitative determination of potential distribution in Stern-Gouy double-layer model. *Canadian Geotechnical Journal*, 31(5), 624-636

**Shang, J.Q. (1997).** Zeta potential and electroosmotic permeability. *Canadian Geotechnical Journal*, 34(4):627-631.

**Somasundaran, P. and Zhang, L. (2006).** Adsorption of Surfactants on Minerals for Wettability Control in Improved Oil Recovery Process. *Journal of Petroleum Science and Engineering* 52: 198-212.

**Stempkowska A, Mastalska-Poplawska J, Izak P, Oglaza L, (2017).** Stabilization of kaolin clay slurry with sodium silicate of different silicate moduli [J]. *Applied Clay Science*, Vol 146: 147-151

**Tan, T. S., T. L. Goh, and Yong, K. Y. 2002.** Properties of singapore marine clays improved by cement mixing. *Geotech. Testing J. (ASTM)* 25(4): 422–433.

**Tang, J., Biggar, K.W., Scott, J.D. and Segoo, D.C. 1997.** Examination of mature fine tailings using a scanning electron microscope, *Canadian Geotechnical Conference, Ottawa, Ontario*, 746-754.

**Tariq, A., & Yanful, E. K. (2013).** A review of binders used in cemented paste tailings for underground and surface disposal practices. *Journal of environmental management*, 131, 138- 149

**Tingle JS and Santoni RL 2003.** Stabilization of Clay Soils with Nontraditional Additives, In *Transportation Research Record 1819*, Transportation Research Board, Washington DC.

**US Army Corps of engineers (1995).** “Engineering and Design, CHEMICAL GROUTING”, Engineer Manual, EM 1110-1-3500, Washington, DC.

**Van Olphen, H. (1963).** An Introduction to Clay Colloid Chemistry. *Soil Science*, 97(4), 290.

**Wild S, Arabi MR, Leng-Ward G. 1993.** Sulphate expansion of lime stabilized kaolinite II: reaction products and expansion. *Clay Minerals*; 28(4):569e83

**Wolter, G.L.L. and Naeth, M.A. 2014.** Dry mature fine tailings as oil sands reclamation substrates. *Journal of Environmental Quality* 43: 1510-1516.

**Wooltorton, F.L.D.** Engineering Pedology and Soil Stabilization. Highway Research Board, n.108, p.29-57, 1955.

**Wu Z, Deng Y, Liu S, Liu Q, Chen Y, Zha F. (2016).** Strength and micro-structure evolution of compacted soils modified by admixtures of cement and metakaolin[J]. *Applied Clay Science*, 127-128: 44-51.

**Xing, H. F., X. M. Yang, C. Xu, and G. B. Ye. 2009.** Strength characteristics and mechanisms of salt-rich soil-cement. *Engineering Geology* 103(1–2): 33–38.

**Yao, Y. (2016).** Dewatering behavior of fine oil sands tailings: an experimental study. Ph.D. Thesis, Delft University of Technology, Delft, Netherlands.

**Yin, J.-H., 2001.** Stress–strain–strength characteristics of soft Hong Kong marine deposits without or with cement treatment. *Lowland Technol. Int.* 3, 1–13

**Zhu Y, X.L. and Qi Liu. (2017).** “Dual Polymer Flocculants for Mature Fine Tailings Dewatering.” *Can. J. Chem. Eng.* 95:3–10.



**Zhang, Y., 2012.** Laboratory Study of Freeze-Thaw Dewatering of Albian Mature Fine Tailings (MFT), MSc thesis. Department of Civil and Environmental Engineering, University of Alberta.

## CHAPTER 3 MATERIALS AND METHODOLOGY

### 3.1 General

The main objectives of this chapter are:

- to introduce and characterize the materials used in this experimental study;
- to present the methods/standards used for investigating the mechanical and physico-chemical properties of the MFT samples;
- to describe the methods for analyzing the microstructures and mineralogical compositions of the MFT samples;

### 3.2 Materials

#### 3.2.1 MFT samples

The MFT examined in this program was received from Shell Canada Limited. Tailings samples were covered by water at the top upon arrival in the laboratory and were placed in the sealed plastic containers. The samples were dark brown in colour and had a strong petroleum odor. The physical properties of MFT were measured and listed in **Table 3.1**. According to the unified soil classification system (USCS), the tailings can be characterized as CL. The liquid limit, plastic limit and plasticity index of MFT was 47.0%, 23.9% and 23.1, respectively. The soil pH was 8.52 and corresponding zeta potential was  $-38$  mV. The results of Inductively Coupled Plasma (ICP) test indicate that the dominant cation in pore water was  $\text{Na}^+$  in (502.07 mg/L), followed by  $\text{K}^+$  (22.65mg/L), and  $\text{Ca}^{2+}$  (4.35 mg/L). It is believed that high concentration of  $\text{Na}^+$  was ascribed to the addition of sodium hydroxide (NaOH) in the bitumen extraction process. Moreover, the particle size analysis of MFT (**Fig. 3.1**) shows that silt (i.e. 81%)<sup>2</sup> was the predominant particle size. The Powder X-ray diffraction (XRD) analysis (**Fig. 3.2**) indicates that Quartz, Kaolinite, Illite and Muscovite were the main minerals present in

---

<sup>2</sup> In this study, the grain size distribution results are adopted based on the laser diffraction method.

the natural MFT. SEM imaging (**Fig. 3.3**) indicates that the particles of the raw MFT were slightly flocculated, forming a mild edge-to-edge ‘card-house’ structure. The EDS analyses (**Fig. 3.4**) confirm the dominance of Si (Quartz) and Al (Kaolinite), and show carbon (Bitumen) and trace of iron (Siderite, FeCO<sub>3</sub>) in MFT (Jeeravipoolvarn, 2005).

### 3.2.2 Chemical stabilizers

The solid stabilizing agent used for this study was Type CAN/CSA-A3001 Portland cement (PC hereafter) that originated from Lafarge Canada Inc, Quebec. The main oxide compositions of PC, determined by an X-ray fluorescence spectrometer (Rigaku ZSX Primus II), are presented in **Table 3.2**. As shown, the dominant compounds in PC were calcium oxide (70.1%) and silica (15.6%). The particles of PC were observed using an SEM image (**Fig. 3.5**), showing that the particles had a rough surface, sharp corners and non-uniform shapes.

Two silicate solutions were also used as the chemical binders (i.e. Ecodrill N<sup>®</sup> Sodium Silicate and Ecodrill Aqueous Alkaline Aluminosilicate) (PQ National Silicates company). The silicates are marketed in commercial names of ‘N sodium silicate (NS)’ and ‘AAAS’ by the manufacturers, respectively. The properties and working mechanisms (i.e. gelation, precipitation, cation exchange and dehydration) of the alkali silicates were described in **Chapter 2 (Section 2.4.3.2-2.4.3.3)**. The NS used in the study is a representative of soluble silicate products. The citric acid (chemical formula C<sub>6</sub>H<sub>8</sub>O<sub>7</sub>), a weak organic acid, was used as the setting agent to initiate the chemical reaction with NS in this study. The citric acid solutions were prepared by dissolving 100g citric acid powders in 1000 ml tap water, as recommended by the manufacturer and supplier. To avoid any evaporation, the solution was used within two days after preparation. AAAS is a relatively new silicate product, which is chemically modified by dissolving aluminum into the traditional aqueous alkali silicate such as NS. Hence, the composite ‘AAAS’ retains the same chemical reactions as NS but can undergo an additional crystallization reaction (McDonald et al., 2014). As such, AAAS can convert to a crystalline phase when it is subjected to high-speed shearing or mixed with other

media such as water (Miller et al., 2013). AAAS itself is amorphous and does not have a porous crystal structure (McDonald et al., 2014). Propylene carbonate solution (an organic compound, chemical formula  $\text{CH}_3\text{C}_2\text{H}_3\text{O}_2\text{CO}$ ) was selected as the setting agent for AAAS in the study, as suggested by the manufacturer. The previous experience showed that the unreactive oil-based drilling fluid became reactive by mixing propylene carbonate with AAAS (McDonald et al., 2014).

**Tables 3.3** represents the typical characteristics of hydrous NS and AAAS. As reported, NS is composed of  $\text{SiO}_2$  solids (28.7%),  $\text{Na}_2\text{O}$  solids (8.9%) and water (62.4%), while AAAS has the same major components as NS but the relative proportions are different. Compared with NS, AAAS has a unique ingredient of  $\text{Al}_2\text{O}_3$  (1.6%). It is believed that the dissolved aluminum in the silicate serves to reduce the syneresis (shrinkage) potential of the resulting products upon aging (Miller et al., 2013). The XRD patterns in **Fig. 3.6** exhibit the broad features (sometimes referred to as ‘halo peak’) between  $20^\circ$  and  $30^\circ$ , therefore confirm the amorphous nature of the silicates. The viscosity measurement results are presented in **Fig. 3.7**, indicating that the viscosity of the products reduces by dilution.

**Figs. 3.8 (a) and (b)** show the photographic images of the NS gel and AAAS gel, respectively. After 60 days of curing, the NS gel exhibited significantly syneresis, whereas AAAS gel had negligible volume change over time. The Environmental scanning electron microcopy (ESEM) observation of pure silicate gels is depicted in Fig 3.7, which suggests that AAAS gel was more consistent than the NS gel, showing no visible internal pores.

### **3.3 Test method**

#### **3.3.1 Water content and solid content**

The water (moisture) content of MFT is defined as the mass of water in MFT to the mass of dry solids in geotechnical engineering applications, note for MFT, dry solids

include bitumen, chemicals and other mineral solids:

$$w = \frac{m_w}{m_s} \times 100\% \quad (3.1)$$

Where  $w$  is the water content (%),  $m_w$  is the mass of water in MFT, and  $m_s$  is the mass of solids in MFT.

The solid content (%) in MFT refers to the mass of dry solids over the total mass of MFT:

$$s = \frac{m_s}{m_s + m_w} \times 100\% \quad (3.2)$$

Based on Eq. 3.1 and Eq. 3.2, the relationship between water content and solid content can be expressed as:

$$s = \frac{1}{1 + w} \quad (3.3)$$

Where  $s$  is the solid content (%) of MFT.

To obtain the mass, MFT samples are dried in an oven at temperature of 105 °C overnight in accordance with ASTM D4959 – 16.

### **3.3.2 Atterberg limit and plasticity**

The Liquid limit (LL) and plastic limit (PL) of all MFT samples are determined by Casagrande percussion cup method and thread rolling method (ASTM D4318-10). The Swedish fall cone method (60g,60°,10mm) is also applied on some of the thick and sticky MFT samples treated by large amounts of silicates, following a Canadian standard CAN/BNQ 2501-092 2006.

Both LL and PL are used to compute the liquidity index and plasticity index. The samples are classified as per the Unified Soil Classification System (USCS) on the Casagrande plasticity chart (ASTM D2487-11).

### **3.3.3 Undrained shear strength**

The strength development of MFT during chemical treatment was measured by a Pilcon hand vane tester (EDECO, England) and a Swedish fall cone device (Geonor model G-200). A pocket penetrometer (HM-500 Gilson) was also used for some MFT samples treated by large amounts of silicates.

### 3.3.3.1 Vane shear test

The hand pocket vane is consisted of four thin steel plates and a rod. When in use the vane is held perpendicular to the specimen surface and inserted into the tailings sample to about 7.5 cm. A torque is applied by rotating the vane head at a constant rate of one revolution per minute until the samples failed in shear (i.e. the vane rotates freely in the sample). The peak shear stress (at the range of kPa) is read directly from the gauge, and the remolded shear strength was measured after remolding without removing the vane blades. The vane head is rapidly rotated by 5 turns and the remolded strength is measured by a uniform rotation speed of one revolution per 10 seconds, following the guidelines of New Zealand Geotechnical Society (2001).

### 3.3.3.2 Swedish fall cone test

The Swedish fall cone test is a simple method to determine the undrained shear strength. The fall-cone apparatus is generally equipped with four different cones, with the mass and cone angle of (1) 60°, 10g; (2) 60°, 60g; (3) 30°, 100g; (4) 30°, 400g. Hansbo (1957) presented an empirical equation to calculate the undrained shear strength of soils from the fall cone test:

$$C_u = K \frac{mg}{d^2} \quad (3.4)$$

Where:

m is the mass of the cone;

d is the penetration depth of the cone into the soil.

K is a constant, which is a function of the cone angle, soil type, and cone bluntness. The referred K values are listed in **Table 3.4**.

The fall cone test procedures are outlined as follows:

- ▶ The cone is suspended vertically first.
- ▶ The tip of the cone is brought into contact with the even surface of the samples by lowering the arm holding the cone.
- ▶ Then, the cone is released for 5 seconds and allowed to drop freely into the specimen under its self-weight.
- ▶ The penetration depth is measured and recorded. Note that the maximum scale for the device is 20mm.
- ▶ The undrained shear strength is calculated based on the **Eq. 3.4**.

For the measurement of remolded shear strength, the disturbed specimen is carefully stuffed into the sample cup and made a smooth levelled surface using a spatula. During this step, special care is taken to preclude the trapped air bubbles in the sample. The sample cup is then placed on the platform of the fall cone unit and the test procedures are repeated. For each sample, a minimum of three cone penetration measurements are taken and the average of the measured values is used for the analysis.

### **3.3.4 Oedometer test**

In this study, one-dimensional consolidation tests (Oedometer tests) were performed to estimate the consolidation behavior of chemically modified MFT at the end of curing period. The conventional consolidometer was developed for soils going through the small strains under step loading, and the Terzaghi's consolidation theory was applied in data analysis and parameter determination. For untreated MFT samples, the compressibility measurement was difficult because of samples' high void ratio and low hydraulic conductivity (S.Proskin et al, 2010).

After curing, the representative samples were selected. The test procedures are specified in ASTM D2435-11. During the process, the sample height change was recorded as the digital LVDT reading and the consolidation cell was submerged in water in order to keep samples saturated. Each loading increment lasted up to 24 hours to ensure that the

primary consolidation was completed. At the end of a test, the apparatus was dismantled and the sample was unloaded. The wet and dry weights of the sample were measured to determine the variations in the moisture content and percent solids.

### **3.3.5 Specific gravity**

In this study, the specific gravity ( $G_s$ ) of MFT solids was also measured (ASTM D854-14). It was noted that, for MFT samples some modifications are needed, as suggested by Jeeravipoolvarn (2005), who reported that the solid-like bitumen might foam and float at the top of the suspension during the process, which disguised the etch mark of the pycnometer. Hence, the gas bubbles in the pycnometer was removed by vacuum.

### **3.3.6 Grain size distribution**

In order to better characterize the property of MFT, grain size distribution analyses were performed by both laser analysis (BT-9300S) and hydrometer/sieve analysis.

The hydrometer tests were conducted first as outlined in ASTM D422-63 (2007), followed by wet sieving. The entire test was finished when the MFT slurry on the sieves were washed under a tap until the wash water ran clear. In the test, the commonly used dispersion agent i.e., sodium hexametaphosphate, was not added into MFT samples, since sodium hydroxide (NaOH) is present in tailings as a dispersion agent during the bitumen extraction process.

### **3.3.7 Water chemistry and zeta potential of solid particles**

In the present study, the MFT pore water was obtained by centrifugal extraction. Both pH and electrical conductivity (EC) of pore fluid were measured using a multimeter (WTW Multi 360i). This instrument was calibrated by buffer solutions prior to the test.

In the test, a mixture of 5 g air-dried, sieved samples and 25 g deionized water was prepared and shaken vigorously in a centrifuge tube, and then let it stand for 24hr. Then the tubes were centrifuged at 5500 rpm for 3 min in a centrifuge machine (Labnet international Inc.). At the end of centrifugation, EC was measured on the free



supernatant, followed by pH measurement. Note that the mass ratio (1:5) of dry soil to water was suggested in standard JGS 0212-2000 (JGD2000). Eades and Grim (1966) suggested that, in pH measurement the periodical shaking of the 1:5 mixture was necessary. Therefore, a Model 75HT ultrasonic was used to facilitate mixing, as the liquid in the mixture was highly separated after centrifugation. Other tests related to the tailings water chemistry were also performed, including the ICP and turbidity using a spectrometry and a turbidimeter, respectively.

To measure the zeta potential of MFT, a zeta potential analyzer (ZetaPlus Brookhaven Instruments Corp.) was employed, which measures the electrophoretic mobility of tailings particles. The aqueous MFT suspension was firstly diluted with distilled water to a solid concentration of  $\sim 500$  ppm. Then the diluted tailings were mixed homogenously by a magnetic stirrer and transferred into a cuvette for zeta potential measurement. The pH of the test suspension was adjusted in the range from 2 to 12 by titration using 0.1M NaOH and 0.1M HCL.

### **3.3.8 SEM and XRD analyses**

For the SEM imaging, MFT samples were either oven-dried or freeze-dried. Oven-drying was performed at the temperature of 45°C for 24hr, as it was reported that this drying temperature would not induce cracks at the surfaces of original MFT samples (Roshani et al, 2017). However, this temperature gave rise to significant shrinkage of silicate-treated samples upon drying. Hence, after oven-drying only the original MFT samples and cement-treated MFT samples were observed by SEM. It was also noted that a higher temperature such as 105°C, which was generally applied in the water content measurement of soils, could cause the particle breakage of MFT samples.

For the freeze-drying of silicate-treated MFT samples, the liquid nitrogen at a temperature of -196°C was used to rapidly freeze the samples, as shown in **Figs. 3.10 (a) and (b)**. Then the samples were transferred to a freeze dryer (**Fig. 3.11(a)**) for ice sublimation under vacuum at a temperature of -50°C. The reason for this step was to minimize the fabric change of specimen during water removal.

After drying, the samples were coated with a thin layer of gold by using a device called “sputter coater (**Fig. 3.11(b)**)”, and then the samples were divided by a cutter without disturbance to the broken surface. After that, the samples were attached to the sample holder by a conducting tape, with the broken surface facing upwards. For some silicate treated samples, the loose fine-grained particles on the weak surface made the entire sample movable at the SEM pin stub when the SEM instrument was running. In these cases, the fresh surface was obtained by a gentle peeling of surface unconsolidated particles, and a conductive carbon glue was used to stabilize the sample, instead of the conducting tape. After sample preparation, the specimens were delivered to the SEM chamber for visual observation. It should be noted that for samples (e.g. silica gel) observed by ESEM, the drying process was not required.

Powder X-ray diffraction (XRD) was used to identify the reaction products formed and mineralogical changes after chemical treatment of MFT. The XRD analysis was carried out in a Rigaku SmartLab X-ray diffraction system using Cu K $\alpha$ 1 radiation source ( $\lambda = 1.54 \text{ \AA}$ ). Air-dried MFT powders finer than  $74 \mu\text{m}$  (#200 sieve) were used. The scans were performed between  $5$  and  $70^\circ 2\theta$ , with an increment of  $0.02^\circ/\text{step}$  and a scan speed of  $6^\circ/\text{min}$ . The peaks were identified using the X’Pert Highscore Plus software.

### **3.4 Summary**

This chapter illustrates the research methodology for the overall experimental tests of MFT. The characterization of basic properties and surface morphology of MFT, as well as the introduction of the chemical stabilizers is presented in this chapter.

**Table 3.1 Characteristics of MFT used in this study**

Parameters	MFT (Oil sand tailings)
Specific gravity, Gs	2.31
Water content, W%	185%
Solid content <sup>1</sup> , S%	35%
Void ratio, e	4.27
Dry density (Mg/m <sup>3</sup> )	0.70
Atterberg limits	
Liquid limit, (%)	47.0
Plastic limit, (%)	23.9
Plasticity index	23.1
USCS classification	CL
Grain size (determined by laser analysis)	
D <sub>25</sub> (µm)	2.93
D <sub>75</sub> (µm)	17.20
D <sub>90</sub> (µm)	30.75
Sand (4.75-0.075mm), %	0.00
Silt (0.075-0.002mm), %	81.00
Clay(<0.002mm) %	19.00
Specific surface area (BET-method)	2.546 m <sup>2</sup> /g
Zeta potential (at natural condition)	-38 mV
Chemical analysis of pore fluid	MFT (Oil sand tailings)
Natural pH of suspension	8.52
Electrical conductivity, µS/cm	1460
Concentration of dissolved cations (ppm)	
[Na <sup>2+</sup> ]	502.07
[K <sup>+</sup> ]	22.65
[Ca <sup>2+</sup> ]	4.35
[Mg <sup>2+</sup> ]	4.34
[Ba <sup>2+</sup> ]	0.21
[Cu <sup>2+</sup> ]	0.01
[Al <sup>3+</sup> ]	1.62
[Zn <sup>2+</sup> ]	0.07

Note: <sup>1</sup> Solid content = 1/ (1+W%);

**Table 3.2 Oxide compositions of Portland cement used in the study.**

Oxide composition	Unit (%w/w)
Silicon dioxide (SiO <sub>2</sub> )	15.6
Alumina oxide (Al <sub>2</sub> O <sub>3</sub> )	2.75
Ferric oxide (Fe <sub>2</sub> O <sub>3</sub> )	5.20
Calcium oxide (CaO)	70.1
Magnesium oxide (MgO)	1.81
Sulfur oxide (SO <sub>3</sub> )	2.43
Potassium oxide (K <sub>2</sub> O)	0.506
Sodium oxide (Na <sub>2</sub> O)	0.154

**Table 3.3 Specification of silicate products used in the study**

Silicates	NS <sup>1</sup>	AAAS <sup>2</sup>
Na <sub>2</sub> O, %	8.9	16.2
SiO <sub>2</sub> , %	28.7	27.9
Al <sub>2</sub> O <sub>3</sub> , %	-	1.6
Solids	37.6%	45.7%
Density, g/cm <sup>3</sup>	1.38	1.6
Weight ratio (Na <sub>2</sub> O:SiO <sub>2</sub> )	3.2	1.7
pH	11.3	-
Characteristics	Syrupy liquid	Syrupy liquid

Note: <sup>1</sup> Reference: PQ Corporation, 2003;

<sup>2</sup> These data were obtained through personal communications with PQ Corporation.

**Table 3.4 Typical values of K for Eq.3.4 <sup>1</sup>.**

Fall Cone angle	30°		60°	
	Undisturbed	Disturbed	Undisturbed	Disturbed
<b>K value</b>	<u>1.0</u> <sup>2</sup> ; Hansbo (1957)	<u>0.85</u> <sup>2</sup> ; 0.8; 0.96 Wood (1985) Karlsson (1977) Houlsby (1982)	<u>0.2</u> <sup>2</sup> -0.25; Hansbo (1957)	<u>0.29</u> <sup>2</sup> ; 0.27 Wood (1985) Karlsson (1977)

Note: <sup>1</sup> Swedish fall cone method, Eq. 3.4:  $C_u = K \frac{mg}{d^2}$ ;

<sup>2</sup> Underlined values are selected for this study.

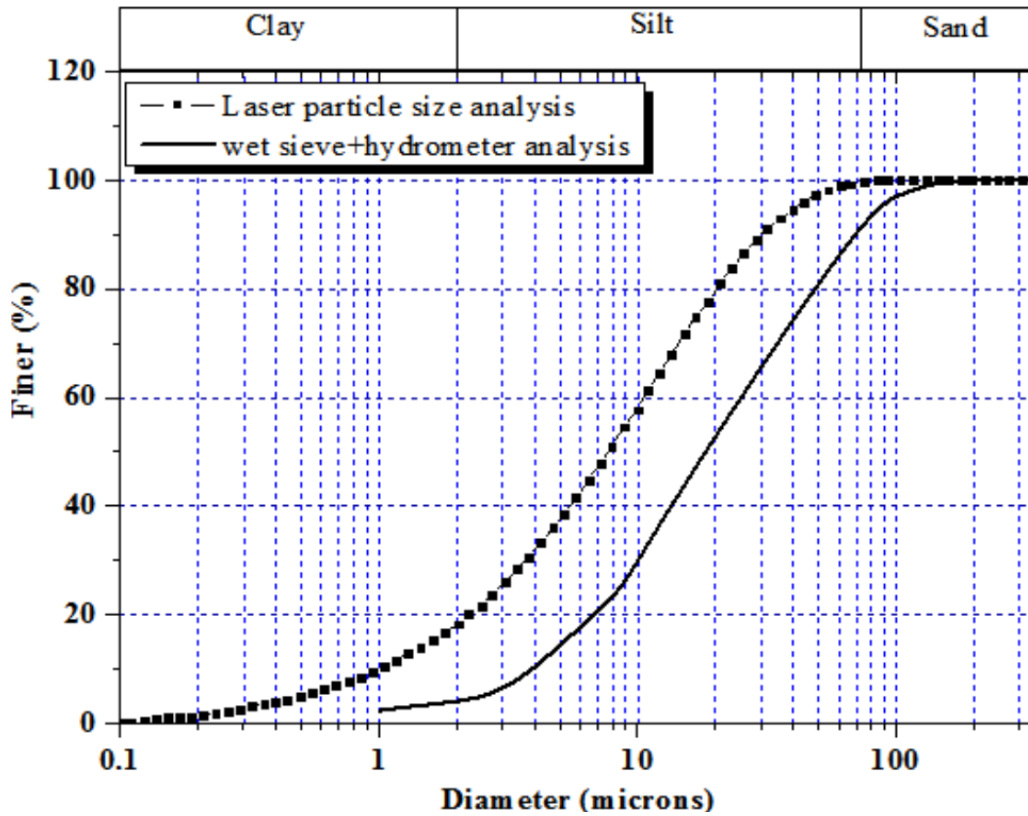


Fig 3.1 Grain size distribution of original MFT

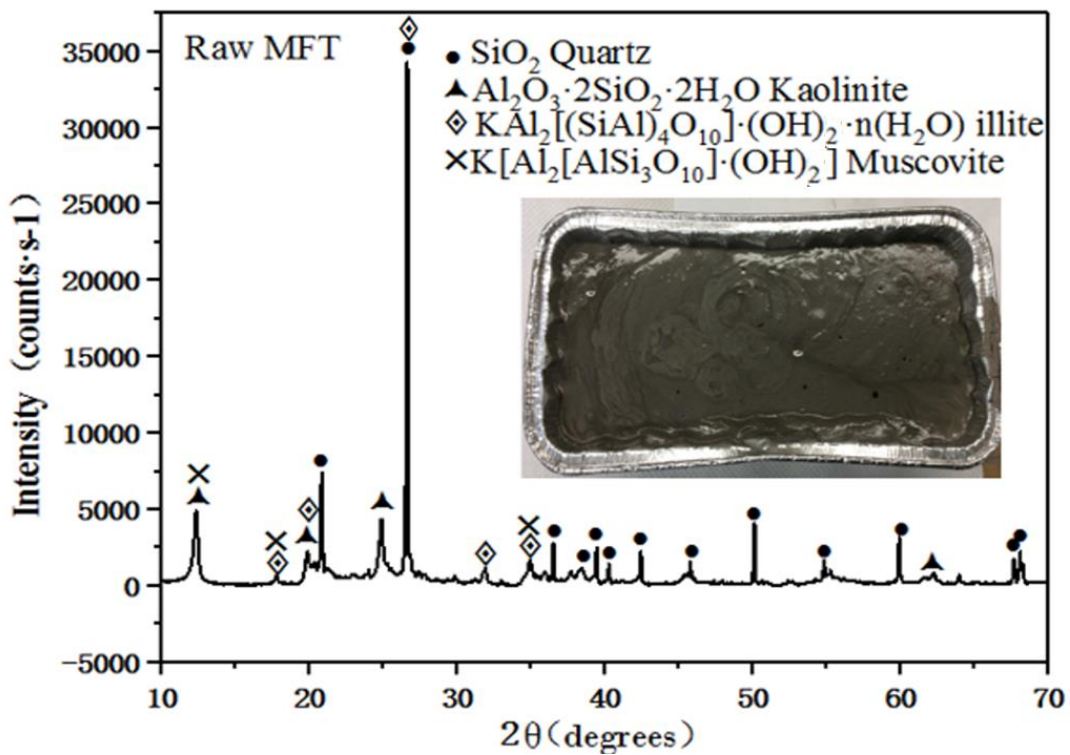
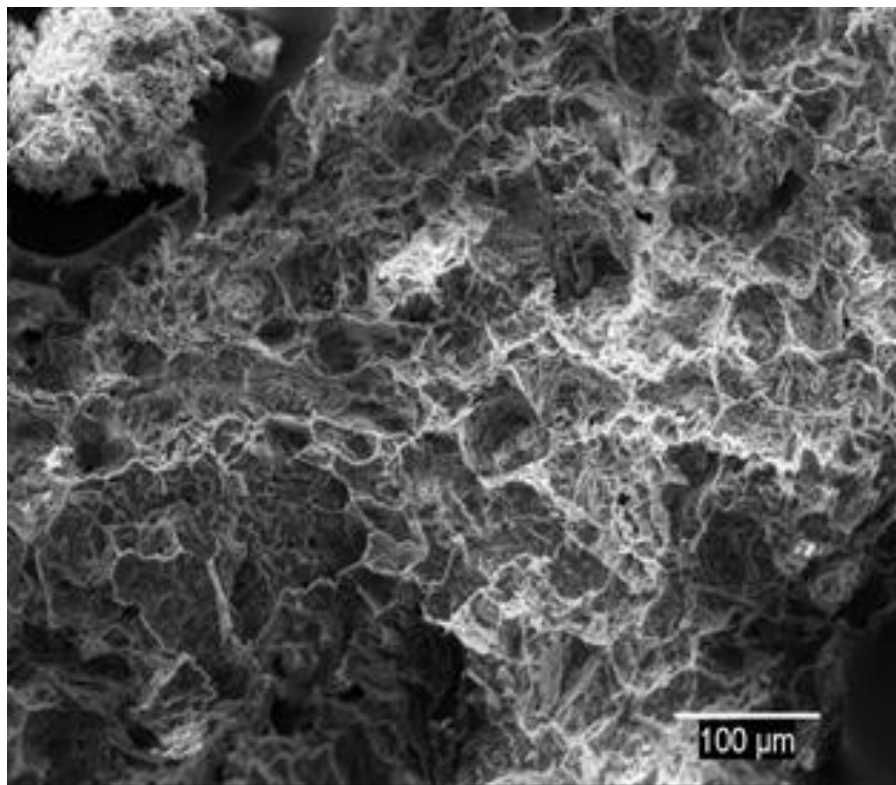
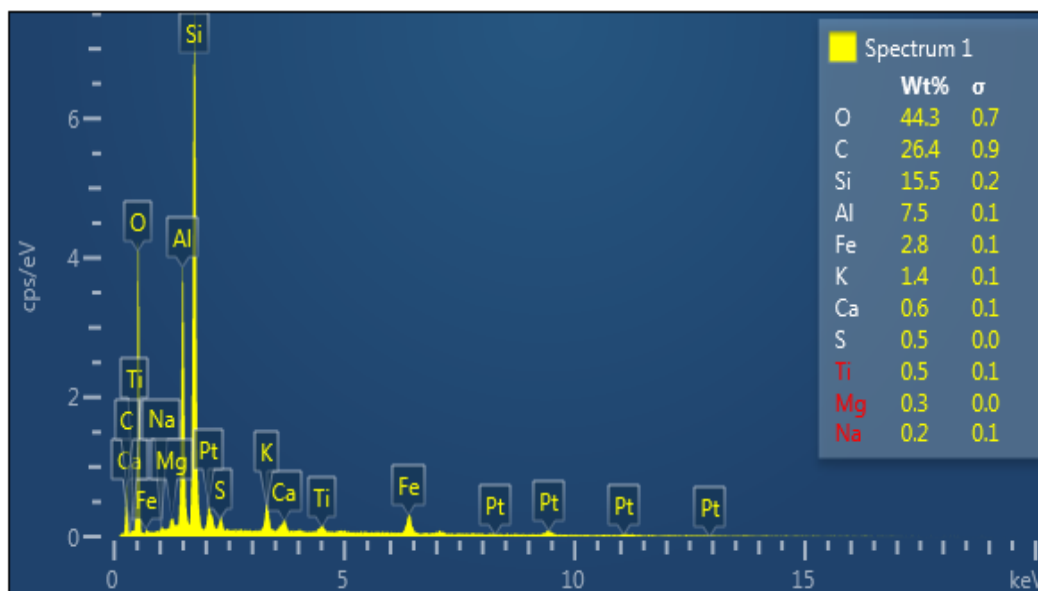


Fig 3.2 X-ray Diffraction (XRD) on original MFT sample



**Fig 3.3 SEM imaging on freeze-dried original MFT (Mag=1,000X)**



**Fig 3.4 EDS analysis on freeze-dried original MFT**

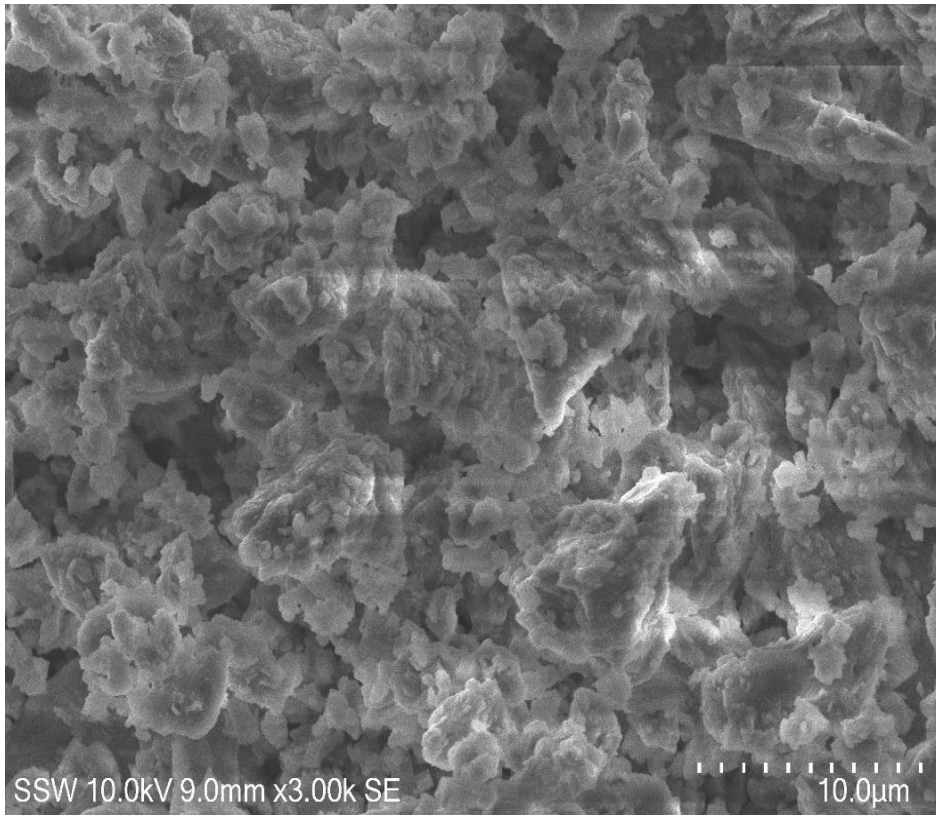


**Fig 3.5 SEM micrograph for as-received cement (3,000x)**

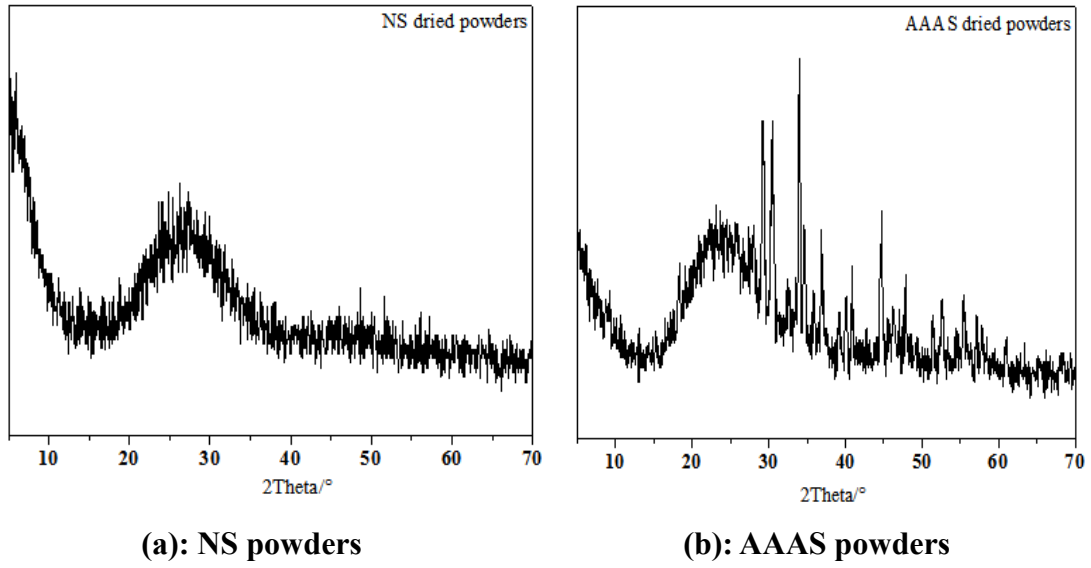


Fig 3.6 XRD pattern of silicate powders

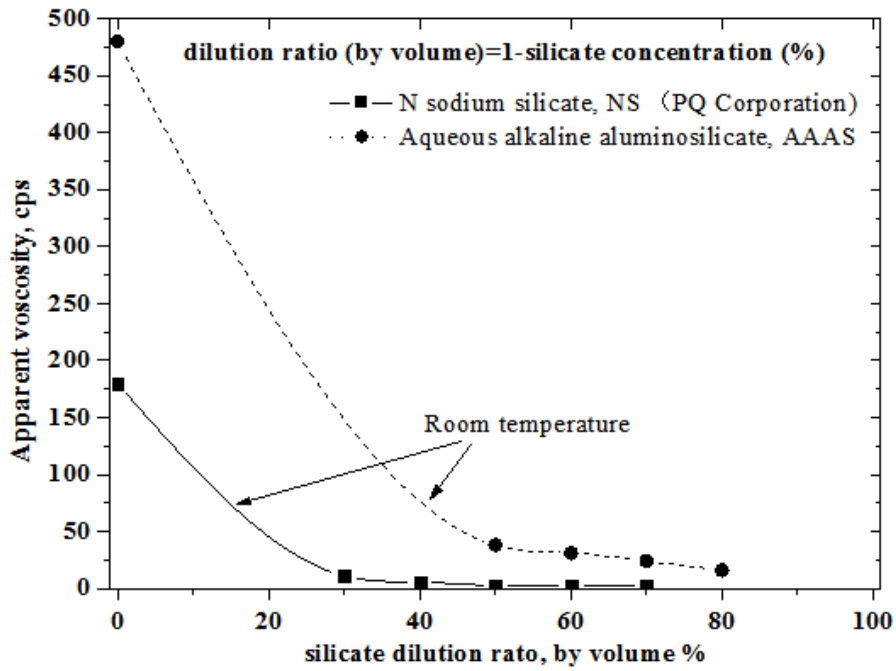
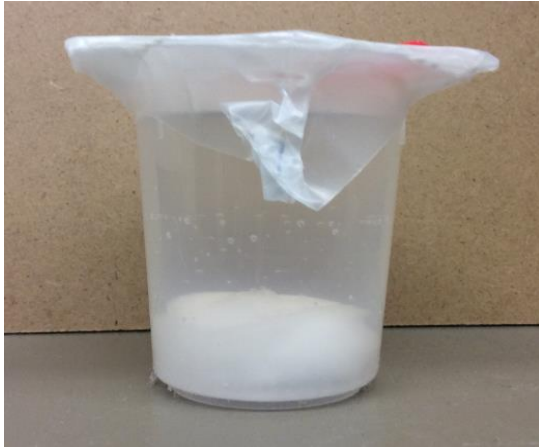


Fig 3.7 Silicate viscosity VS silicate dilution ratios



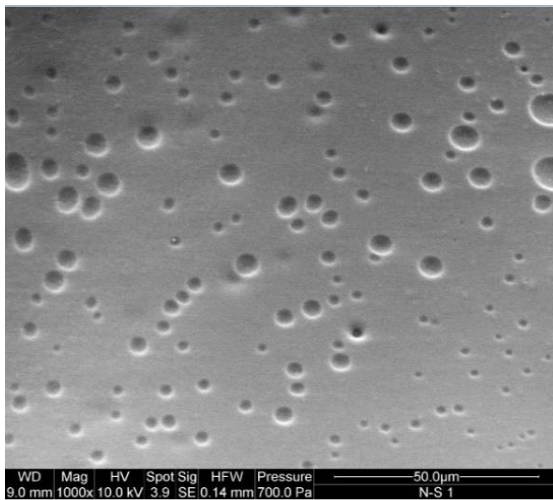


**(a): NS gel after 60 days curing**

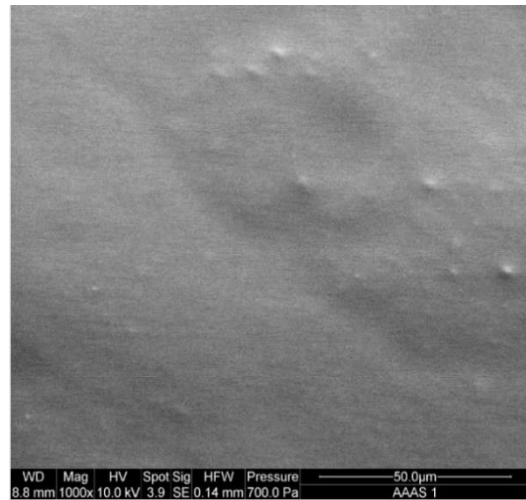


**(b): AAAS gel after 60 days curing**

**Fig 3.8 Close-up view of the colloidal Silicate gel**



**(a): Mag=1,000X (NS gel)**



**(b): Mag=1,000X (AAAS gel)**

**Fig 3.9 ESEM imaging on the colloidal Silicate gel**



**(a) Liquid nitrogen**



**(b) Frozen MFT samples**

**Fig 3.10 Freeze-drying of MFT samples**



**(a): Freeze-dryer**



**(b): Sputter coater**

**Fig 3.11 Device for the sample preparation of SEM observation**

## References

**ASTM 2435/D2435M-11.** Standard Test Methods for One-dimensional Consolidation Properties of Soils Using Incremental Loading, ASTM International, West Conshohocken, PA, 2011, DOI: 10.1520/D2435\_D2435M-11.

**ASTM D2487-11.** Standard Practice for Classification of Soils for Engineering Purposes (Unified Soil Classification System), ASTM International, West Conshohocken, PA, 2011, DOI: 10.1520/D2487-11.

**ASTM D422-63 (2007) e2.** Standard Test Method for Particle-Size Analysis of Soils. ASTM International, West Conshohocken, PA, 2007, DOI: 10.1520/D422-63.

**ASTM D4318-10.** Standard test methods for liquid limit, plastic limit, and plasticity index of soils. ASTM International, West Conshohocken, PA, 2007, DOI: 10.1520/D4318-10.

**ASTM D4959-16.** Standard Test Method for Determination of Water Content of Soil By Direct Heating, ASTM International, West Conshohocken, PA, 2016, DOI: 10.1520/D4959-16.

**ASTM D854-14.** Standard Test Methods for Specific Gravity of Soil Solids by Water pycnometer, ASTM International, West Conshohocken, PA, 2014, DOI: 10.1520/D854-14.

**Canadian Standards Association and Bureau de normalization du Quebec, Standard CAN/BNQ 2501-092 (2006).** Soils-determination liquid limit by the fall cone penetrometer and determination of plastic limit. Bureau de normalization du Quebec, Quebec

**Eades JL, Grim RE. 1966.** A quick test to determine requirements for lime stabilization. Highway Research Board Bulletin; 139: 61e72.

**Hansbo, S. 1957.** A new approach to the determination of the shear strength of clay by the fall cone test. Proceedings of the Royal Swedish Geotechnical Institute, Stockholm,

NO. 14.

**Houlsby, GT 1982.** Theoretical analysis of the fall cone test. *Geotechnique* 32, No.2, 111-118.

**Japan Geotechnical Society (JGS). (2000).** “Test method for electrical conductivity of soils.” 0212-2000, Tokyo (in Japanese)

**Jeeravipoolvarn, S. (2005).** Compression behaviour of thixotropic oil sands tailings. M.A.Sc. thesis, Department of Civil and Environmental Engineering, The University of Alberta, Edmonton, Alberta.

**McDonald M J, Miller N, Hamilton J. (2014)** USE OF AQUEOUS ALKALI ALUMINOSILICAE FOR PROFILE MODIFICATION, WATER CONTROL AND STABILIZATION. United States Patent Application Publication 20140076568A1 Mar. 20, 2014.

**Miller ML, Scorsone JT, Whitfill DL, McDonald M., Miller N., 2013.** “The Development of a Geopolymer-based Pill as an Engineered Solution to Lost Circulation”, SPI 166123, SPE Annual Conference, New Orleans, LA

**New Zealand Geotechnical Society, 2001.** Guideline for hand held shear vane test. New Zealand Geotechnical Society (NZGS). Available at: <http://www.nzgs.org/library/guideline-for-hand-held-shear-vane-test/>

**Proskin S, Segó D, Alostaz M. 2010** Freeze-thaw and consolidation tests on Suncor mature fine tailings(MFT)[J]. *Cold Regions Science and Technology*, 63(3):110–120.

**PQ Corporation, 2003.** Soluble silicate in geotechnical grouting applications. Bulletin 52–53, USA.

**Roshani, A., Fall, M., and Kennedy, K. (2017).** "Drying Behavior of Mature Fine Tailings Pre-Dewatered with Super-Absorbent Polymer (SAP): Column Experiments," *Geotechnical Testing Journal*, Vol. 40, No. 2, 2017, pp. 210-220.

**Wood, D.M. 1985.** Some fall-cone tests. *Geotechnique*, 35(1):64-68

# CHAPTER 4 STABILIZATION OF OIL SANDS MATURE FINE TAILINGS (MFT) BY PORTLAND CEMENT

## 4.1 Introduction

Chemical stabilization of soft ground by shallow and deep cement mixing is a commonly used technique in earthwork projects. Many studies have been conducted to characterize the properties of artificially cemented clays. The results showed that cement was effective in increasing the strength and stiffness of weak soils (e.g. Pakbaz and Alipour, 2012; Zhang et al., 2014). Portland cement was also used to stabilize wastes such as mine tailings for underground mining operations, and the resulting material was called ‘cemented paste tailings’ (CPT) (Fall and Pokharel, 2010; Tariq and Yanful, 2013). Hydraulic cement served to develop cohesion within CPT and provide sufficient strength for CPT applications as backfill materials (Belem and Benzaazoua, 2004). Paste technology was widely adopted in Australia and Canada for tailings management (Ercikdi et al., 2017).

Soil-cement reactions are responsible for the strength development of soft soils (Mitchell, 1981). As described in **Chapter 2 (Section 2.4.2.2)**, these reactions mainly include cement hydration and pozzolanic reaction, during which cementitious products are produced. This creates a structured soil typically with a higher strength. It is reported that the strength improvement was controlled by the cement type, amount of cement added, curing period and soil properties (e.g. Horpibulsuk et al., 2004; Consoli, et al., 2011; Sasanian and Newson, 2014).

The main objective of this chapter is to investigate the influence of Portland cement addition on the geotechnical properties of MFT. The focus of discussion is on the effect of treatment on the solid content and undrained shear strength of MFT. The changes in the microstructure of stabilized MFT samples were observed using a scanning electron microscope (SEM). X-ray diffraction (XRD) analysis was performed to identify the minerals present and the new reaction products in the cement-stabilized MFT samples.

## 4.2 Sample Preparation

In order to ensure that MFT used throughout the study had consistent properties, test samples were taken from the mid-height of the bucket by a scoop sampler and then stirred thoroughly. The initial water content of 185% was adjusted for the test samples to simulate the in-situ water content of MFT in tailing ponds. The test samples were dried for 3 days under air-tight condition, then a prescribed amount of deionized water was added and mixed by a stirring machine (**Fig. 4.1**).

In this study, the dry method was applied (i.e. MFT slurry was mixed with dry cement). Pulverized cement powders passing #200 sieve were directly added to the test samples (original MFT hereafter) to ensure rapid chemical reactions. Then the specimen was mixed by machine (**Fig. 4.1**) at a high speed within 10 minutes, as suggested by Kamruzzaman et al., (2006). The cement content was adopted based on regular dosages in the practice, i.e., 1%, 5%, 10% and 15% (w/w), i.e. the mass ratio of dry cement to the dry MFT solids. After thorough mixing with cement, the MFT slurry became a homogenous paste. Then the paste was transferred to 2” cylindrical plastic molds (50mm in diameter and 100mm in height) and 4” molds (100mm in diameter and 200 mm in height), as shown in (**Fig. 4.2**). Air bubbles on top surface of the specimens were removed through slight vibrations. The molds were capped and each of them was assigned with a number. All prepared samples were cured under the room temperature ( $20\pm 2^{\circ}\text{C}$ ) for 7,14, and 28 days before testing. Samples for each curing period were tested in triplets and the average results were taken, including the water content and undrained shear strength. After the specified curing time, a hole was drilled at the bottom of the mold, then the sample was extracted by air pump for testing. The overall experimental program is summarized in **Table 4.1**.

## 4.3 Results and discussion

### 4.3.1 Water content and Solid content

For each curing period (7, 14 and 28 days), the water contents (W%) of the MFT samples were measured. As indicated before, the initial water content of MFT was 185%. After adding cement powders into MFT, pore water was mainly removed by two pathways: a) evaporation due to heat generated by cement hydration and atmospheric interactions; b) consumption by cement hydrated products. It is noted that the water incorporated into the structures of cementitious products cannot be depleted by heating to 105°C (Chew et al., 2004).

In the study, the moisture loss of MFT due to evaporation was monitored by daily weighing ( $\pm 0.01$ g), and the results are shown in **Fig. 4.3**. It is seen that the weight of the samples slightly decreased due to evaporation, but changes in water contents were negligible. This suggested that the chemical reactions between the MFT particles and binders should be the main reason for dewatering of MFT.

In general, as shown in **Fig. 4.4**, the water content of MFT samples decreased as cement content increased. After mixing, the water content was immediately reduced. The majority of reduction in water content took place within the first 7 days of curing, and the decreases slowed down at later curing stage (7 to 28 days). This was attributed to that hydration reaction was faster than pozzonlanic reaction, hence water was mainly consumed by the time-dependent pozzonlanic reaction (Chew et al., 2004). It is also noted that, at a relatively high cement content (e.g., 10% and 15%), the water content decreased almost linearly with the cement content. In addition, the corresponding increase in solid content was illustrated in **Fig. 4.4**. As shown, on addition of 15% cement, the stabilized MFT paste exhibited the highest solid content of 41.72% among other treated samples after 28 days, compared to 35% of the original MFT sample.

### **4.3.2 Index properties**

The influence of cement additives on the liquid limit (LL) of MFT samples is presented in **Fig. 4.5**. It is observed that, the LL of all MFT samples increased immediately after mixing. The increase became more prominent with curing time. For example, as shown in **Fig. 4.5**, adding a small amount of cement (5%) increased the LL of MFT to 67.5%

at 7 days and 96.5% at the end of curing period (28 days), eventually doubled the initial LL (47.0%) of MFT. The maximum increase in LL (i.e. 136.5% at 28 days) was registered in 15%-PC-MFT sample. As shown, the LL value of 15%-PC-MFT sample increased linearly with curing time and higher than other cement-treated MFT samples at all ages of curing. However, after mixing the LL of 1%-PC-MFT samples did not change much with curing time, as shown in **Fig 4.5**.

The variations of plastic limit (PL) are also presented in **Fig 4.5**. In general, the plastic limit of MFT samples slightly increased upon mixing, and gradually increased with time (7 days and 28 days). As expected, the most significant increase in PL was also registered in the 15%-PC-MFT (61.56% at 28 days). With higher cement amounts (e.g. 10%, 15%), the admixed MFT samples formed semi-hard to hard bodies due to aggregation of solid particles into larger clusters (Hassan et al., 2008).

**Fig. 4.6** shows the Casagrande plasticity chart, containing LL and plasticity index (PI) data of cement-treated MFT samples. It is seen that after mixing and curing, the PI of MFT samples increased. This was due to that the increase in LL was more significant than the increase in PL, as illustrated in **Fig. 4.5**. The points of the MFT samples mixed with 10% and 15% cement were located below A-line in inorganic MH region of the plasticity chart, as shown in **Fig. 4.6**, indicating that the MFT samples were characterized as elastic silts.

Overall, an increase in the cement content and curing period are associated with increases in the Atterberg limits of MFT. It has been reported that cement addition promotes the flocculation and aggregation of the soil particles (e.g. Chew et al., 2004; Kumar and Janewoo, 2016), and the soils with a higher degree of particle flocculation can enclose large void spaces holding water. This increases the LL value of soils (Wang and Siu, 2006; Bhuvaneshwari et al., 2014). It was also reported that surfaces and pores of the gelatinous materials (e.g., C-S-H products) could imbibe water, thereby giving rise to an enhanced LL of soils, especially the SiO<sub>2</sub>-rich soils (Dash and Hussain, 2011). The notion that the aggregation and cementation of MFT fine particles after cement treatment was consistent with the particle size distribution curves shown in **Fig. 4.7**.



The figure indicates that the particle sizes of MFT increased with curing time and cement content. It should be also noted that during sample preparation some degree of bond breaking occurred and the actual sizes of aggregates were underestimated. In addition, the formation of cementitious products and fabric changes occurred in the cement-treated MFT samples were examined by the XRD and SEM analyses, as shown in **Section 4.3.5** and **Section 4.3.6**.

### **4.3.3 Undrained shear strength**

The undrained shear strength of MFT samples was evaluated using the fall cone method. This method was commonly adopted to measure the strength properties of geomaterials, e.g., marine clays (Rajasekaran and Rao, 2004), soft clays (Tanaka et al., 2012) and mine tailings (Dimitrova and Yanful, 2011; Chen et al., 2013). The Swedish fall cone has also been used to measure the strength of oil sands MFT (Boxill, 2016). In this study, the laboratory vane shear tests were carried out to compare with the results obtained by the falling cone on MFT samples. The original MFT slurry was placed in an Electrokinetic testing cell (Liu and Shang, 2014), and the surcharges were applied to consolidate the sample. Then a series of vane shear tests and falling cone tests were performed following the procedures described in **Chapter 3**. **Fig. 4.8** shows that two sets of data had a high correlation ( $r=0.9617$ ) and the ratios of  $S_{u1}(\text{Fall cone})$  to  $S_{u2}(\text{vane shear})$  were between 0.83 and 1.33; At low strength range, the data points were close to the  $45^\circ$  line, especially within 3 kPa. The comparison between two methods agreed with other previous works (e.g., Wasti and Bezirci, 1986; Rajasekaran and Rao, 2004). The calibration indicates that the use of Swedish fall cone method to measure the shear strength of cement-treated MFT is reliable.

**Fig. 4.9** illustrates the variations in the  $S_u$  of MFT with respect to the cement dosages. In general,  $S_u$  increased with curing time and cement content. However, no measurable shear strengths were recorded at the cement content of 1% with curing time up to 28 days. It is also noted that the strength improvement was practically negligible for the 5%-PC-MFT samples, displaying an approximate value of 1kPa throughout the entire

curing period. This suggested that a minimum percentage of cement (i.e. >5%) was required to generate any noticeable strengthening effect on MFT. At cement contents of 10% and 15%, the MFT samples could reach 5 kPa (one-year management requirement for MFT) and 10 kPa (five-year management requirement of MFT) (Directive 074, 2009). In particular, after 28 days the  $S_u$  of 10%-PC-MFT and 15%-PC-MFT sample was 7.65 kPa and 15.5 kPa, respectively. Also, it is found that more significant strength development of MFT occurred between the 7th and 28th days at higher cement content levels, which was mainly governed by the pozzonlanic reaction (Chew et al., 2004).

The results are consistent with the study of Chew et al., (2001) and Kamruzzaman et al., (2009). They reported that the cementation effect was insignificant when cement content was less than 5%<sup>3</sup> (termed as inactive zone), and the strength increase was more pronounced when cement content was between 5%-40% (termed as active zone), while beyond 40% (termed as inert zone) the cementitious reactions proceeded at a slower rate. It was also reported that the initial water content of soils greatly affected the distance between the soil and cement particles, as well as the efficiency of calcium ion diffusion in pore fluid (Chew et al., 2001).

#### **4.3.4 Consolidation tests**

Standard oedometer tests (ASTM D2435-11) were carried out on MFT samples treated by 5%, 10% and 15% Portland cement after 28-day curing. The results are presented in **Fig. 4.10**. Initially, the void ratio of MFT decreased with increasing cement content, and this was due to the immediate pore water consumption by hydraulic cement. It is also observed that for 5%-PC-MFT sample, there was no obvious preconsolidation pressure from the  $e$ - $\log \sigma'$  relationship. However, the preconsolidation pressure increased with the cement content (10% and 15%), showing an approximate value of 45 kPa and 95 kPa, respectively. This indicated a higher degree of cementation bonding between solid particles in these MFT samples in comparison to that of 5%-PC-MFT sample. Also, for MFT samples mixed with 10% and 15% cement, the void ratios

---

<sup>3</sup> The ratio has the same definition with this study, i.e., mass ratio of dry cement to dry soil.

remained relatively constant within the range of preconsolidation pressure, and beyond this pressure the curves were almost parallel. This suggested that once the bond strength was exceeded, the inter-particle cementitious bonds were destroyed (Bhuria and Sachan, 2014). In this case the cement-treated MFT samples exhibited typical behavior of normally consolidated clays. Moreover, **Fig. 4.11** shows the similar patterns of 14-day consolidation results with lower preconsolidation pressure. As shown, after 14 days, the preconsolidation pressure of 10%-PC-MFT sample and 15%-PC-MFT sample was as high as 25 kPa and 30 kPa, respectively. The increase in preconsolidation pressure with time and cement content was believed to be associated with the formation of new cementitious products, which resulted in a greater resistance to compression (Rao and Shivananda, 2005).

It is also noted that a stress ranging from 100 to 400 kPa was adopted to calculate the compressibility index ( $C_c$ ). **Table 4.2** shows the values of compression indexes of MFT samples at different contents of PC (10% and 15%), and at various curing times (14 and 28 days). In general, the compressibility properties of the treated MFT samples reduced with time and cement dosages. For example, the compressibility index of 15%-PC-MFT sample was 2.04 at 14 days of curing and further decreased to 1.81 after 28 days. The decrease in the compressibility characteristics of the treated MFT were believed to be due to the formation of cementitious products and flocculation of particles which increased the resistance to compression at same stress degrees (Nalbantoglu and Tuncer, 2001; Latifi et al., 2016).

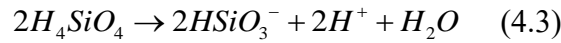
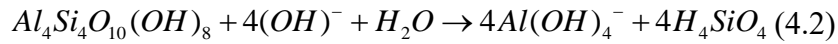
#### **4.3.5 X-ray diffraction analysis**

Typical XRD results for the original MFT slurry and 28-day cured MFT samples mixed with 5%, 10% and 15% cement are shown in **Fig. 4.12**. The crystalline phases of Quartz, Kaolinite and Illite in MFT were clearly seen, particularly in the region of  $19-25^\circ$  and  $35-45^\circ$ , as mentioned in Chapter 3. The XRD patterns for the cement-stabilized MFT samples revealed extra peaks. The development of C-S-H gel at  $2\theta=29.36^\circ$  was observed, and the C-S-H peak was more predominant as the percentage of cement

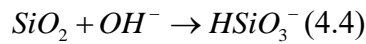
increased. It is noted that the slight camber at  $2\theta=31.98^\circ$  was identified for both 10% and 15% cement-treated MFT samples, which also indicated the formation of C-S-H gel. However, the peaks of calcite ( $\text{CaCO}_3$ ) were not detected by XRD, suggesting that the carbonation of cement was absent. In addition, other phases related to the cement hydration, e.g., C-A-H and C-A-S-H gel, were not observed in the XRD patterns, which implied that the strength improvement of MFT samples was mainly attributed to the formation of C-S-H compounds.

Comparison between peaks of original and treated MFT samples also demonstrated that the reflections of clay minerals, e.g., Kaolinite ( $2\theta=12.32^\circ, 24.86^\circ$ ) and Illite ( $2\theta=17.74^\circ$ ) reduced as a result of cement stabilization. Moreover, the peak intensity of Quartz (e.g.  $2\theta=20.82^\circ, 26.6^\circ, 40.06^\circ$ ) also decreased to some extent.

It is known that when pH of the pore liquid exceeds 10.5, dissolution of the clay surface (e.g. Kaolinite) will take place (Davidson et al., 1965; Hunter, 1988):



Silica ( $\text{SiO}_2$ ) will also be dissolved under this alkaline environment:



As a result, dissociated hydrogen silicate ions  $\text{HSiO}_3^-$  can react with calcium ions in pore fluid, producing cementitious products by the following equation (Ma et al., 2015):

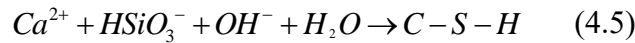
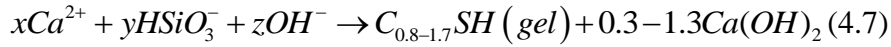


**Fig. 4.13** presents the pH values of cement-stabilized MFT samples at different dosages, showing that after 28 days MFT sample treated by 5%, 10% and 15% cement had pH values greater than 10.5. This suggested that Kaolinite, Illite and  $\text{SiO}_2$  in MFT samples were consumed by the reactions (Eqs. 4.2, 4.3 and 4.4), which is reflected in the XRD patterns (**Fig. 4.12**), i.e. the diffraction intensities of clay minerals reduced after cement treatment. The appearance of C-S-H peaks in the XRD patterns of MFT (**Fig. 4.12**) was believed to be associated with pozzolanic reaction (Eq. 4.5), as well as the cement

hydration (Eqs. 4.6 and 4.7) after mixing (Ma et al., 2015):



Referring to **Fig. 4.13**, the increase in pH of MFT paste after cement treatment is related to the fact that, Portland cement is an alkaline material increasing the alkalinity of the MFT paste, and the high pH condition can induce the microfabric changes, such as the formation of flocculated structure (Chew et al, 2004; Ahmed and EI Naggar, 2016). The microstructure of cement-stabilized MFT samples will be discussed in next section.

### 4.3.6 Scanning electron microscope analysis

**Figs. 4.14-4.17** show a series of micrographs taken by SEM of cement-treated MFT samples. As observed from **Figs. 4.14(a) and (b)**, after 28 days of curing, edge-to-edge and edge-to-face flocculated and aggregated patterns dominated in MFT fabrics. It was reported that the flocculated structure can be ascribed to the cation exchange process, which results in the  $Ca^{2+}$  ions replacing the  $Na^+$  or  $K^+$  cations (Mengue, et al., 2017). **Figs. 4.15 (a) and (c)** show the presence of fibrous-type C-S-H gels in 10%-PC-MFT sample, which was consistent with the XRD test results. Indeed, the needle-shaped C-S-H gels formed in pore spaces and enwrapped solid particles, resulting in a denser MFT sample. However, no hexagonal shaped  $Ca(OH)_2$  crystals were observed. At higher magnification, **Figs. 4.15 (b) and (d)** show that the long and slender cementitious products were heterogeneously distributed within the cement-MFT matrix. It also appears that the solid particles formed small and condensed clots or large irregular agglomerates. Bhuvaneshwari et al., (2014) stated that this cluster formation was attributed to the dissociation of the clay particles at the edges.

**Fig. 4.16 and Fig. 4.17** present the surface morphology of MFT samples stabilized with 15% cement at 7 days and 28 days of curing, respectively. In **Fig. 4.16**, It is observed that the fine bundles of needle-like gels were interspersed by laminated compounds

(another type of C-S-H morphology). The packing of these cement hydration products contributed to a reticular texture of the MFT microstructure after 28 days of curing. However, in **Fig. 4.17**, very few fibrous C-S-H products were observed but fine particles were cemented and formed a film that coating around the larger-sized particles such as Quartz (see white dashed circle in Fig. 4.18(a)). The difference between **Fig. 4.16 and Fig. 4.17** indicates that, as curing time increased, the amount of cementitious products increased and the binding effect was more significant.

The formation of the cementitious products, as well as the overall cemented morphology enables the MFT samples to sustain higher load. From the images, it is evident that the cementitious crystals were connected and the voids were filled. This is believed to be the reason that the mechanical properties of MFT are improved after cement treatment.

#### **4.4. Summary**

This chapter presents the effects of Portland cement as chemical additive on the mechanical, physicochemical and microstructural properties of MFT. The effects of curing time and cement dosage on MFT are investigated. The advantages of using Portland cement to stabilize MFT in terms of increase in undrained shear strength and solid content are evaluated, followed by the assessment of compressibility and Atterberg limits. The XRD and SEM analyses are conducted to evaluate changes in mineralogy and microscopy of MFT samples after cement treatment. The main results are summarized as follows:

- The undrained shear strength of MFT samples increases as cement content increases. The undrained shear strength of 10%-PC-MFT sample and 15%-PC-MFT sample reaches 5 kPa after 28-day curing, showing 7.65 and 15.5 kPa, respectively. However, MFT samples with 1% cement content do not show any strength improvement.
- The solid content of MFT increases with cement content and curing time. The dewatering effect is most significant in the first 7 days, and further reduction of water content is also observed between 7 and 28 days. 15%-PC-MFT sample has the highest

solid content of 41.72% at the end of curing period (28 days).

- The Atterberg limits and plasticity index of MFT increase with cement content and curing time, due to the augmented flocculated fabrics and the formation of cementitious products. The plastic limit is practically constant for a cement content less than 5%; The liquid limit for the 1%-PC-MFT samples remains relatively stable with curing time.
- MFT samples mixed with cement contents of 10% and 15% exhibit a preconsolidation pressure of 45 kPa and 90 kPa at 28 days, respectively. The preconsolidation pressure increases with curing time. However, addition of 5% cement shows no effectiveness on the consolidation behavior of MFT. The compressibility index of treated MFT samples reduced with curing time and cement dosages.
- The pH of MFT samples increases with cement content and curing period. The maximum pH value is registered in 15%-PC-MFT sample, indicating the significant pozzonlanic activities.
- The XRD results indicate the growth of secondary minerals, i.e. cement hydrated products (C-S-H gel) and show the decay of clay mineral peaks in MFT paste after cement treatment.
- The SEM observations confirm the existence of C-S-H gels after cement treatment, and indicate that the main C-S-H morphology in MFT is slender needle-like in shape. The cement-treated MFT samples have typical flocculated structure, with the C-S-H gels binding the solid particles together and forming aggregates.

**Table 4.1 Overall test plan for this study.**

PC (Portland cement) tests								
Sample description <sup>1</sup>	Water (Solid) content	Undrain shear strength	Atterberg limits	Consolidation	Particle sizes	pH	XRD	SEM
1%-PC-MFT	7, 14, 28 D	-	7, 14, 28 D	-	-	1, 7, 14, 21, 28 D	-	-
5%-PC-MFT	7, 14, 28 D	7, 14, 28 D	7, 14, 28 D	28 D	-	1, 7, 14, 21, 28 D	28 D	-
10%-PC-MFT	7, 14, 28 D	7, 14, 28 D	7, 14, 28 D	14, 28 D	7, 14, 28 D	1, 7, 14, 21, 28 D	28 D	28 D
15%-PC-MFT	7, 14, 28 D	7, 14, 28 D	7, 14, 28 D	14, 28 D	-	1, 7, 14, 21, 28 D	28 D	7, 28 D

Note: <sup>1</sup>: Sample description (Mix name): For example, 1%-PC-MFT denotes the MFT samples were treated by Portland cement at mixing ratio of 1%.

**Table 4.2 Compressibility index<sup>1</sup> (C<sub>c</sub>) of MFT samples treated by Portland cement.**

	10%-PC-MFT		15%-PC-MFT	
Curing time	14	28	14	28
C <sub>c</sub>	2.09	1.90	2.04	1.81

Note: <sup>1</sup>: compressibility index=  $e_1 - e_2 / \log(p_1/p_2)$





**Fig. 4.1 Laboratory mixing device used in the study**



**Fig. 4.2 Cylindrical plastic mold for curing, left: 50mm\*100mm; Right:  
100mm\*200mm**

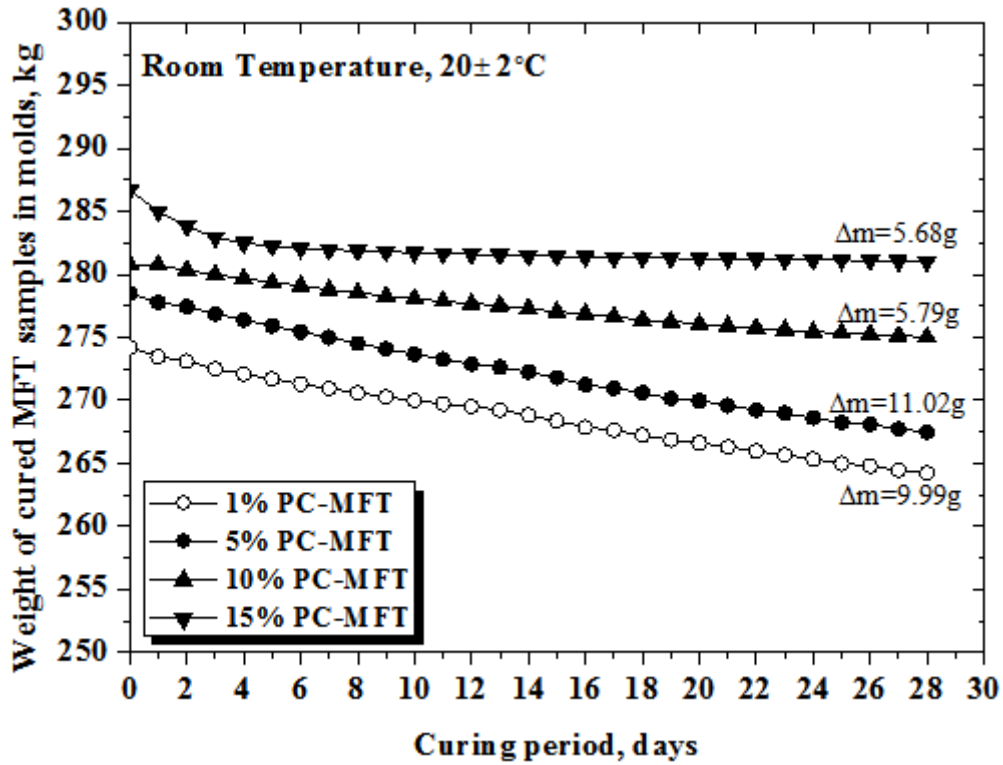


Fig. 4.3 Daily weight of cement-treated MFT samples in 2'' mold (50mm\*100mm) versus curing time

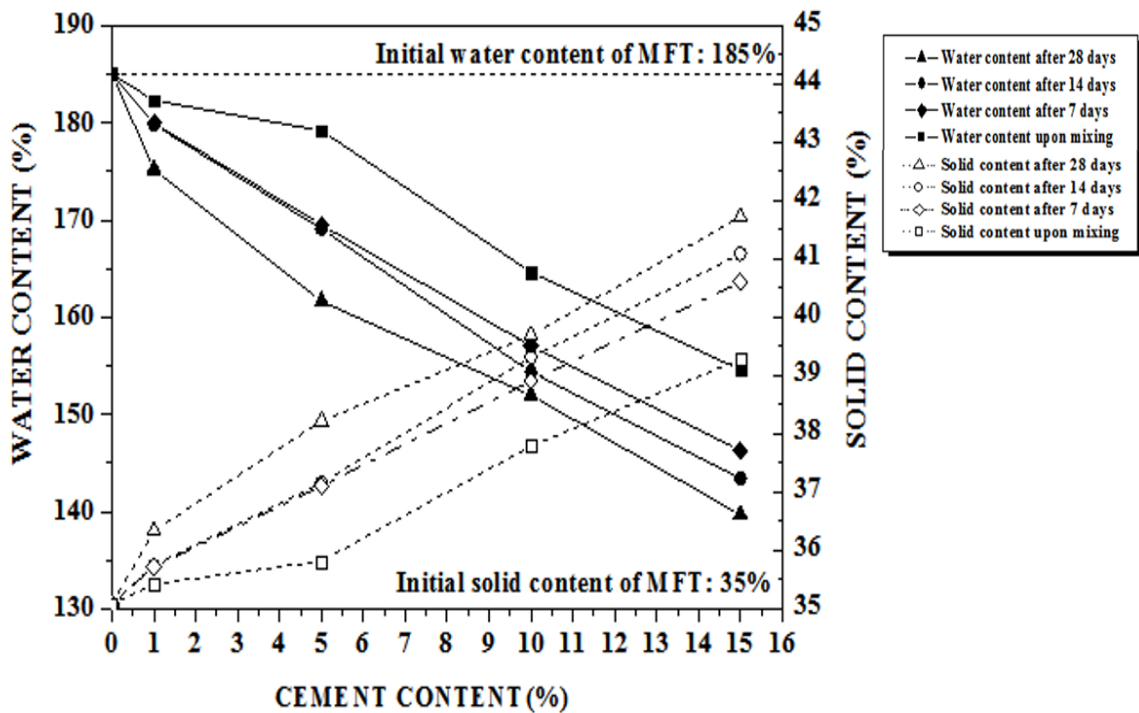


Fig. 4.4 Water content and solid content of cement-treated MFT samples

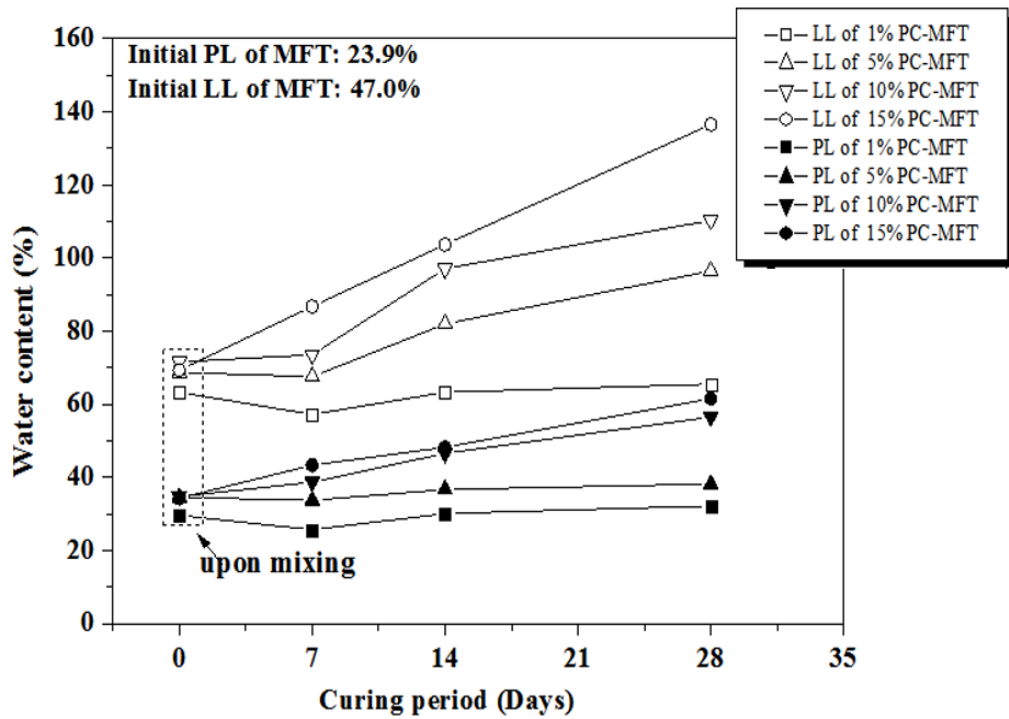


Fig. 4.5 Atterberg limits of cement-treated MFT samples

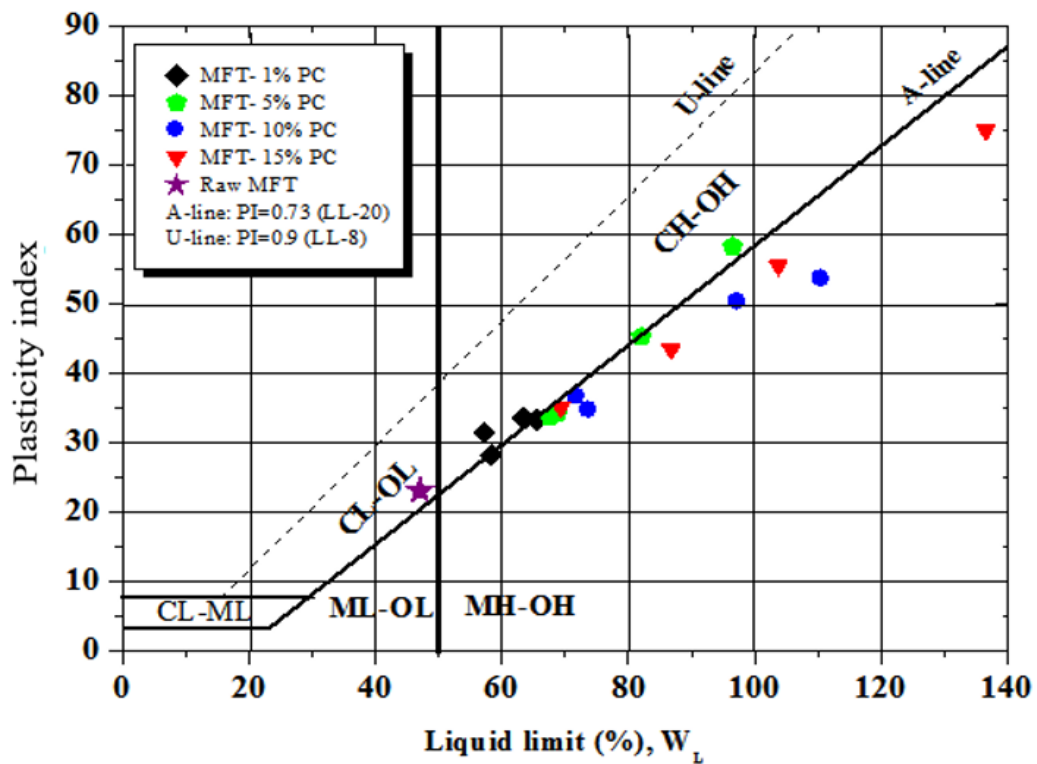


Fig. 4.6 Casagrande plasticity chart

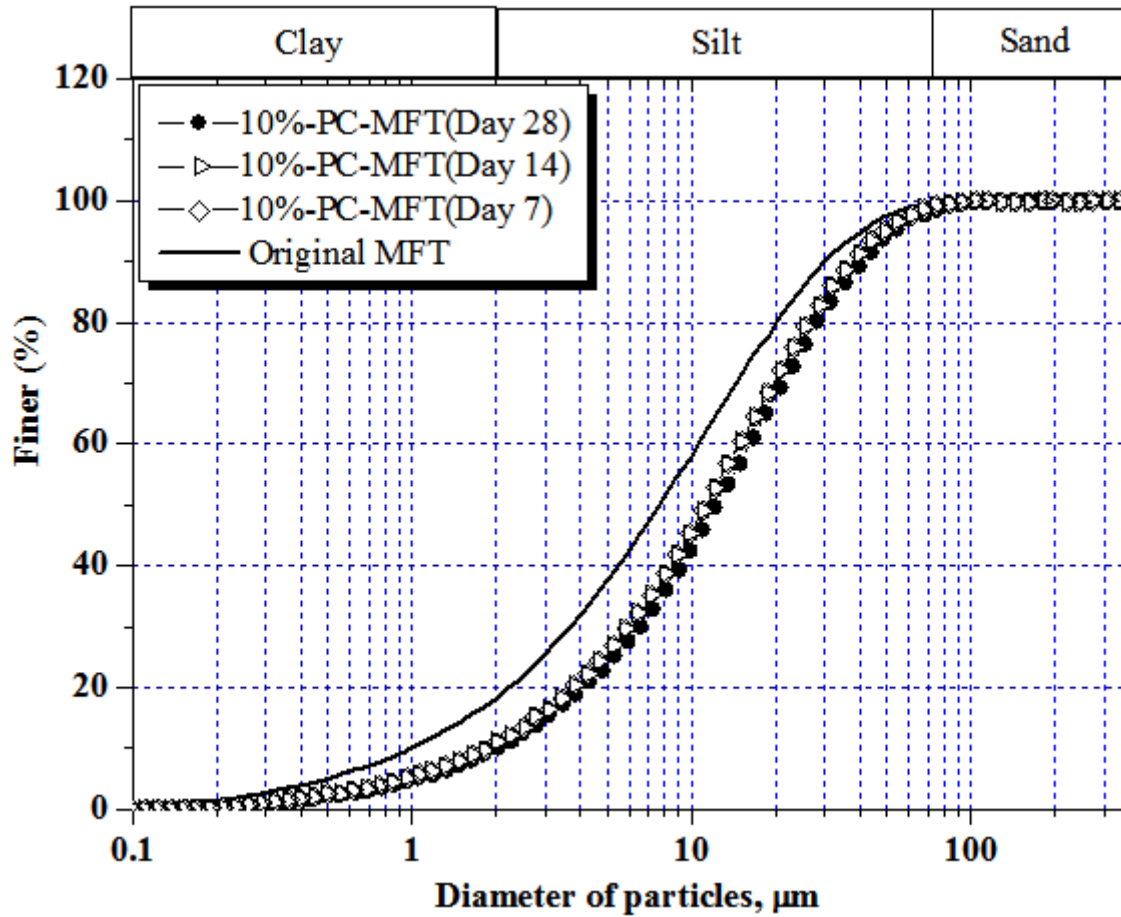


Fig. 4.7 Effect of curing time on particle size distribution curves of 10%-PC-MFT sample (measured from laser BT-9300S)

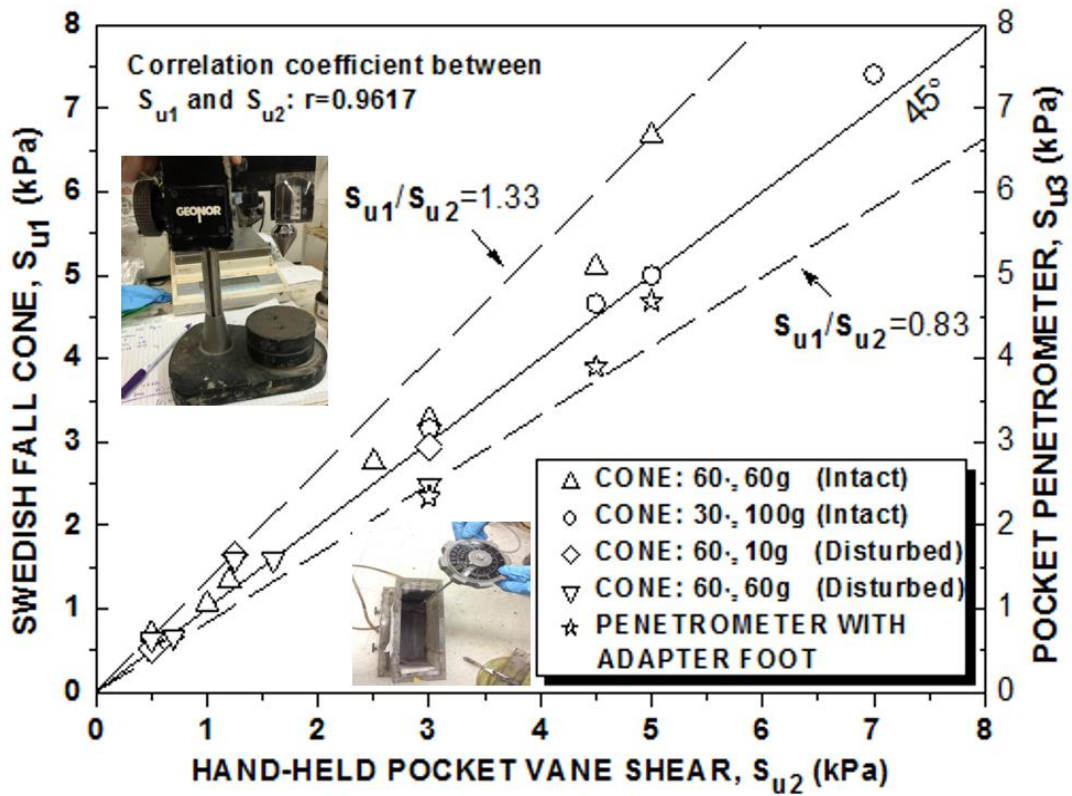


Fig. 4.8 Correlation between falling cone, pocket penetrometer and laboratory shear vane tests

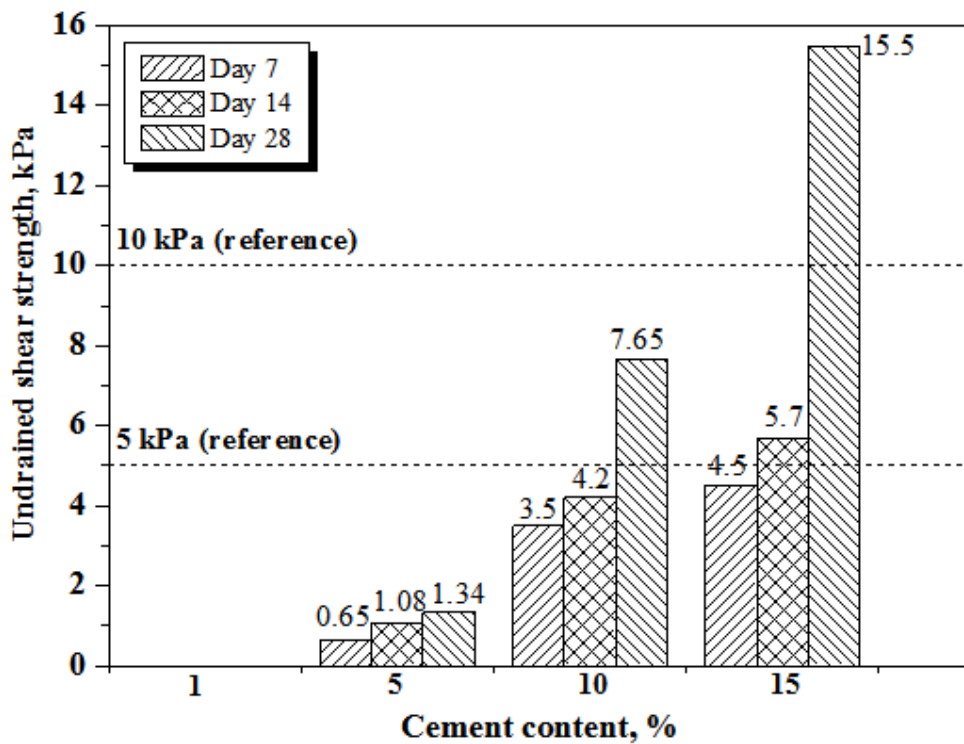


Fig. 4.9 Undrained shear strength of cement-treated Oil sands MFT

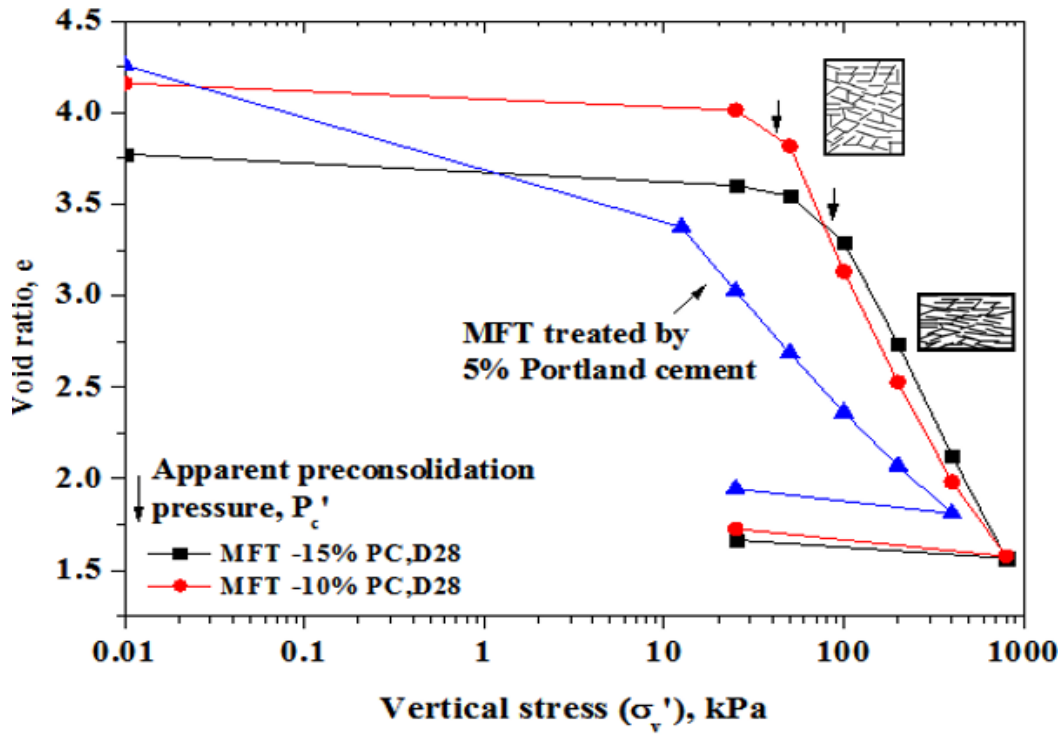


Fig. 4.10 1-D consolidation curves of cement-treated MFT after 28 days

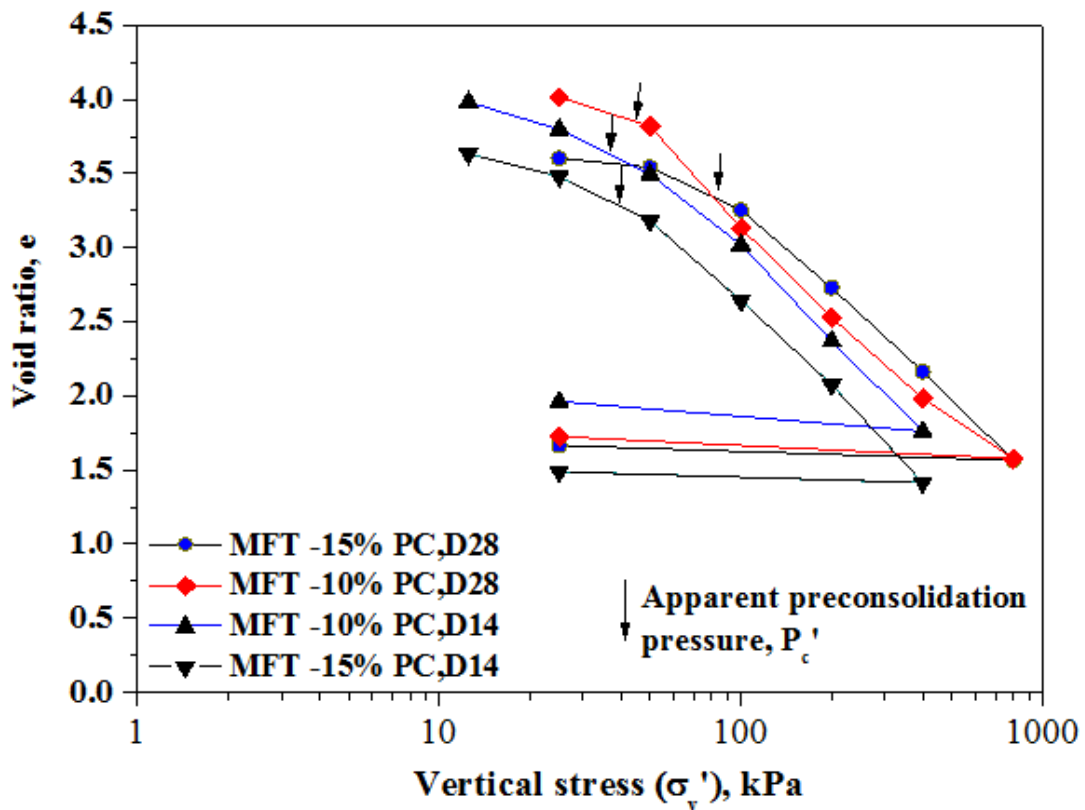


Fig. 4.11 1-D consolidation curves of cement-treated MFT after 14, 28 days

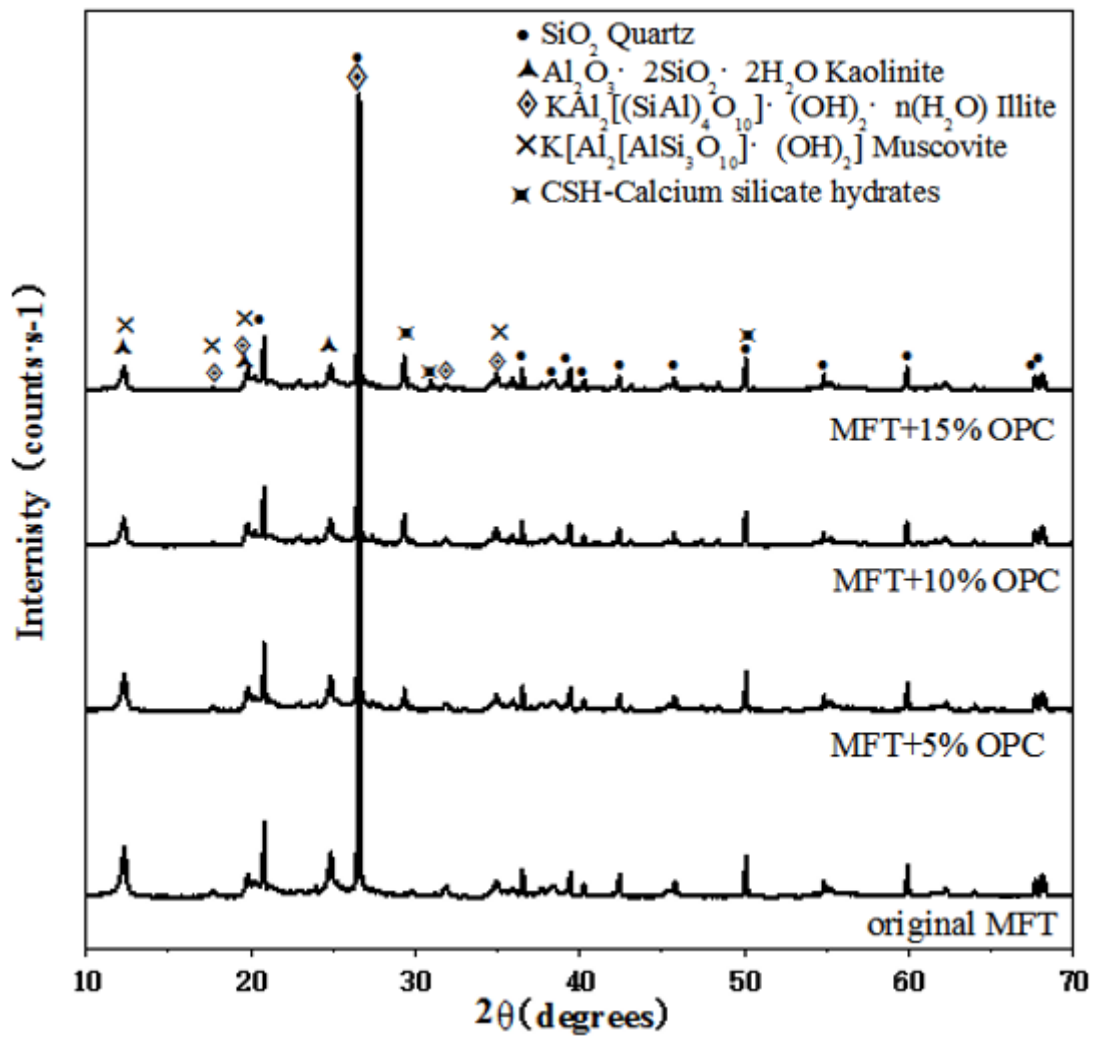


Fig. 4.12 XRD patterns of original and cement-treated MFT samples after 28 days



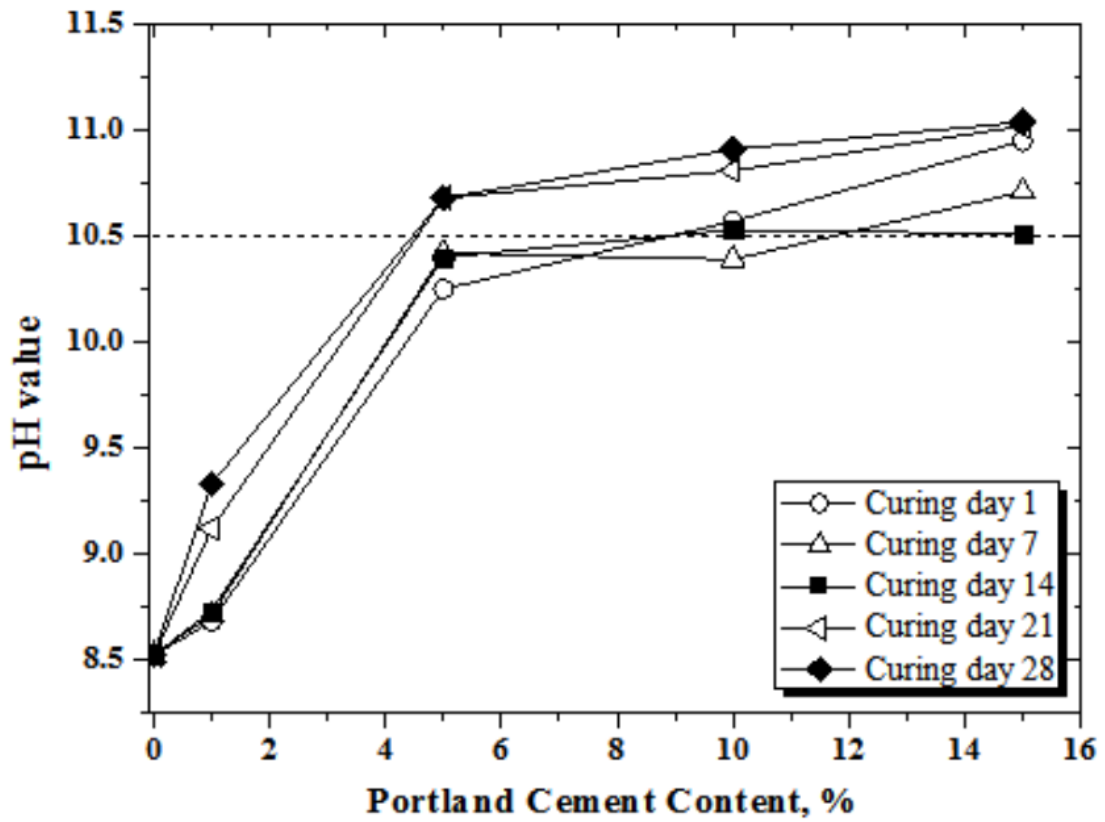
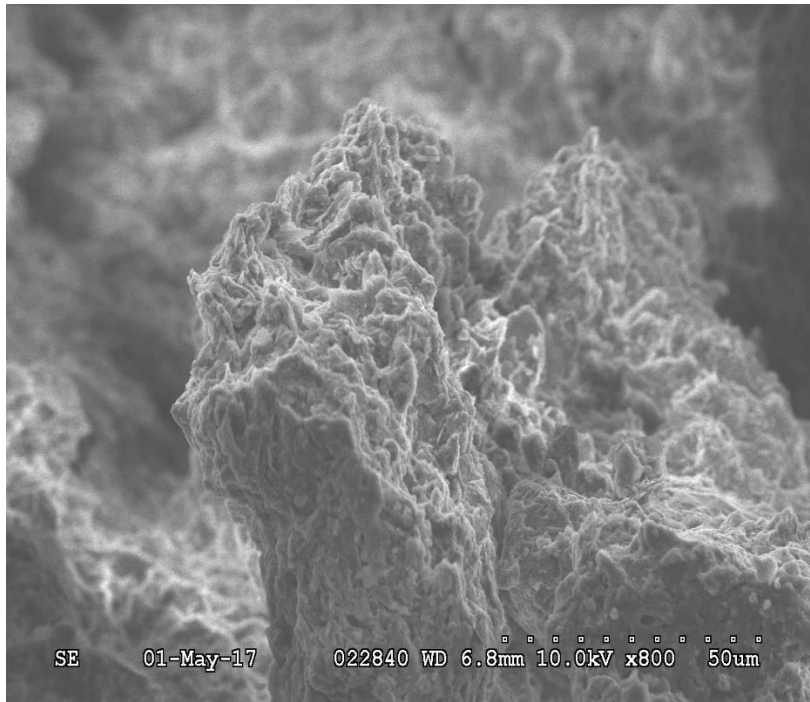
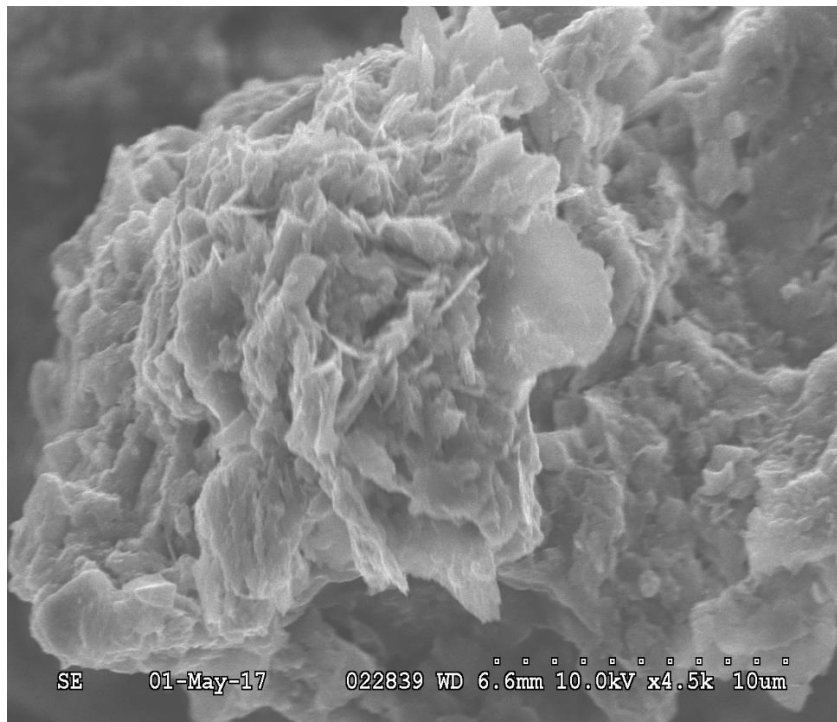


Fig. 4.13 pH of cement-treated MFT samples at various curing periods





(a): 800



(b): 4,500x

**Fig. 4. 14 SEM photos of 10% PC-stabilized MFT sample after 28-day curing,**

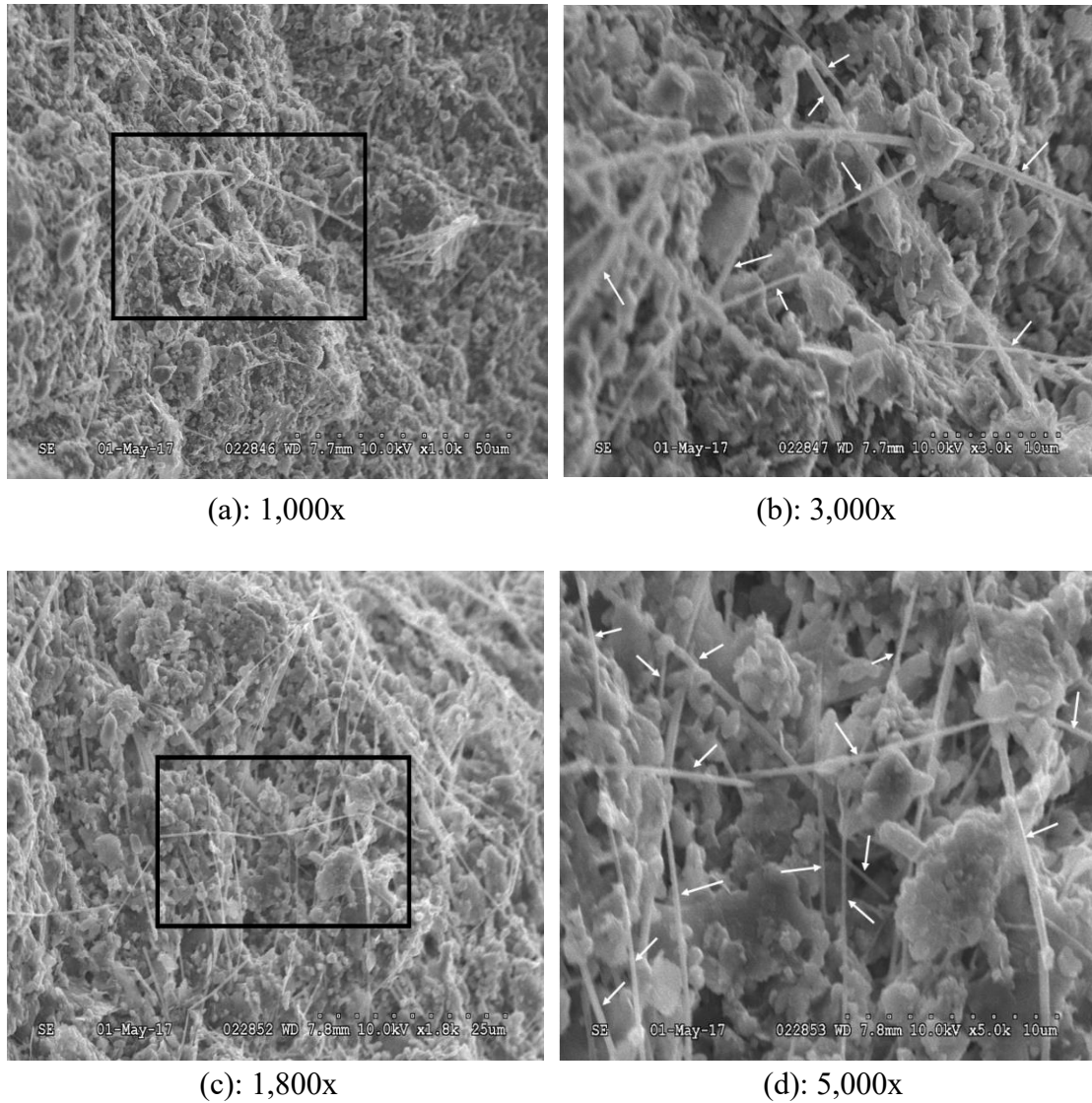


**Fig. 4.15 SEM photos of 10% PC-stabilized MFT sample after 28-day curing, (the black rectangular in figure (a) and (c) mark the zoomed-in areas in figure (b) and (d); the while arrows label the fibrous C-S-H morphology)**

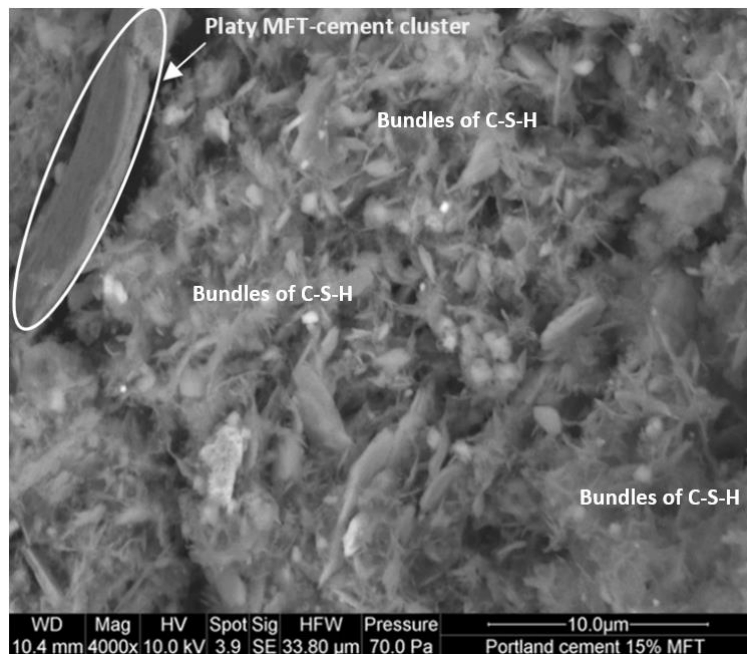
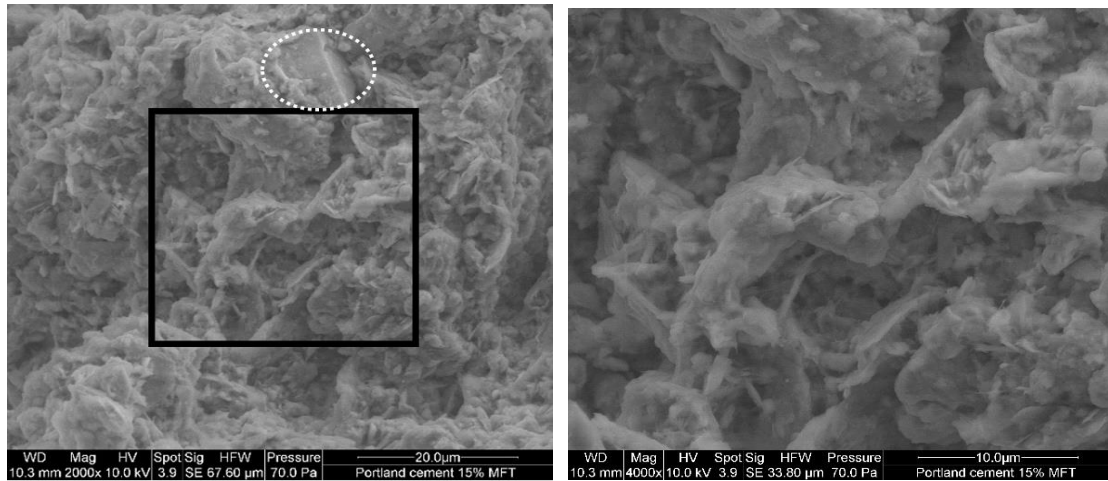
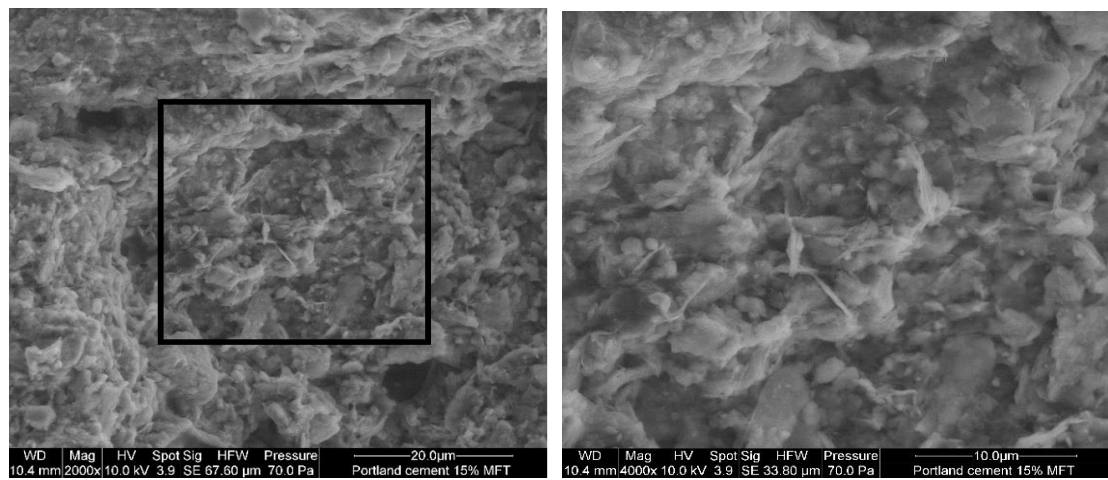


**Fig. 4.16 SEM photos of 15% PC-stabilized MFT sample after 28-day curing, (4,000x; the white circle in figure mark the MFT-cement cluster)**



(a): 2,000x

(b): 4,000x



(c): 2,000x

(d): 4,000x

**Fig. 4.17 SEM photos of 15% PC-stabilized MFT sample after 7-day curing (the black rectangular in figure (a) and (c) mark the zoomed-in areas in figure (b) and (d); the white circle in figure (b) mark Quartz mineral);**

## References

**ASTM 2435/D2435M-11.** Standard Test Methods for One-dimensional Consolidation Properties of Soils Using Incremental Loading, ASTM International, West Conshohocken, PA, 2011, DOI: 10.1520/D2435\_D2435M-11.

**Ahmed A, El Nagggar MH. (2016)** “Swelling and geo-environmental properties of bentonite treated with recycled bassanite”. *Applied Clay Science*, 121: 95-102.

**Belem T., Benzaazoua M. 2004.** An overview on the use of paste backfill technology as a ground support method in cut-and-fill mines. Proceedings of the 5th Int. Symp. on Ground support in Mining and Underground Construction. Villaescusa & Potvin (eds.), 28-30 September 2004, Perth, Western Australia, Australia, Tayler & Francis Group, London, pp. 637 – 650.

**Bhuria, N. R. & Sachan, A. (2014).** Shear strength and constant rate of strain consolidation behavior of cement-treated slurry-consolidated soft soil, *Current Science*, Vol. 106, No. 7, pp. 972- 979.

**Bhuvaneshwari, S., Robinson, R. G., & Gandhi, S. R. (2014).** Behaviour of lime treated cured expansive soil composites. *Indian Geotechnical Journal*, 44(3), 278-293.

**Boxill L.E, (2016).** The impact of fabric and surface characteristics on the engineering behavior of polymer-amended mature fine tailings Ph.D thesis. The University of British Columbia, Canada.

**Chen, R., Zhang, L., & Budhu, M. (2013).** Biopolymer stabilization of mine tailings. *Journal of geotechnical and geoenvironmental engineering*, 139(10), 1802-1807.

**Chew SH, Kamruzzaman HM, Lee FH (2001).** “Strength and Deformation Characteristics of Cement Treated Marine Clay” *Geotechnical Engineering: Meeting Society's Needs: Proceedings of the Fourteenth Southeast Asian Geotechnical Conference*, Hong Kong, 10-14 December 2001, Volume 1, 285-290.

**Chew SH, Kamruzzaman HM, Lee FH (2004).** Physicochemical and engineering behaviour of cement treated clays. *J Geotech Geoenviron Eng* 130(7):696–706

**Consoli, N.C., Rosa, D.A., Cruz, R.C., Rosa, A.D., 2011.** Water content, porosity and cement content as parameters controlling strength of artificially cemented silty soil. *Eng. Geol.* 122 (3–4), 328–333.

**Dash, S.K., and Hussain, M. (2011)** “Lime stabilization of soils: Reappraisal,” *Journal of Materials in Civil Engineering*, Vol.24, No.6, pp.707-714.

**Davidson, L. K., Demirel, T. and Handy, R. I., 1965.** Soil Pulverization and Lime Migration in Soil Lime Stabilisation. *Highway Research Record.* 92, 103-126

**Dimitrova, R.S., and Yanful, E.K. 2011.** “Undrained Strength of Deposited Mine Tailings Beds: Effect of Water Content, Effective Stress and Time of Consolidation.” *Geotechnical and Geological Engineering*, 29: 935-951

**Directive 074 (2009).** Tailings performance criteria and requirements for oil sands mining schemes, Energy Resources Conservation Board (ERCB), Alberta

**Ercikdi, B., Cihangir, F., Kesimal. A., Deveci, H. (2017)** “Practical Importance of Tailings for Cemented Paste Backfill” Chapter 2 in Book *Paste Tailings Management*, pp.7-32. DOI: 10.1007/978-3-319-39682-8\_2

**Fall, M., & Pokharel, M. (2010).** Coupled effects of sulphate and temperature on the strength development of cemented tailings backfills: Portland cement-paste backfill. *Cement and Concrete Composites*, 32(10), 819-828.

**Hassan M. M., Lojander M., and Ravaska O. 2008.** Characteristics of soft clay stabilized for construction purposes *Advances in Transportation Geotechnics.* 651-656

**Horpibulsuk, S., Miura, N., Bergado, D.T., 2004.** Undrained shear behavior of cement admixed clay at high water content. *J. Geotech. Geoenviron. Eng., ASCE* 130 (10), 1096–1105

**Hunter, D., 1988.** Lime-induced heave in sulfate-bearing clay soils. *J. Geotech. Eng.* 114 (2), 150–167

**Kamruzzaman, A.H.M., Chew, S.H. and Lee, F.H. (2006).** Microstructure of cement-treated Singapore marine clay. *Ground Improvement*, Vol. 10, No. 3, pp. 113-123

**Kamruzzaman, A.H.M., Chew, S.H., Lee, F.H., 2009.** Structuration and destructure behavior of cement-treated Singapore marine clay cement-treated Singapore marine clay. *J. Geotech. Geoenviron. Eng.* 135 (4), 573–589.

**Kumar, J.S. and Janewoo, U. (2016).** Stabilization of expansive soil with cement kiln dust and RBI grade 81 at subgrade level. *Geotechnical and Geological Engineering*, 34(4), pp.1037-1046.

**Liu, P and Shang J.Q. (2014).** Improvement of marine sediment by combined electrokinetic and chemical treatment, *International Journal of Offshore and Polar Engineering*, 24(3):232-240.

**Latifi, N., Marto, A., Eisazadeh, A., 2015.** Physicochemical behavior of tropical laterite soil stabilized with non-traditional additive. *Acta Geotech.* 1–11. <http://dx.doi.org/10.1007/s11440-015-0370-3>.

**Ma, C., Qin, Z. H., Zhuang, Y. C., Chen, L. Z., and Chen, B. (2015).** “Influence of sodium silicate and promoters on unconfined compressive strength of Portland cement-stabilized clay.” *Soils and Foundations*, Vol. 55, No. 5, pp. 1222-1232.

**Mengue, E., Mroueh, H., Lancelot, L., & Eko, R. M. (2017).** Physicochemical and consolidation properties of compacted lateritic soil treated with cement. *Soils and Foundations*, 57(1), 60-79.

**Mitchell, J.K. (1981).** “Soil Improvement-State of the art report.” *Proc., 10<sup>th</sup> Int. Conf. on Soil Mechanics and Foundation Engineering*, Vol.4, Balkema, The Netherlands, 509-565.

**Nalbantoglu Z, Tuncer E R. (2001).** Compressibility and hydraulic conductivity of a chemically treated expansive clay. *Canadian Geotechnical Journal*, 38 (1): 154–160.

**Pakbaz, M. S., & Alipour, R. (2012).** Influence of cement addition on the geotechnical properties of an Iranian clay. *Applied Clay Science*, 67, 1-4.

- Rajasekaran, G., Narasimha Rao, S., 2004.** Falling cone method to measure the strength of marine clays. *Ocean Engineering* 31, 1915–1927
- Rao SM, Shivananda P (2005) Compressibility behaviour of lime-stabilized clay.** *Geotech Geol Eng* 23(3): 309-319
- Sasanian, S., Newson, T.A., 2014.** Basic parameters governing the behaviour of cement-treated clays. *Soils Found.* 54 (2), 209–224.
- Tanaka, H., Hirabayashi, H., Matsuoka, T., Kaneko, H., 2012.** Use of fall cone test as measurement of shear strength for soft clay materials. *Soils Found.* 52, 590e599.
- Tariq, A., and Yanful, E. K. (2013).** "A review of binders used in cemented paste tailings for underground and surface disposal practices." *Journal of environmental management*, 131, 138-149.
- Wang, Y. H., and Siu, W. K. (2006).** Structure characteristics and mechanical properties of kaolinite soils. I. Surface charges and structural characterizations. *Canadian Geotechnical Journal*, 43, No.6, 587-600.
- Wasti, Y. & Bczirci, M. H. (1986).** Determination of the consistency limits of soils by the fall cone test. *Can. Ceo/echo J.* 23, No.2, 241-246.
- Zhang, T., Yue, X., Deng, Y., Zhang, D., & Liu, S. (2014).** Mechanical behaviour and micro-structure of cement-stabilised marine clay with a metakaolin agent. *Construction and Building Materials*, 73, 51-57.



# CHAPTER 5 STABILIZATION OF OIL SANDS MATURE FINE TAILINGS (MFT) BY SILICATE GROUTS

## 5.1 Introduction

Liquid silicates have been used in geotechnical applications for ground improvement. Grouting with sodium silicates is best suitable for sandy soils (Sherwood, 1961), whereas it may negatively affect clayey soils as clay particles become dispersed attributed to the increased negative charges on clay surfaces (Ding et al., 1996; Moayedi et al., 2011). In addition, sodium silicates have been reported to act as an alkali activator when blended with coal fly ash in preparing geopolymers (Pangdaeng et al., 2014).

Setting agents are added to trigger chemical reactions. To date, most studies on effects of silicate grouts on soil improvement were conducted using inorganic hardeners, such as lime (Maaitah, 2012), cement (Ma et al., 2015), and metal salts (e.g. calcium chloride). The research on using organic setting agents, which are considered more flexible in their gelling response (PQ Corporation, 2003), is limited.

In this study, soluble silicates are used in conjunction with organic setting agents for the treatment of MFT. The properties and working mechanisms of silicates have been introduced in chapter 2 (**Section 2.4.3.2-2.4.3.3**) in detail. The chemistry of silicates used in the study (NS and AAAS) has been described in chapter 3 (**Section 3.2.2**). This chapter is mainly devoted to present experimental results to study the influence of silicate dosages, and curing time on geotechnical properties of MFT. An experimental program was designed and carried out in three steps, i.e. firstly, to develop a mixing formula for MFT with specific gel times; secondly, to estimate the optimal amount of silicates required to improve MFT properties in terms of short-term strengthening and solidifying effects; and thirdly, to study the mechanisms of MFT stabilization by silicate grouts based on the microscopic analyses, including scanning electron microscope (SEM) and X-ray diffraction (XRD).

## 5.2 Experimental set up

### 5.2.1 Design consideration for testing program

Liquid silicates have high viscosity, whereas MFT has low permeability and high natural water content. In this study, silicate products are mixed with MFT in sample preparation. The commercially available silicates and setting agents, are in the form of solutions. The silicates are added into MFT with the natural water content by a syringe, without dilution. To compare with the results of cement stabilization, the short-term curing period is also prescribed to 28 days to allow for the completion of gel hardening process.

The experiments are divided into two groups based on the silicate usage: The high concentration group and low concentration group. The silicate concentration (content) is defined as the volume of silicate to the volume of grouts (v/v). The high concentration group tests (i.e. 30%, 40% and 50% for NS; 40%, 50%, 60% for AAAS) are started first according to an empirical formula (**Tables 5.1-5.2**). The formula recipes provide proportions of each components (i.e. tap water, silicates, setting agents) in the chemical grout, as well as their resulting gel times. The starting point of this formula is suggested by PQ Corporation, the manufacturer of the silicates used in the study and industrial partner of the project. Since the supernatant of MFT as received contains more cations compared to the tap water, the precipitation reactions induced by dissolved metal ions (e.g.,  $\text{Ca}^{2+}$ ) and silicate anions are much stronger. This may cause the actual time for the gel formation using the supernatant of MFT somewhat shorter than that by tap water. Therefore, the gel time of 4-5 hours by using tap water is selected. Then the ingredient proportions in the grout are followed.

In the second phase, the low concentration group tests (e.g., 3%, 5%, 8%, 10% for both NS and AAAS) are carried out, with the aim of determining the optimal dosages in the treatment of MFT. Each sample is assigned an ID and the overall program design is summarized in **Table 5.3**.

## 5.2.2 Sample preparation

In order to investigate the influence of silicate grouts on MFT, NS and AAAS with corresponding setting agents were mixed with MFT suspension under different volumetric ratios, as summarized in **Tables 5.4-5.5**. For preparing the samples, the chemicals were added through a two-step process. The predetermined quantity of setting agents (e.g. citric acid) was first added to the MFT by a pipette and mixed thoroughly by a miniature mixing machine (**Fig. 5.1(a)**). Subsequently, the predetermined amount of silicate solutions was added and stirred rapidly until a homogenous paste was formed. Then the mixture was transferred to plastic cylindrical molds and stored under room temperature for curing. After pre-set curing time, the samples were removed from the molds following a procedure similar to the cement stabilization described in Chapter 4.

The procedure of adding and mixing of the silicates is critical to the stabilization outcome. Silicates are viscous and difficult to mix homogeneously throughout the tailings slurry, especially for MFT samples mixed with high silicate contents. Hence, the mixing was carried out quickly and vigorously to prevent the partial gel accumulation in the vicinity of the impeller blades (**Fig. 5.1(b)**).

## 5.3 Results and discussion

With reference to **Table 3.2**, AAAS has a higher total solids content<sup>4</sup> of 45.7% (i.e. 16.2% Na<sub>2</sub>O, 27.9% SiO<sub>2</sub> and 1.6% Al<sub>2</sub>O<sub>3</sub>) than NS of 37.6% (i.e. 8.9% Na<sub>2</sub>O and 28.7% SiO<sub>2</sub>). AAAS has an additional crystallization process (autocatalysis) when diluted with water (**Section 3.2.2**). The chemical compositions of NS and AAAS play an important role in the resulting engineering behaviors of silicate-treated MFT samples.

### 5.3.1 Gel time

The gel time of the silicate grouts is defined as the interval between mixing of the

---

<sup>4</sup> Total solids content (%)=The weight ratio of the total active ingredients dissolved in silicate solution to the silicate solution.

chemicals and formation of the silica gel. **Fig. 5.2 (a)** and **Fig. 5.3 (a)** present the gel times of NS grouts and AAAS grouts, respectively. When the gel time was fixed (either 1-2hr, 3hr or 4-5hr), the concentration ratio of silicate solutions to the setting agent was nearly constant ( $R^2$  is close to 1.0). Also, the figures indicate that the gel formation was delayed in solutions of higher silicate concentrations with the same amount of setting agent. **Fig. 5.2 (b)** and **Fig. 5.3 (b)**. It is observed that when the silicate concentration level was maintained the same, the gel time was reduced by increasing the concentration of setting agents. The setting agent (i.e. Propylene carbonate) was not needed when the AAAS concentration was lower than 40%, as AAAS formed gel just by adding water. On the other hand, NS required a large amount of setting agent (i.e. citric acid solution) to complete the transition, and 50% of NS was found to be the threshold concentration in practice. When the concentration of NS exceeds 50%, the gel time less than 5 hours cannot be controlled, as the process of gel formation is extremely rapid.

### **5.3.2 Water content and Solid content**

As mentioned earlier, the initial water content (W%) and solid content (S%) of the MFT samples were adjusted to 185% and 35%, respectively. The results of W% and S% for NS- and AAAS-treated MFT samples at 7, 14 and 28 days are plotted versus the silicate concentration in **Fig. 5.4** and **Fig. 5.5**, respectively. As expected, after treatment the water content of MFT samples decreased as silicate concentration raised. For example, after 28 days, 10%-NS-MFT sample exhibited a water content of 170% and a solid content of 37.02%, whereas 10%-AAAS-MFT sample showed a lower water content of 144.2% and a higher solid content 40.95%. The difference in W% or S% between two silicates treated MFT samples became more noticeable when the silicate concentration went up to 40% or higher. As indicated earlier, AAAS has a higher density ( $1.6 \text{ g/cm}^3$ ) and inherent solid content of 45.7% than NS, and gel formation can be triggered just by water. In the experiments, adding setting agent solution increased the water content of MFT samples upon mixing, and this was believed to be the main

reason behind the fact that at the same silicate concentration level, the dewatering/solidification effect on MFT using two silicates products were not the same.

The most significant increase in the solid content was registered in 60%-AAAS-MFT sample at the end of the 28 days, where the sample achieved nearly 50% solid content (i.e. 49.24%). It is noted that after 7-day curing, the solid content of the sample has reached up to 48.22%. This indicated that the increase in the solid content was near completion within 7 days. This observation is consistent with other NS-treated MFT samples with varying silicate concentrations, including 10%- and 50%-NS-MFT samples, as shown in **Fig. 5.4 (b)**.

### **5.3.3 Strength properties**

#### **5.3.3.1 Undisturbed undrained shear strength**

The effects of silicate concentrations and aging on the undrained shear strength ( $S_u$ ) development of MFT are shown in **Fig. 5.6** and **Fig. 5.7**, respectively. **Fig. 5.6** reveals that the  $S_u$  of MFT samples increased with the increasing NS and AAAS concentrations. It is also noted that for NS-treated MFT samples, at least 5% of silicate concentration was needed to cause a strength increase. After 28 days, the  $S_u$  of 10%- and 15%-NS-MFT samples reached 4.83 and 7.55 kPa, while the specimens treated with 5% and 8% AAAS reached 4.8 and 5.5 kPa of  $S_u$ , respectively. These data suggested that, the undrained shear strength of 5 kPa, a one-year minimum requirement for the MFT treatment (Directive 074 (2009)), was achieved in a short duration (28 days) by adding 15% NS or 8% AAAS. In addition, as shown in **Fig. 5.6**, all MFT samples treated under high silicate contents showed a strength gain in excess of 10 kPa. For example, at curing period of 7 days, 40%-NS-MFT sample and 40%-AAAS-MFT sample exhibited a significant strength gain of 39.2 kPa and 28.6 kPa, respectively. It should be mentioned that 10 kPa shear strength was five-year criterion of MFT depositions regulated by Directive 074 (2009). **Fig. 5.6** also shows the trend lines of the shear strength data for all treated MFT samples in the concentration range tested.

Furthermore, as illustrated in **Fig. 5.7**, for all MFT samples with low concentrations (i.e. 3%-10% for NS and AAAS), the undrained shear strength exhibited an initial increase at first 7 days of curing but did not further increase with time. This was consistent with the solid content results shown before, indicating that most reactions between MFT and silicate solutions completed within 7 days. For MFT samples treated by high concentration (e.g. 30-50%) NS solutions, a sharp strength increase in the second curing period (7 to 14 days) and then a relatively slow increase at the later stage between 14 days and 28 days were observed. On the other hand, for MFT samples treated by high concentration (e.g. 40-60%) of AAAS solutions, the strength gain was nearly completed after 7 days, as shown in **Fig. 5.7**. This suggested that the strength development of AAAS-treated MFT samples was more rapid than the NS-treated samples at high silicate concentrations.

### 5.3.3.2 Remolded undrained shear strength and sensitivity

The remolded undrained shear strength ( $S_{ur}$ ) of the stabilized MFT samples was measured by fall cone immediately after the measurement of undisturbed shear strength. **Fig. 5.8 and Fig. 5.9** present the  $S_{ur}$  results of NS- and AAAS-treated MFT samples, respectively. It is observed that, the remolded strength of AAAS-treated MFT was slightly higher than that of the NS-treated samples at the low silicate concentrations, e.g., 1.58 kPa and 2.43 kPa for 8%-NS-MFT sample and 8%-AAAS-MFT sample at 28 days of curing, respectively. It should be also noted that 3%- and 5%-NS-MFT samples, as well as 3%-AAAS-MFT sample virtually had no measurable remolded shear strength ( $S_{ur}$ ), as shown in **Figs. 5.8 and 5.9**.

The sensitivity ( $S_t$ ) describes the effect of the disturbance on the undrained shear strength ( $S_u$ ). The sensitivity can be quantitatively determined using the equation (Terzaghi, 1944):

$$S_t = \frac{S_u}{S_{ur}} \quad (5.1)$$

Where  $S_t$  is the sensitivity,  $S_u$  is the undisturbed undrained shear strength,  $S_{ur}$  is the

remolded undrained shear strength.

**Figs. 5.10-5.11 and Table 5.6** presents the sensitivity results of the silicate-treated MFT samples. As shown, the sensitivity of all MFT samples treated by low silicate concentration solutions varies in the range of 1 to 4. However, there was a significant increase in sensitivity values ( $S_t=4-16$ ) on samples treated with high silicate concentrations (e.g. 50% for NS and AAAS). In general, the sensitivity of AAAS-treated MFT samples was lower than that of NS-treated MFT samples on the same silicate concentration level.

Many factors can contribute to the low remolded strength and sensitive nature of cemented clays and other geomaterials, including the cementation bond (e.g., **Fig. 5.24(e)**), high water content (i.e., **Fig. 5.4(a)**), increased zeta potential (i.e., **Fig. 5.20**), ion exchange and addition of dispersing agent (Boone and Lutenegeger, 1997; Mitchell and Soga, 2005). Furthermore, Beier et al., (2013) summarized the available field data provided by Shell Canada Energy and indicated that, chemically amended MFT samples generally exhibited sensitive and metastable behavior, and thus after chemical treatment further consolidation and dewatering were generally required to achieve a higher degree of densification of the treated MFT samples.

### **5.3.4 Index Properties**

#### **5.3.4.1 Atterberg limit**

The effects of NS (5%, 10% and 15%) and AAAS (3%, 5% and 10%) additions on the index properties of the treated MFT samples at 7, 14, and 28 days are plotted in **Figs. 5.12-5.13**, respectively. The details of the data including the liquidity index are listed in **Table 5.7**. **Fig. 5.12** shows a steady increase in both liquid limit (LL) and plastic limit (PL) of NS-treated MFT samples at increasing silicate contents and curing time. The LL of the NS-treated MFT samples varied from 116 to 174.4% and notably attained a peak value (174.4%) at 28 days in 15%-NS-MFT sample. The similar increasing trend is also observed in AAAS-treated MFT samples, as shown in **Fig. 5.13**. For example,

the LL of 3 %-AAAS-MFT sample increased rapidly to 95.5% after 7 days and continuously increased with curing time, eventually reached up to 123.5% at 28 days. However, under the same conditions (i.e., curing time, silicate content), the magnitude of the LL increase in AAAS-treated MFT samples was found to be lower than that of NS-treated MFT samples. It is believed that the increase in LL in all silicate-treated MFT samples was associated with changes in the geometric arrangement of particles due to the presence of cementing agents, i.e., silica gels (e.g., **Figs. 5.24(b) and (c)**), and entrapped water in pore spaces between flocculated (edge-to-edge) particles (**Fig. 5.24(e)**) (Sridharan 1988, 1991; Chew et al., 2004).

Changes in the PL of MFT samples during curing period of 28 days are also presented in **Figs. 5.12-5.13**. With a rather low (5%) NS concentration, the PL of MFT samples obviously increased, starting from 23.9% (natural state) to 38.4% after 7 days and peaking at 43.6% after 28 days. The rate of the PL increase is observed to be nearly constant with increasing NS concentrations. It is noted that after 28 days, the PL of 15%-NS-MFT sample reached 77.4%, and this was approximately two times greater than that of the untreated MFT sample. However, the PL of AAAS-treated MFT samples showed marginal changes with elevating AAAS concentrations.

It is noted that MFT samples treated by high concentration silicates (e.g., 40% NS, AAAS solutions) became rather brittle due to the presence of excess hardened gels, thus the measurement of liquid limit could not be done (**Fig. 5.14**). The measurement of the plastic limits (**Fig. 5.15**) was also unsuccessful due to operational difficulties caused by the high viscosity of the MFT paste.

#### **5.3.4.2 Plasticity**

**Fig. 5.16** shows the Casagrande plasticity chart containing LL and plasticity index (PI) data of the silicate-treated MFT samples. It is found that, the points of AAAS-treated MFT samples on the chart moved upwards over the A-line, while for the NS-treated MFT samples, the points shifted below the A-line. This indicated that MFT samples typically behaved as inorganic silts of high plasticity (MH) after NS treatment, while



the MFT samples treated by AAAS behaved as inorganic clays of high plasticity (CH).

### 5.3.5 Water chemistry

**Figs. 5.17 (a) and (b)** show the electrical conductivity (EC) of the extracted pore water from NS- and AAAS-treated MFT samples, respectively. In general, the EC increased with silicate content and curing time. Note that after 28 days the decrease of EC in MFT samples treated by 10% silicates (NS and AAAS) was possibly due to a measurement error. As shown, at the lower silicate concentration range (5%-10%), the AAAS-treated MFT samples have higher EC than those NS-treated MFT samples. For example, on addition of 5% silicates, the ECs of NS-treated MFT samples were 2.71 mS/cm at 7 days and 3.01 mS/cm at 28 days, while the ECs of AAAS-treated MFT samples were 2.99 mS/cm at 7 days and 7.52 mS/cm at 28 days, respectively. The difference was more evident when the silicate contents increased to 40%, suggesting higher concentrations of dissolved cations in the AAAS-treated MFT solutions. As expected, the pH of MFT increased by mixing with alkaline silicates solutions, as illustrated in **Figs. 5.18 (a) and (b)**. However, in the cases of low silicate contents (i.e. 5%-10%), there was not significant difference observed between the effects of NS and AAAS on increasing the pH of MFT samples, and the pH values varied within a narrow range from 10 to 11. While as silicate concentration grew up to 40%, the pH of AAAS-treated MFT samples were clearly higher than the pH of NS-treated MFT samples.

Moreover, significant sample shrinkage was observed from the MFT samples treated with high concentration of NS (i.e. 30%-50%). As seen in **Fig. 5.19**, the volume of decanted liquid after sample shrinkage increased with an extension of curing time and an increase in the NS concentration. It is noted that, after 28 days, the 50%-NS-MFT sample had the largest volume reduction of nearly 50%. This was believed to be associated with the silica gel syneresis (see **Section 2.4.3.2, Section 3.2.2 and Fig. 3.6**). However, syneresis was not observed in AAAS-treated MFT samples throughout the experimental program.

**Table 5.8** summarizes the experimental results of the supernatant chemistry, including pH, EC and turbidity. The results indicate that, after chemical grouting, the collected supernatant was more basic (pH in the range of 10 to 11) and saline (EC in the range of 35 to 39 mS/cm) compared to the supernatant of initial tailings (pH=8.52, EC=1.46 mS/cm). Also, it is found that the supernatant of 50%-NS-MFT sample was clearer (e.g., 69.7 NTU at 28 day) than that of 30%-NS-MFT sample (e.g., 109.6 NTU at 28 day) and 40%-NS-MFT sample (e.g., 89.4 NTU at 28 day).

### 5.3.6 Zeta potential

The Zeta potential (ZP) measurements were carried out on the silicate-treated MFT samples after the curing time of 28 days, to establish the surface electrical characteristics of stabilized samples. The variations in ZP for the MFT samples treated by 5% and 10% silicates, as well as that for the original MFT sample, are presented in **Fig. 5.20**. As shown, the natural pH of MFT is 8.52 and the zeta potential is -38mV. After addition of silicate grouts, the magnitude of zeta potential for MFT samples increased (became more negative). For example, 10%-NS-MFT sample showed -44.5 mV of ZP (at pH=10.16), while 10%-AAAS-MFT sample showed -51.24 mV of ZP (at pH=10.88). It is well recognized that the sodium concentration increase contributed to ZP increase in soils containing Kaolinite minerals (Kaya and Yukselen, 2005). Suganya and Sivapullaiah (2016) reported that the negatively charged silicate ions that adsorbed on positive charge sites (edges) of clay minerals, enhanced the ZP of solid particles, and as a result, the net electrostatic repulsion forces of particles led to a dispersed fabric of soil. This notion can be evidenced by SEM images shown in **Section 5.3.8**.

### 5.3.7 XRD analysis (Mineralogy)

X-ray diffraction analysis was employed to determine whether silicate treatment caused alternations in clay mineralogy of MFT samples. Typical 28-day XRD patterns for the stabilized MFT samples at NS concentrations of 5%, 10% and 40% are presented in

**Fig. 5.21**, along with the untreated MFT sample for comparison. As shown, the quartz peaks were significant in the pattern, indicating that quartz was the dominant non-clay mineral in MFT. No significant changes of quartz ( $\text{SiO}_2$ ) spectra in 5%- and 10%-NS-MFT samples were observed compared to the original sample. The decrease in the intensity of  $\text{SiO}_2$  peaks, such as quartz plane (100) at  $2\theta$  of  $20.82^\circ$  and (101) at  $2\theta$  of  $26.6^\circ$ , was noticed in 40%-NS-MFT sample. Since the NS solution contains silica, it was difficult to evaluate the effects of silicate stabilization to quartz crystals in MFT. In addition, though the XRD pattern of 5%-NS-MFT sample exhibited very little difference with that of the original sample, some reflections of clay minerals, e.g., Kaolinite (001) and (002) in 10%- and 40%-NS-MFT samples were weaker, and peaks of illite (002) and (004) almost disappeared in this alkaline environment ( $\text{pH} > 10.5$ ). The results suggested that the interactions of NS solution with MFT solids occurred and the mechanism of these changes should be further investigated.

As shown in **Fig. 5.22**, the peak intensities of clay minerals in MFT samples slightly reduced after mixing with AAAS solutions. **Fig. 5.23** combined the XRD patterns of original MFT and MFT samples treated by 5% silicates (NS and AAAS). After treatment, the peak intensities of Kaolinite (001) and (002), Illite (002) in 5%-AAAS-MFT sample were more significant than those in 5%-NS-MFT. This comparison suggested that at the same concentration level, AAAS solutions were more active than the NS solutions in engaging in the chemical reactions with MFT solid particles.

Furthermore, it is found that for silicate treated MFT samples, no new peaks in XRD patterns are observed, which is a distinguished difference to the XRD results of MFT samples treated by Portland cement as discussed in Chapter 4. This is presumably due to the amorphous nature (gel-form) of the resulting reaction products from silicate grouts (Tingle et al., 2007; Latifi et al., 2014).

### **5.3.8 SEM imaging (Morphology)**

**Figs. 5.24 (a)-(e)** provide the SEM photos of the MFT samples mixed with 5%, 10%

and 40% NS and AAAS at curing age of 28 days. The micro fabrics are characterized at a magnification of 2000x at 10kV. As shown in **Fig. 5.24 (a)**, MFT treated by 5% NS exhibited a fairly open microstructure, with the solid particles assembled in a random orientation. The particles were slightly flocculated with a rosette-like morphology, and the pores were visible in the micrographs. On the other hand, less distinct pores and relatively denser matrix were observed in 5%-AAAS-MFT sample, as shown in **Fig. 5.24 (b)**. It appears that discrete particles were covered by gel-like amorphous substances, giving rise to the hazy patches around solid particles. After detailed examination of **Fig. 5.24 (c)**, it is observed that the flocculation of fabric was more evident than that in **Fig. 5.24 (a)**, as a result of an increase in NS concentration (10%). In **Fig. 5.24 (d)**, solid particles were significantly coated by gelling products, forming larger clusters. Therefore, a more compact microstructure was observed, compared to **Fig. 5.24 (b)**.

**Fig. 5.24 (e)** exhibits a distinct interlocking network structure on the MFT sample after 40% NS treatment. The NS gels formed the chemical crosslinks between solid particles with some sign of reticulation, and hence the microstructure of the entire NS-treated MFT sample emerged as a crusty web. In addition, salt precipitation (mostly sodium and calcium) at contacts between particles was captured as white spots in **Fig. 5.24 (e)** (Roshani et al., 2017). In contrast, solid particles in the 40%-AAAS-MFT sample were well-bonded together in a packet fabric, as observed in **Fig. 5.24 (f)**. The AAAS gel appeared to have irregular and vague outlines, and the pores of the specimen are less visible in comparison with **Fig. 5.24 (e)**. This suggested that AAAS gel had better space-filling effects than NS gel. In the former case, the gelling products formed by the chemical reactions filled the porous areas inside the mixture, leading to a stronger aggregate of particles and a denser microstructure.

Comparing the SEM images between the original (**Fig. 3.3**) and solidified (**Fig. 5.24**) MFT samples, it is observed that the surface morphology of original MFT was modified through silicate treatments. In **Figs. 5.24 (a)(c)(e) and (b)(d)(f)**, the gelling products became readily apparent as the silicate concentration increases, exhibiting as the small

irregular lumps or roughly undulating shapes. The NS gel (especially in **Fig. 5.24 (e)**) connected the solid particles, while AAAS gel (especially in **Fig. 5.24 (f)**) encapsulated the particles and filled the gaps. This results in a flocculated microstructure of MFT. Hence, the mechanical properties (e.g. shear strength) of MFT are improved. Furthermore, **Figs. 5.25 (a)** and **(b)** show the SEM configuration of 10%-NS-MFT sample and 10%-AAAS-MFT sample consolidated under 5 kPa. In **Fig. 5.25 (a)**, the individual particles were discernible with their angular edges, whereas in **Fig. 5.25 (b)**, the particles were still cemented together by silicate grouts.

## **5.4 Practical implications**

The use of silicates is aimed to increase the shear strength and solid content of MFT. The test results presented in this chapter show that a relatively small amount (e.g. 8% and 10% concentrations) of silicates can generate the shear strength gain within 28 days, suggesting that silicate treatment is an alternative solution for the strengthening of MFT in short time. On the other hand, due to the high viscosity of the silicate products, the treatment requires large-scale equipment for mixing and dosage control system. It should be noted that the predominant effect of silicate treatment of MFT is the strength gain, whereas the reduction of water content is secondary.

## **5.5 Summary**

The influence of silicate type, concentration and curing period on mechanical and physicochemical properties of MFT are presented in this chapter. In general, the undrained shear strength, Atterberg limits, plasticity index, solid content, zeta potential of the silicate-stabilized MFT samples increase with silicate concentrations and curing time. The undrained shear strength and water content data indicate the rapid reactions between MFT and silicates taking place within 7 days. The factors controlling gel time of the silicate grouts are also discussed. With the aid of SEM, the cementing morphology in silicate-stabilized MFT samples is qualitatively investigated. Based on

the study, the following conclusions are drawn:

- After 28 days, a required undrained shear strength value (5 kPa) can be achieved by adding 15% NS (7.55 kPa) and 8% AAAS (5.5kPa), respectively. To achieve equivalent shear strengths of MFT, a lower content of AAAS is needed relative to NS. The sensitivity of NS-treated MFT samples is higher than that of AAAS-treated MFT samples.
- AAAS is more effective than NS in increasing the solid content of MFT at same curing period. The most significant increase in solid content (49.24%) is registered in the MFT sample treated by 60% AAAS at 28 days.
- The liquid limit (LL) and plastic limit (PL) of MFT samples increase after silicate treatment. In general, the magnitude of the LL increase in AAAS-treated MFT samples is lower than that of NS-treated MFT samples. All measured liquid limits exceed a value of 95%, and the increasing trend in LL is more significant than in PL, leading to an increase in plasticity index (PI).
- The use of silicates increases the pH and electrical conductivity (EC) of MFT pore fluid. At the low silicate concentration level (5%-10%), there is no significant difference between NS- and AAAS- treated MFT samples in terms of pH and EC results. However, MFT sample treated by AAAS has a much higher pH and EC than the MFT sample treated by NS, at the silicate concentration of 40%.
- The volume of MFT samples treated by high concentrations of NS reduces with time, i.e., supernatant liquid is released from the specimen. However, the volume of AAAS-treated MFT samples remain almost the same during the curing process.
- For silicate-stabilized MFT samples, the gel-like substances play an important role in binding the detached particles and filling the voids, rendering a dense microstructure responsible for a higher undrained shear strength of MFT sample. AAAS-treated MFT samples have a much denser structure than NS-treated MFT specimens, showing a greater number of fine particle aggregates.
- The XRD patterns show no trace of new crystalline phases for all NS- and AAAS-

treated MFT samples, but reveal the suppression of the existing minerals due to the stabilizer effect, i.e., reactions between silicate additives and active minerals in MFT.

**Table 5.1 Grouting formula for TYPE N sodium silicate (NS)**

Gel time: 4-5hr						
Component A(ml)		Component B(ml)		%silicate <sup>1</sup>	% CA <sup>2</sup>	Gel time
N silicate	Tap water	Citric acid	Tap water			
20	26	20	34	<b>20</b>	<b>20</b>	<b>4-5 hr</b>
25	25	22	28	<b>25</b>	<b>22</b>	
30	30	25	15	<b>30</b>	<b>25</b>	
35	20	27	18	<b>35</b>	<b>27</b>	
40	20	30	10	<b>40</b>	<b>30</b>	
45	11	34	10	<b>45</b>	<b>34</b>	
50	7	36.6	6.4	<b>50</b>	<b>36.6</b>	
Gel time:3hr						
Component A(ml)		Component B(ml)		%silicate <sup>1</sup>	% CA <sup>2</sup>	Gel time
N silicate	Tap water	Citric acid	Tap water			
20	26	21	33	<b>20</b>	<b>21</b>	<b>3 hr</b>
25	25	22.8	27.2	<b>25</b>	<b>22.8</b>	
30	30	25.5	14.5	<b>30</b>	<b>25.5</b>	
35	20	27.8	17.2	<b>35</b>	<b>27.8</b>	
40	20	31	9	<b>40</b>	<b>31</b>	
45	10	34.2	10.8	<b>45</b>	<b>34.2</b>	
50	7	36.7	6.3	<b>50</b>	<b>36.7</b>	
Gel time: 1-2hr						
Component A(ml)		Component B(ml)		%silicate <sup>1</sup>	% CA <sup>2</sup>	Gel time
N silicate	Tap water	Citric acid	Tap water			
20	23	22	35	<b>20</b>	<b>22</b>	<b>1-2 hr</b>
25	25	23.3	26.7	<b>25</b>	<b>23.3</b>	
30	30	26	14	<b>30</b>	<b>26</b>	
35	20	28	17	<b>35</b>	<b>28</b>	
40	20	32	18	<b>40</b>	<b>32</b>	
45	10	34.3	10.7	<b>45</b>	<b>34.3</b>	
50	7	36.8	6.2	<b>50</b>	<b>36.8</b>	

Note: 1: % silicate= volume of silicate / volume of the grouts (component A + B)

2: % CA= volume of citric acid / volume of the grouts (component A + B)



**Table 5.2 Grouting formula for Aqueous Alkaline Aluminosilicate (AAAS)**

<b>Gel time: 4-5hr</b>						
Component A(ml)		Component B(ml)		%silicate <sup>1</sup>	% PC <sup>2</sup>	Gel time
AAAS	Tap water	PC	Tap water			
40	<b>60</b>	0	<b>0</b>	40	0	<b>4-5 hr</b>
45	<b>0</b>	1	<b>54</b>	45	1	
50	<b>0</b>	2	<b>48</b>	50	2	
55	<b>0</b>	2.2	<b>42.8</b>	55	2.2	
60	<b>0</b>	3.4	<b>36.6</b>	60	3.4	
<b>Gel time: 3hr</b>						
Component A(ml)		Component B(ml)		%silicate <sup>1</sup>	% PC <sup>2</sup>	Gel time
AAAS	Tap water	PC	Tap water			
40	<b>0</b>	0.4	<b>59.6</b>	40	0.4	<b>3 hr</b>
45	<b>0</b>	1.1	<b>53.9</b>	45	1.1	
50	<b>0</b>	2.2	<b>47.8</b>	50	2.2	
55	<b>0</b>	2.6	<b>42.4</b>	55	2.6	
60	<b>0</b>	3.6	<b>36.4</b>	60	3.6	
<b>Gel time: 1-2hr</b>						
Component A(ml)		Component B(ml)		%silicate <sup>1</sup>	% PC <sup>2</sup>	Gel time
AAAS	Tap water	PC	Tap water			
35	<b>0</b>	0	<b>65</b>	35	0	<b>1-2 hr</b>
40	<b>0</b>	0.8	<b>59.2</b>	40	0.8	
45	<b>0</b>	1.3	<b>53.7</b>	45	1.3	
50	<b>0</b>	2.4	<b>47.6</b>	50	2.4	
55	<b>0</b>	2.8	<b>42.2</b>	55	2.8	

Note: 1: % silicate= volume of silicate / volume of the grouts (component A + B)

2: % PC= volume of propylene carbonate / volume of the grouts (component A + B)

**Table 5.3 Overall test plan for this study.**

NS Series tests									
Sample ID <sup>1</sup>	Water (Solid) content	strength property	Atterberg limits	pH	Electrical conductivity	Zeta potential	Turbidity	XRD	SEM
3%-NS-MFT	● <sup>2</sup>	●	●	-	-	-	-	-	-
5%-NS-MFT	●	●	●	●	●	○ <sup>3</sup>	-	○	○
8%-NS-MFT	●	●	●	●	●	-	-	-	-
10%-NS-MFT	●	●	●	●	●	○	-	○	○
15%-NS-MFT	●	●	●	●	●	-	-	-	-
30%-NS-MFT	●	●	●	-	-	-	●	-	-
40%-NS-MFT	●	●	●	●	●	-	●	○	○
50%-NS-MFT	●	●	●	-	-	-	●	-	-
AAAS Series tests									
Sample ID <sup>1</sup>									
3%-AAAS-MFT	●	●	●	-	-	-	-	-	-
5%-AAAS-MFT	●	●	●	●	●	○	-	○	○
8%-AAAS-MFT	●	●	●	●	●	-	-	-	-
10%-AAAS-MFT	●	●	●	●	●	○	-	○	○
40%-AAAS-MFT	●	●	●	●	●	-	-	○	○
50%-AAAS-MFT	●	●	●	-	-	-	-	-	-
60%-AAAS-MFT	●	●	●	-	-	-	-	-	-

**Note:** <sup>1</sup>: Sample ID: For example, 3%-NS-MFT denotes MFT samples treated by 3% concentration NS solution.

<sup>2</sup>: The tests were performed on the curing period of 7 days, 14 days and 28days.

<sup>3</sup>: The tests were performed only after 28days

**Table 5.4 Mixing ratio for N sodium silicate (NS)**

Sample ID	Concentration <sup>1</sup>	MFT (g)	Water (ml) <sup>2</sup>	NS (ml)	CA (ml) <sup>3</sup>
3%-NS-MFT	3%	200	130	4	2
5%-NS-MFT	5%	200	130	7	2.3
8%-NS-MFT	8%	200	130	11.3	2.4
10%-NS-MFT	10%	200	130	14.5	2.5
15%-NS-MFT	15%	200	130	23	5
Sample ID	Concentration <sup>1</sup>	MFT (g)	Water (ml) <sup>2</sup>	NS (ml)	CA (ml) <sup>3</sup>
30%-NS-MFT	30%	100	65	43.3	36.1
40%-NS-MFT	40%	80	52	69.3	52.0
50%-NS-MFT	50%	30	19.5	72.8	53.3

**Note:** <sup>1</sup>Definition of concentration ratio= Volume of silicate/ Volume of silicate grouts;

<sup>2</sup>Volume of water in MFT= [MFT/(1+185%)]\*185%. 185% is the water content of raw MFT;

<sup>3</sup>CA denotes the citric acid (setting agent for NS).

**Table 5.5 Mixing ratio for Aqueous Alkaline Aluminosilicate (AAAS)**

Sample ID	Concentration <sup>1</sup>	MFT (g)	Water (ml) <sup>2</sup>	AAAS (ml)	PC (ml) <sup>3</sup>
3%-AAAS-MFT	3%	200	130	4	0
5%- AAAS-MFT	5%	200	130	7	0
8%- AAAS-MFT	8%	200	130	11.3	0
3%- AAAS-MFT	10%	200	130	14.5	0
Concentration <sup>1</sup>	Concentration <sup>1</sup>	MFT (g)	Water (ml) <sup>2</sup>	AAAS (ml)	PC (ml) <sup>3</sup>
40%-AAAS-MFT	40%	120	77.9	51.9	0
50%-AAAS-MFT	50%	100	64.91	67.61	2.71
60%- AAAS-MFT	60%	80	51.93	85.1	4.82

**Note:** <sup>1</sup>Definition of concentration ratio= Volume of silicate/ Volume of silicate grouts;

<sup>2</sup>Volume of water in MFT= [MFT/(1+185%)]\*185%. 185% is the water content of raw MFT;

<sup>3</sup>PC denotes the propylene carbonate (setting agent for AAAS).

**Table 5.6 Summary of Sensitivity of silicate-treated MFT samples.**

Test series	Sample ID <sup>1</sup>	Curing (days)		
		Day 7	Day 14	Day 28
NS	3%-NS-MFT	- <sup>1</sup>	-	-
	5%-NS-MFT	-	-	-
	8%-NS-MFT	2.7	2.69	2.38
	10%-NS-MFT	3.44	2.98	2.24
	15%-NS-MFT	2.55	1.86	1.94
	30%-NS-MFT	3.7	4.7	5.0
	40%-NS-MFT	8.5	8.9	9.0
	50%-NS-MFT	17.5	13.1	13.2
AAAS	3%-AAAS-MFT	-	-	-
	5%-AAAS-MFT	3.37	2.09	2.68
	8%-AAAS-MFT	2.51	2.45	2.27
	10%-AAAS-MFT	3.24	2.72	2.22
	40%-AAAS-MFT	6.0	6.87	7.94
	50%-AAAS-MFT	8.3	8.44	8.59
	60%-AAAS-MFT	9.6	9.61	ND

**Note:** <sup>1</sup> The remolded undrained shear strength of 3%-NS-MFT, 5%-NS-MFT, 3%-AAAS-MFT were virtually zero;

**Table 5.7 Index properties of silicate-treated MFT samples.**

NS Series												
Sample ID	Curing period, days											
	D7				D14				D28			
	LL, %	PL, %	PI	LI <sup>2</sup>	LL, <sup>1</sup> %	PL, %	PI	LI <sup>2</sup>	LL, <sup>1</sup> %	PL, %	PI	LI <sup>2</sup>
<b>5%-NS-MFT</b>	116.0	38.4	77.6	1.8	125.0	41.6	83.4	1.6	134.8	43.6	91.2	1.4
<b>10%-NS-MFT</b>	140.1	52.3	87.8	1.4	142.4	61.4	81.0	1.3	157.0	64.9	92.1	1.1
<b>15%-NS-MFT</b>	168.4	69.4	99.0	1.0	169.1	75.6	93.5	1.0	174.4	77.4	97.0	0.9
AAAS Series												
Sample ID	Curing period, days											
	D7				D14				D28			
	LL, %	PL, %	PI	LI <sup>2</sup>	LL, <sup>1</sup> %	PL, %	PI	LI <sup>2</sup>	LL, <sup>1</sup> %	PL, %	PI	LI <sup>2</sup>
<b>3%-AAAS-MFT</b>	95.5	42.5	53.0	2.4	116.2	45.0	71.2	1.7	123.5	51.0	72.5	1.5
<b>5%-AAAS-MFT</b>	128.1	41.9	86.2	1.5	134.3	47.9	86.4	1.3	122.7	54.3	68.4	1.5
<b>10%-AAAS-MFT</b>	135.9	44.3	91.6	1.2	138.3	43.5	94.8	1.1	143.2	47.8	95.4	1.0

**Note:** <sup>1</sup>Liquid limit (LL) determined by Swedish Falling Cone method (cone of 60g,60°; 10mm);

<sup>2</sup>LI denotes the liquidity index.

**Table 5.8 Aquatic chemistry of decanted liquids from NS-treated MFT samples.**

Sample ID	30%-NS-MFT			40%-NS-MFT			50%-NS-MFT		
Time(days)	7	14	28	7	14	28	7	14	28
pH (22±1°C)	11.0	10.9	11.0	11.1	10.9	10.8	10.9	10.9	11.0
EC, mS/cm	36.9	38.2	35.4	38.0	36.7	37.7	38.9	35.6	38.4
Turbidity, NTU	188	167	101.3	109.6	94.6	89.4	60.8	72.1	69.7
liquid collected <sup>1</sup>	10	18	25	32	42	56	45	60	85

**Note:** <sup>1</sup> Unit: milliliter (ml). The MFT samples were cured in 2” molds, and the volumes of the samples were 157ml (30%-NS-MFT), 192ml (40%-NS-MFT) and 161 ml (50%-NS-MFT).

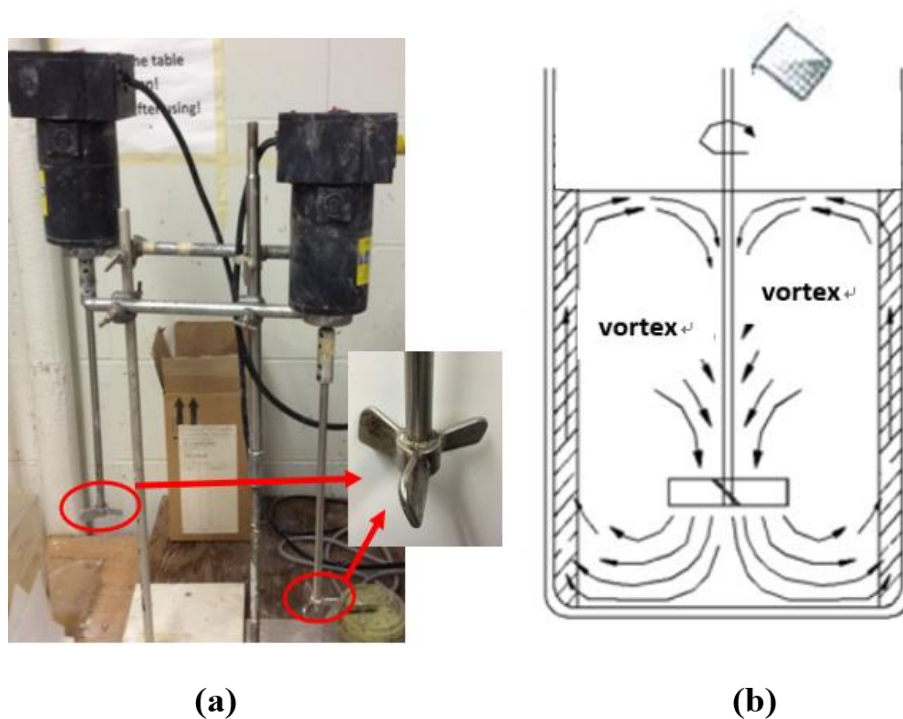


**Fig. 5.1 (a) Mixing device and impeller blade; (b) Flow pattern during mixing (modified from Yao, 2016)**

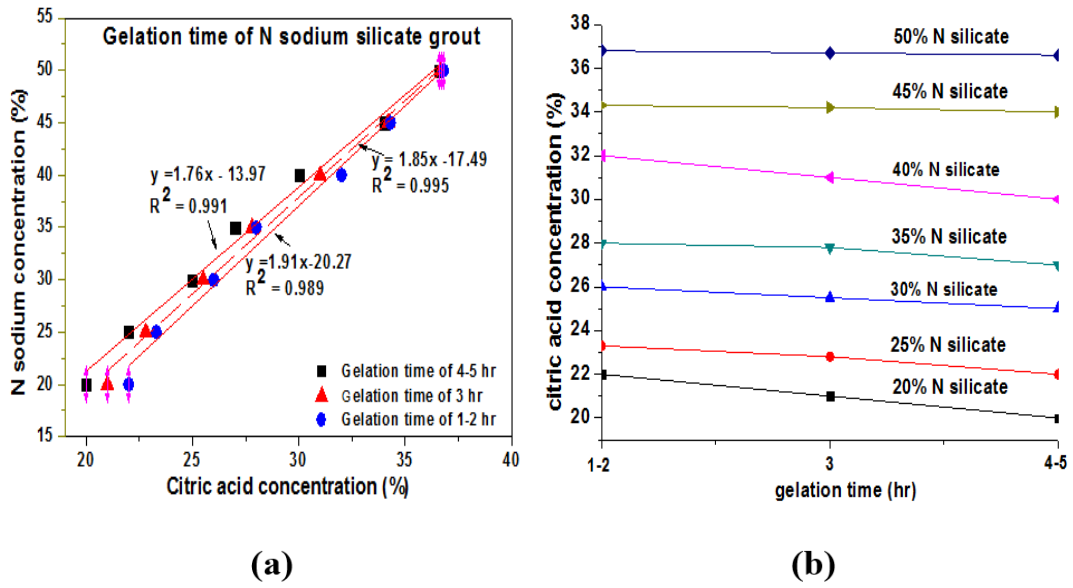


**Fig. 5.2 (a) Gel time determination of NS grout system; (b) Effects of setting agent and silicate concentration on the gel time of NS grout**

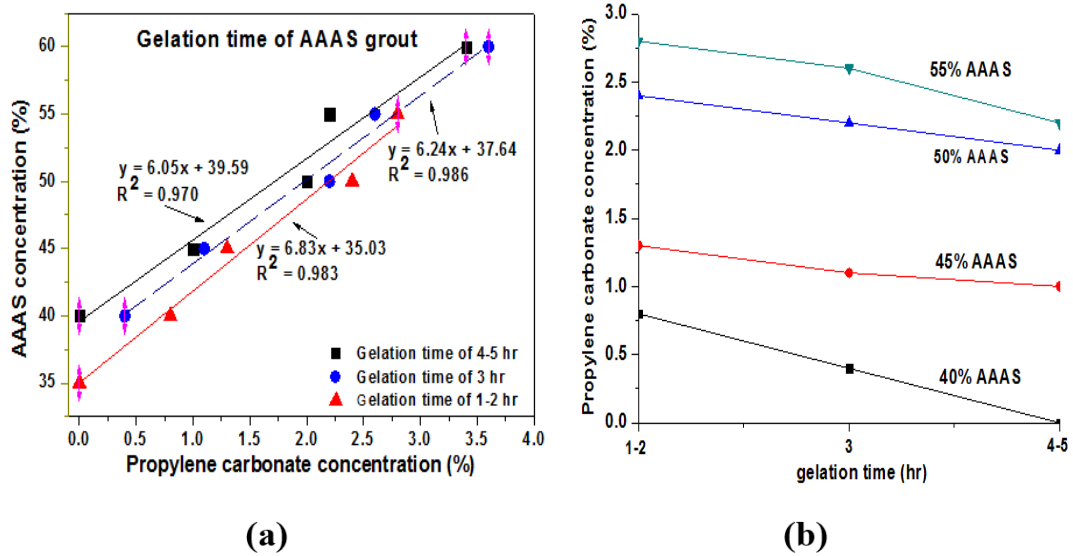


**Fig. 5.3 (a) Gel time determination of AAAS grout system; (b) Effects of setting agent and silicate concentration on the gel time of AAAS grout**

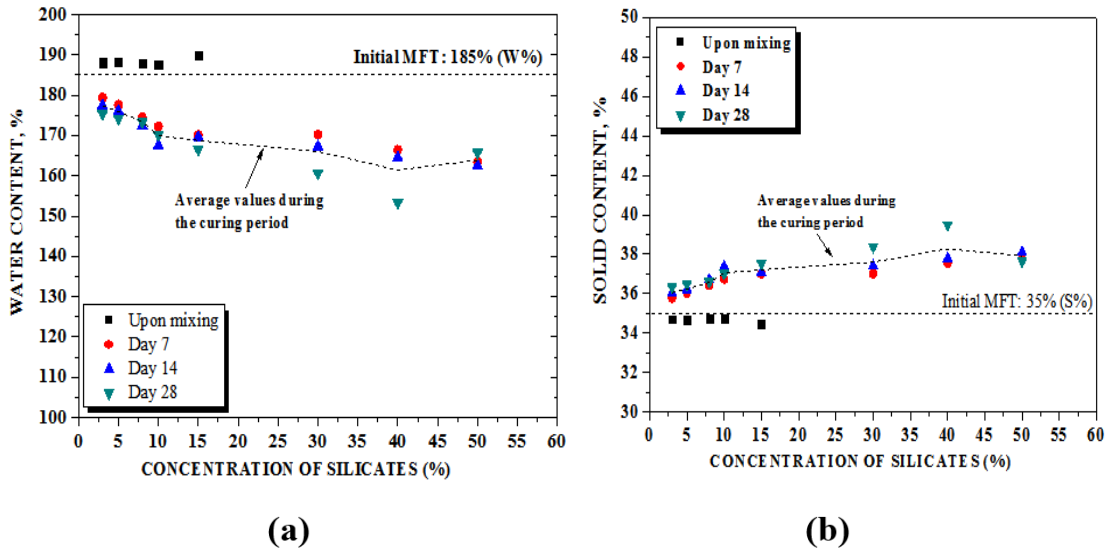


Fig. 5.4 (a) Water content of NS treated MFT; (b) Solid content of NS treated MFT

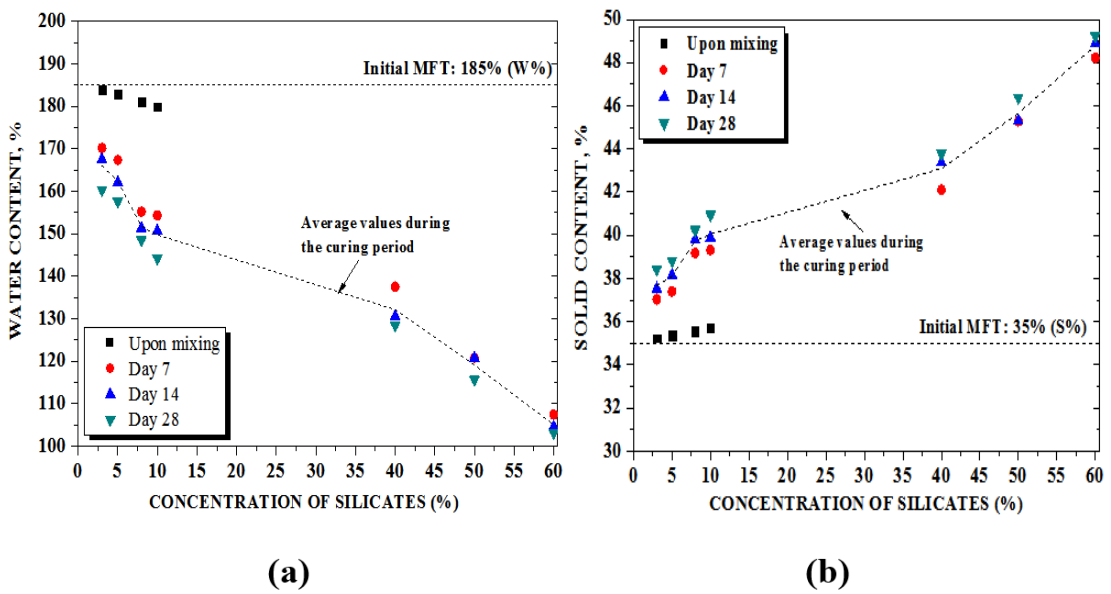


Fig. 5.5 (a) Water content of AAAS treated MFT; (b) Solid content of AAAS treated MFT



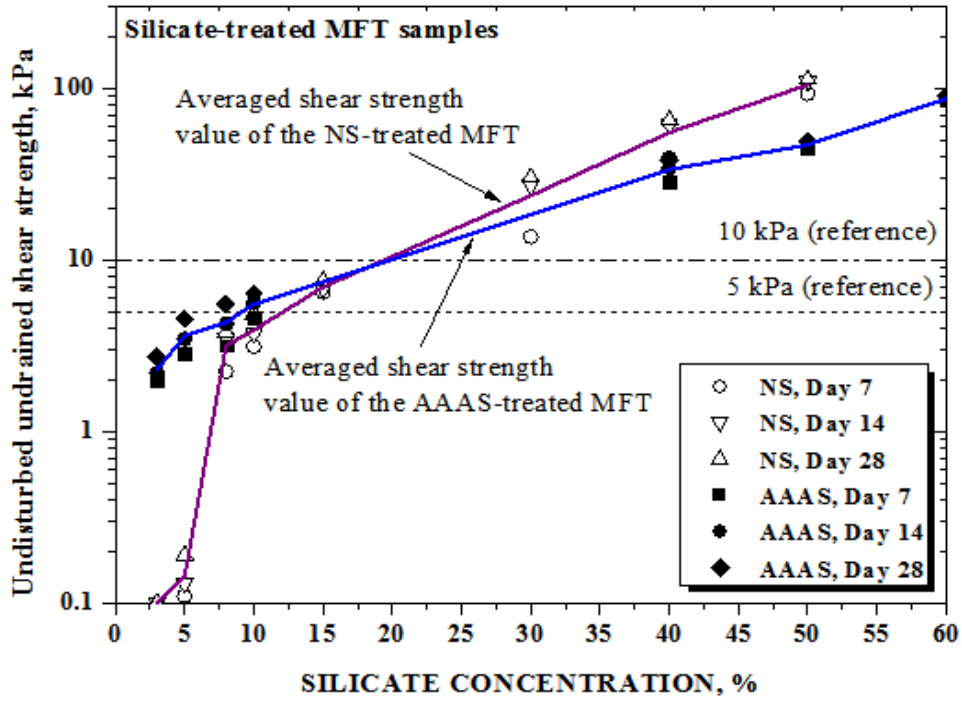


Fig. 5.6 Effects of silicate type and concentrations on the undrained shear strength gain of MFT samples

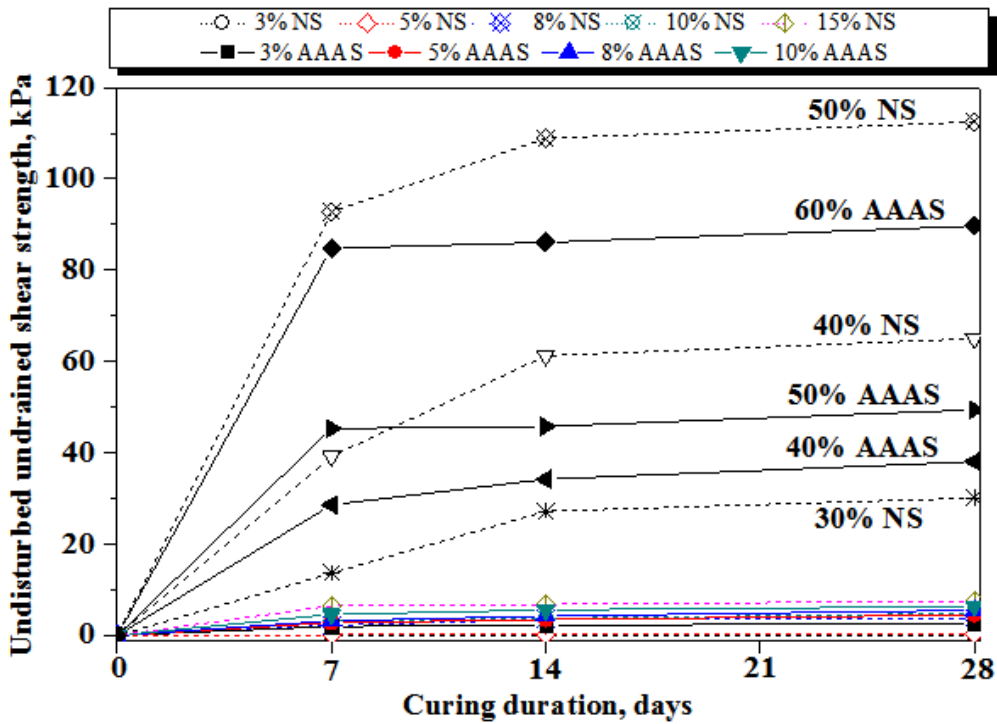


Fig. 5.7 Effects of curing period on the undrained shear strength gain of silicate-treated MFT samples

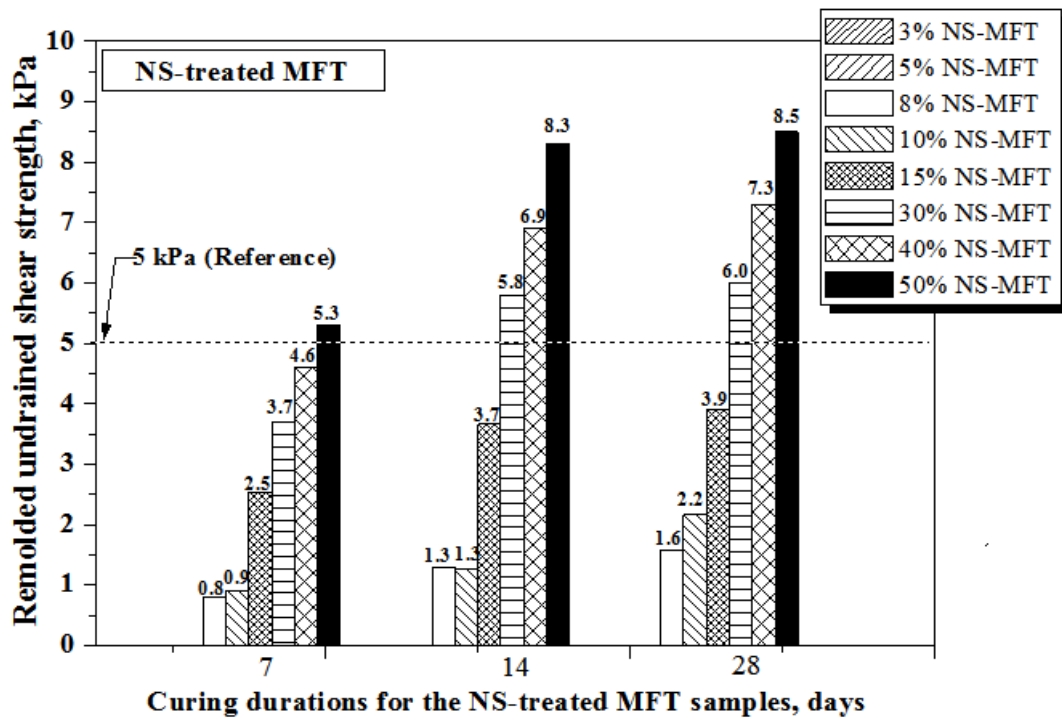


Fig. 5.8 Remolded undrained shear strength of NS treated MFT samples

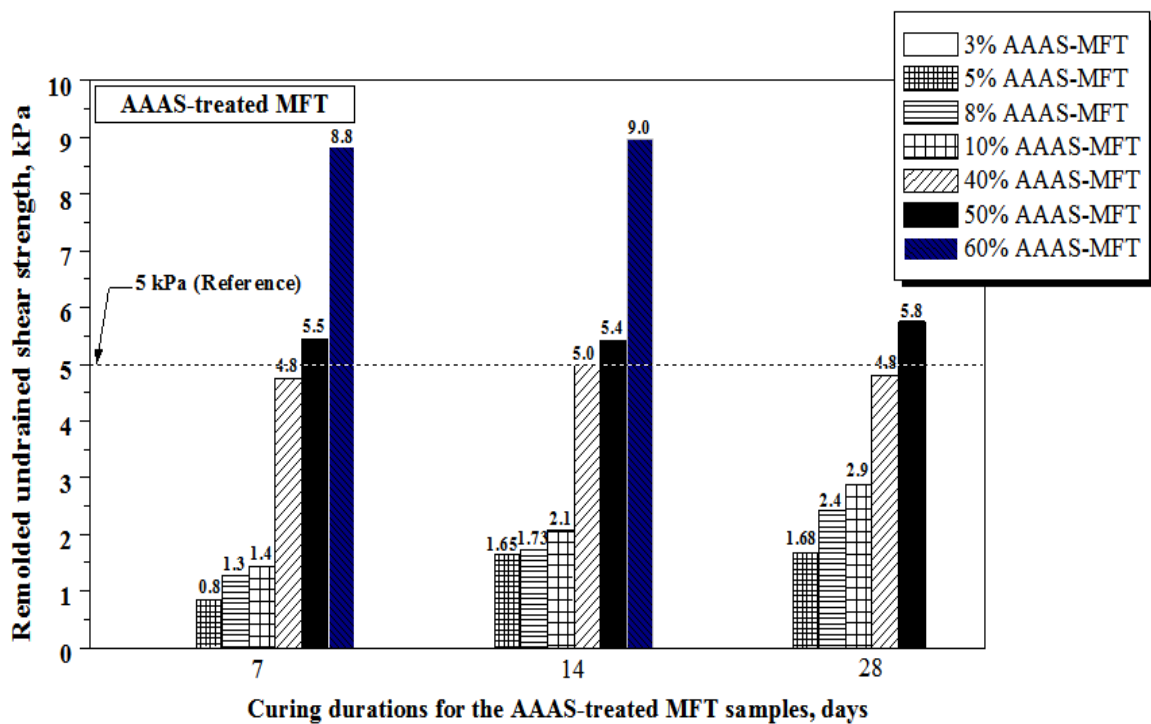


Fig. 5.9 Remolded undrained shear strength of AAAS treated MFT samples

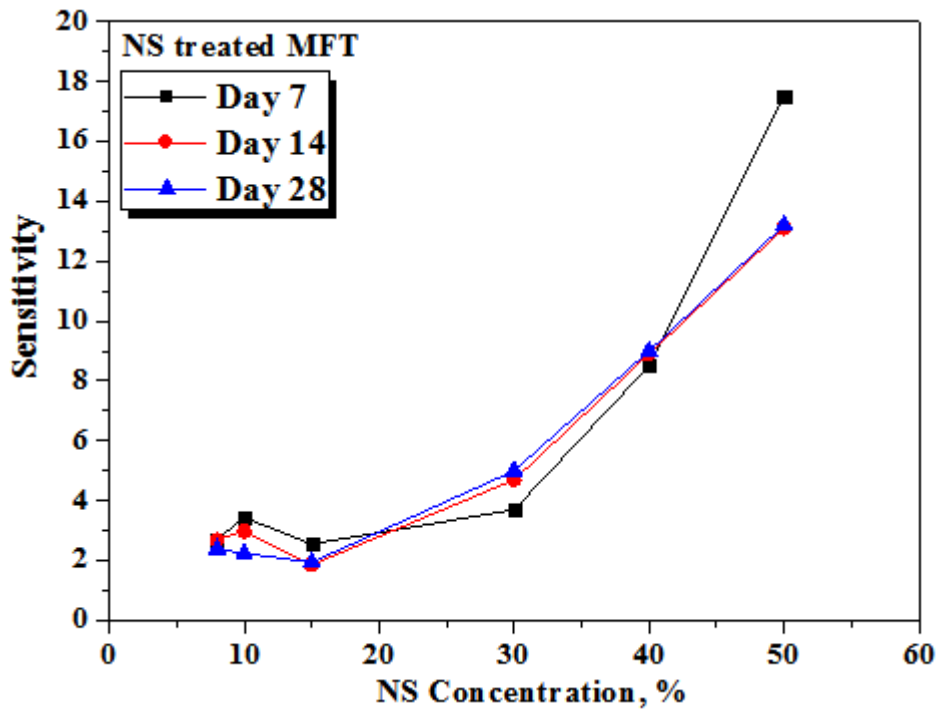


Fig. 5.10 Sensitivity of NS treated MFT samples

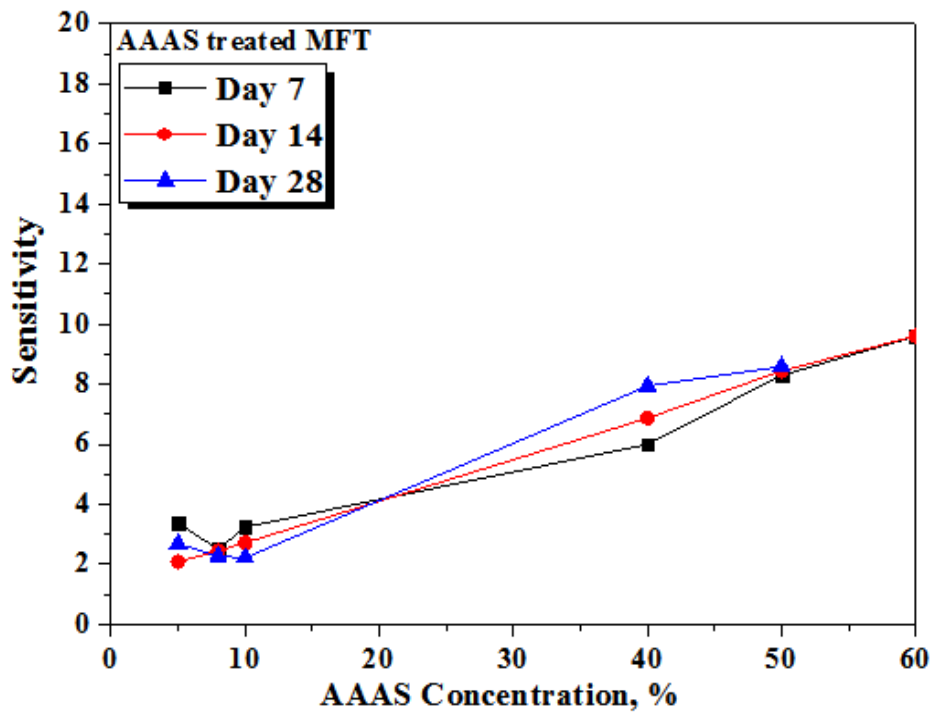
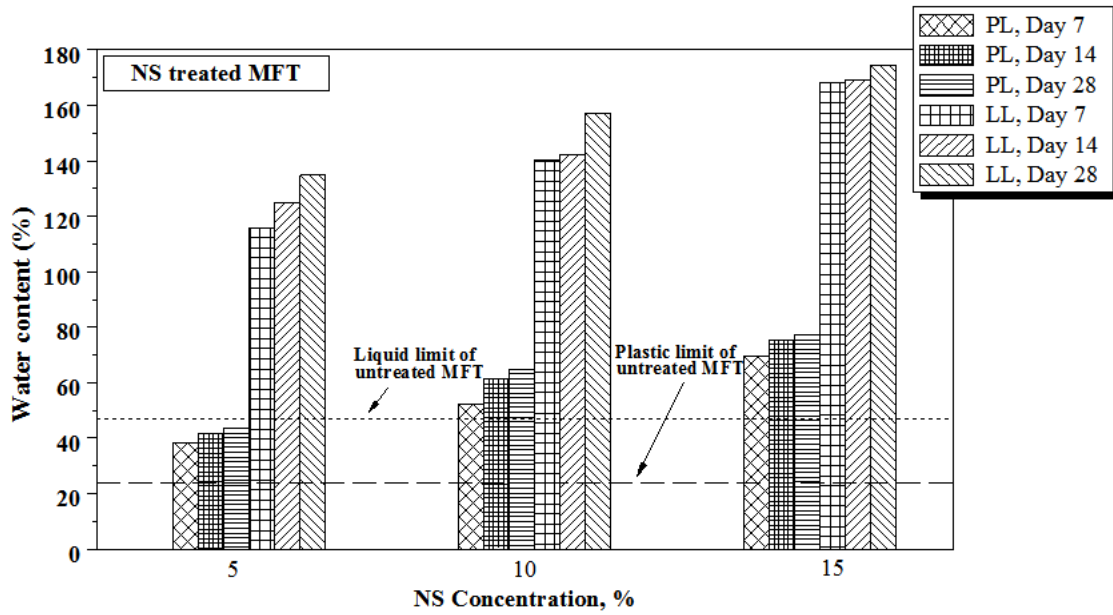
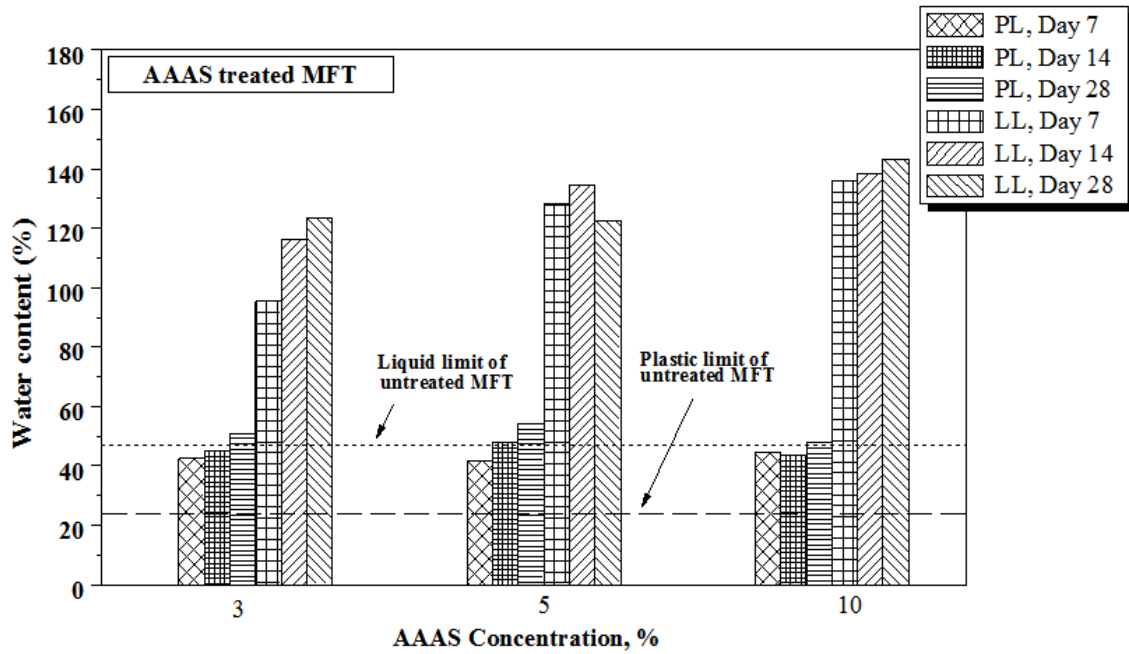


Fig. 5.11 Sensitivity of AAAS treated MFT samples



**Fig. 5.12 Atterberg limits of NS treated samples**



**Fig. 5.13 Atterberg limits of AAAS treated MFT samples**

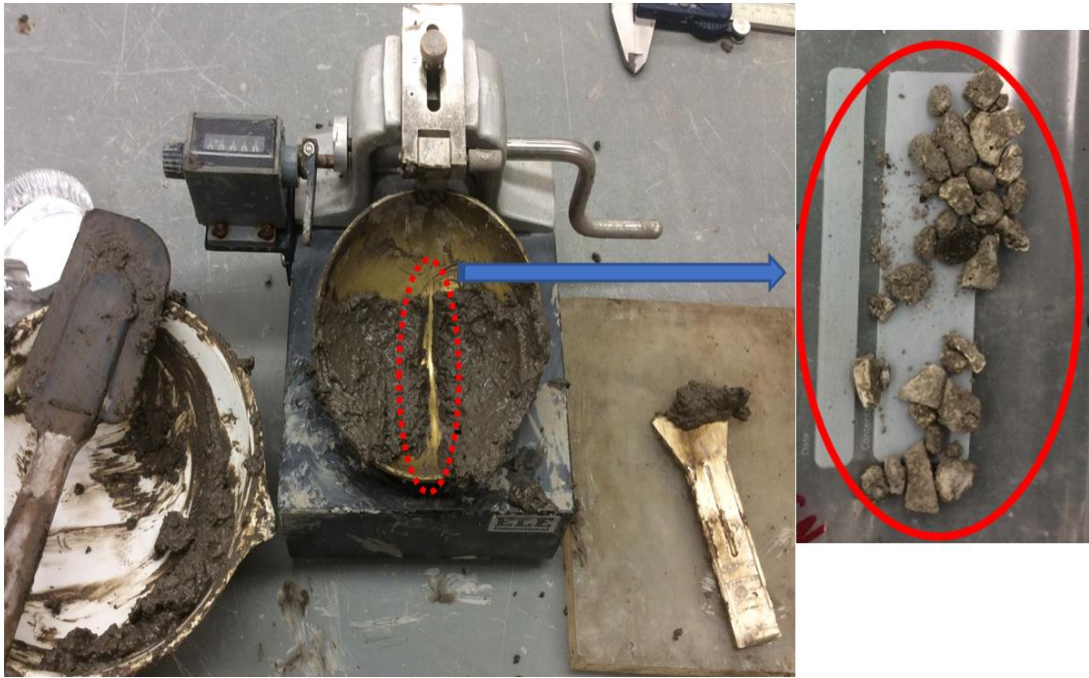


**Fig. 5.14** Liquid limit test of MFT samples treated by high amount of silicates



**Fig. 5.15** Plastic limit test of MFT samples treated by high amount of silicates

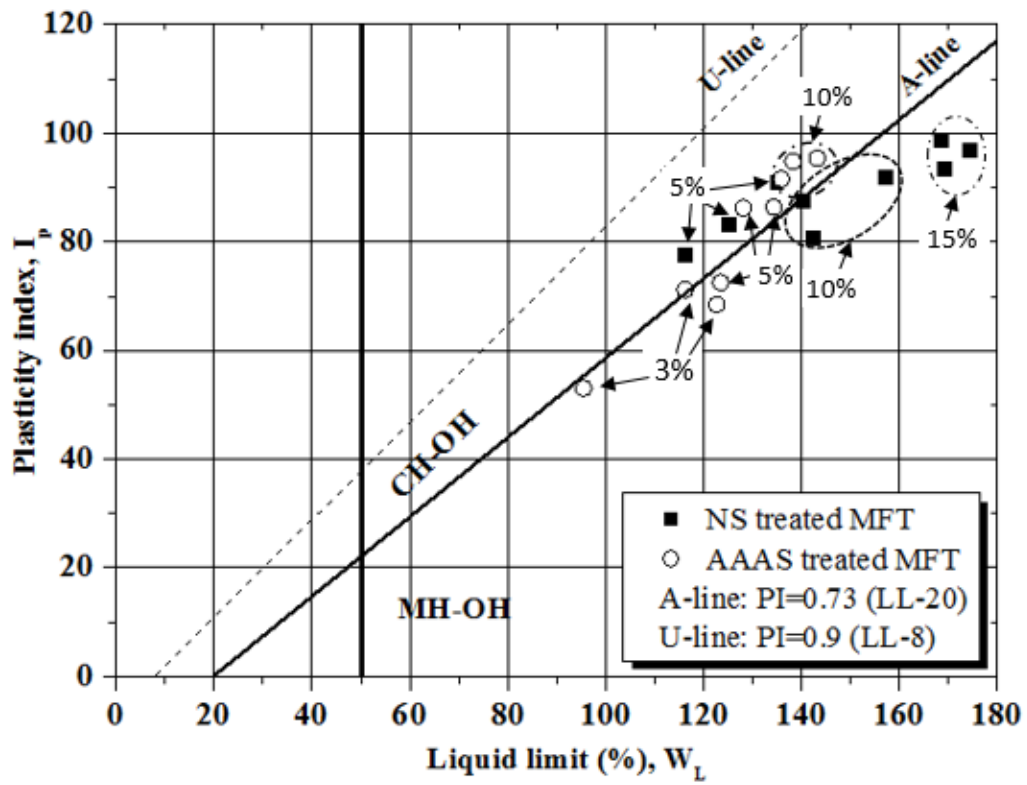
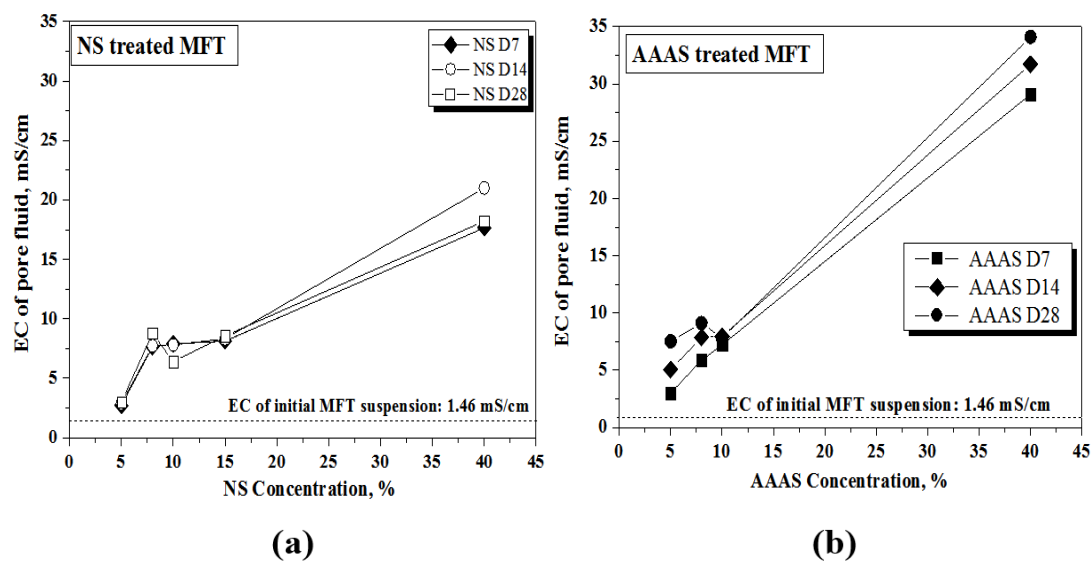
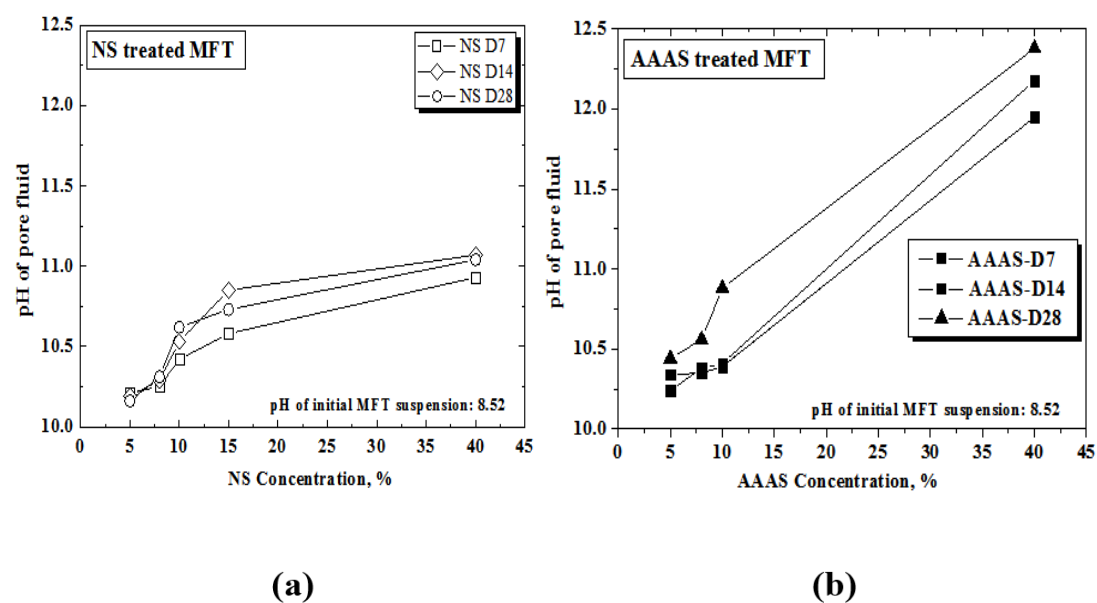


Fig. 5.16 Casagrande plasticity chart



**Fig. 5.17 (a) Electrical conductivity of NS-treated MFT samples; (b) Electrical conductivity of AAAS-treated MFT samples;**



**Fig. 5.18 (a) pH of NS-treated MFT samples; (b) pH of AAAS-treated MFT samples;**



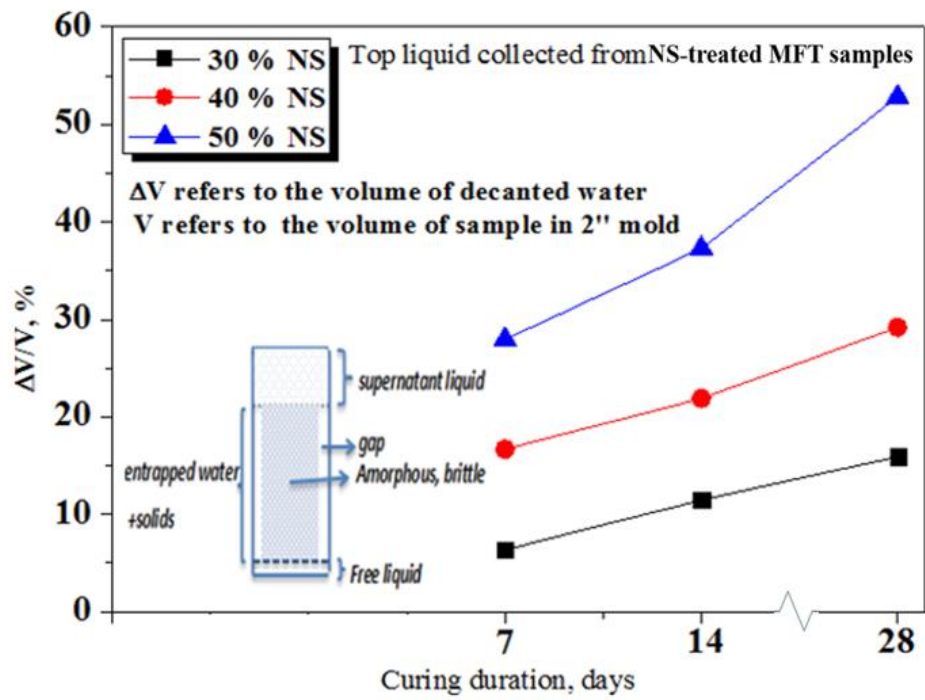


Fig. 5.19 The volume of decanted liquid of NS-treated MFT samples

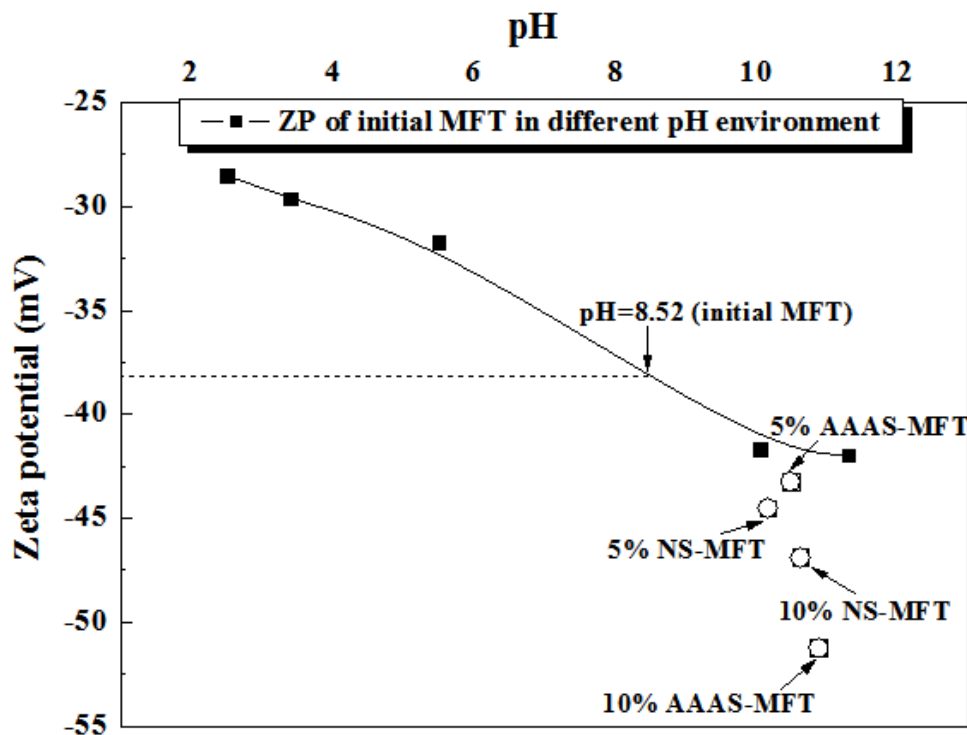


Fig. 5.20 Zeta potential of the solid particles in silicate-treated MFT samples



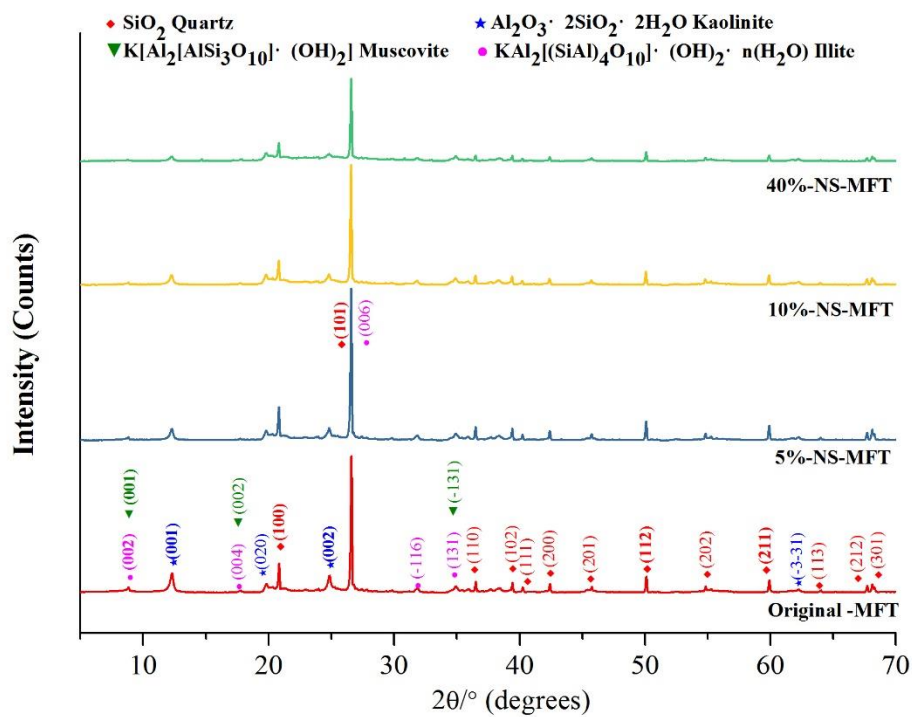


Fig. 5.21 XRD pattern of NS-treated MFT samples

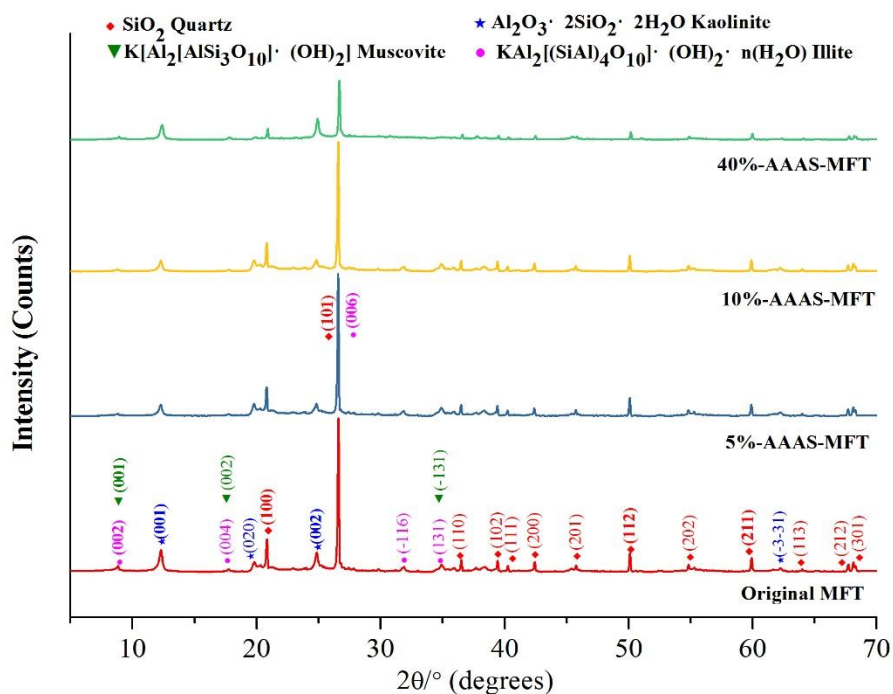
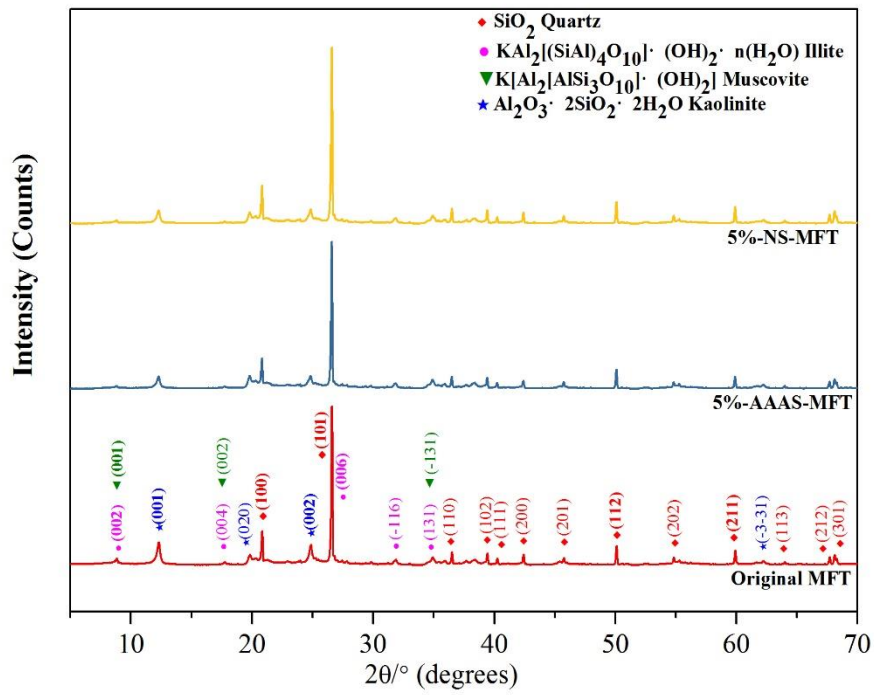
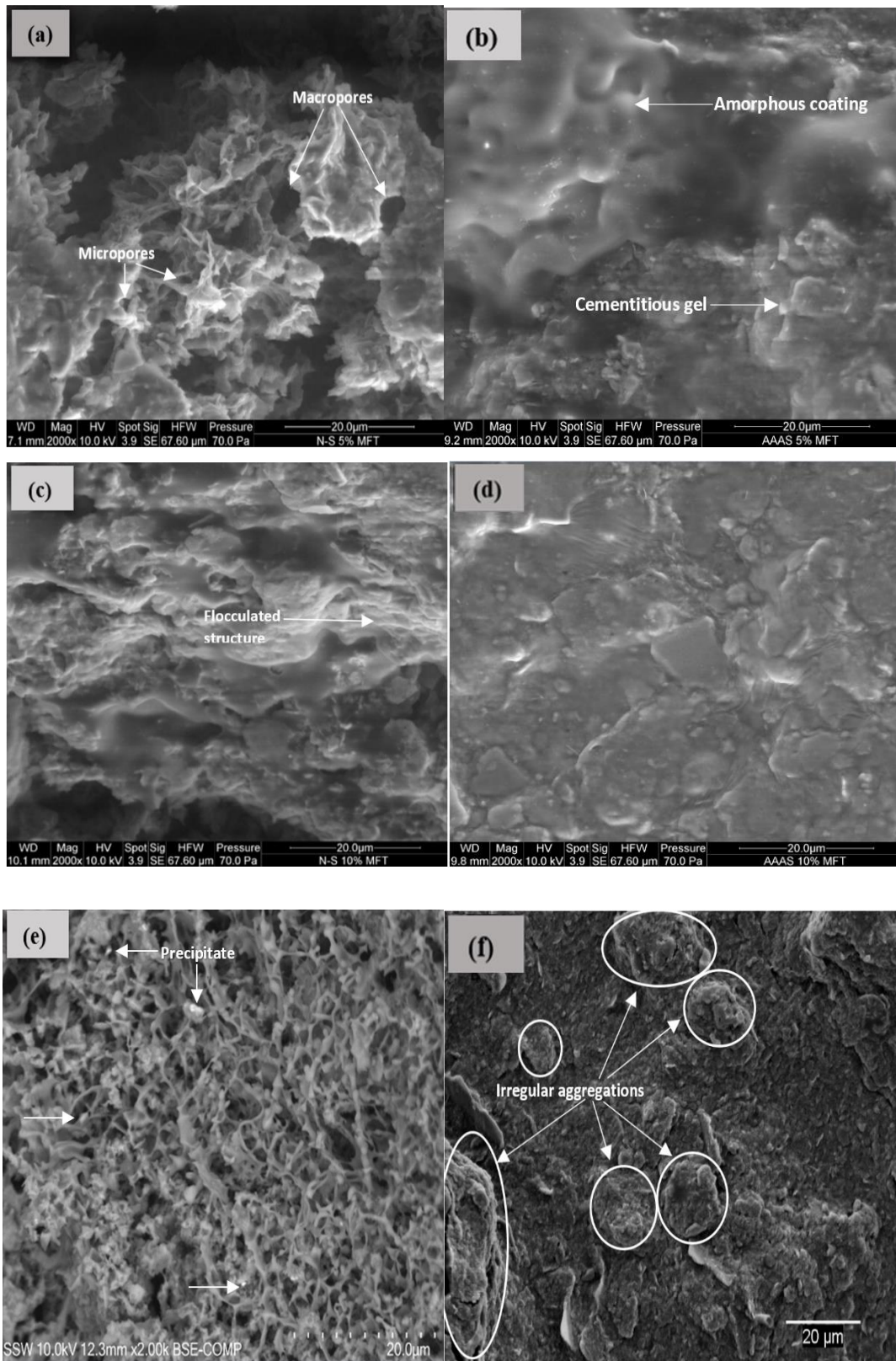


Fig. 5.22 XRD pattern of AAAS-treated MFT samples



**Fig. 5.23 XRD pattern of initial MFT sample and 5% silicates treated MFT samples**



**Fig. 5.24 SEM photos after 28-day curing (Mag=2000x). (a) 5% NS-MFT; (b) 5% AAAS-MFT; (c) 10% NS-MFT; (d) 10% NS-MFT; (e) 40% NS-MFT; (f) 40% AAAS-MFT;**

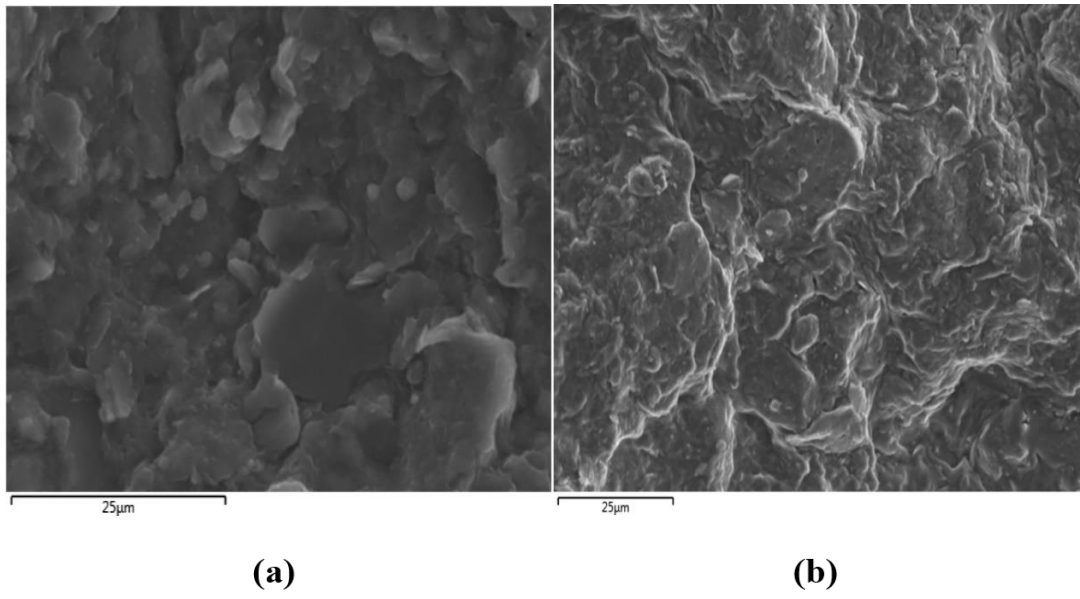


**Fig. 5.25 SEM photos for 10% silicate-treated MFT samples consolidated up to a stress level of 5 kPa after 28-day curing (Mag=2000x): (a) NS; (b) AAAS**

## References

**Beier N., Wilson W., Dunmola A., and Segó D., (2013)** “Impact of flocculation-based dewatering on the shear strength of oil sands fine tailings,” *Can. Geotech. J.*, vol. 50, pp. 1001-1007.

**Boone, S.J. and A.J. Lutenegeger. 1997.** Carbonates and cementation of glacially derived cohesive soils in New York State and southern Ontario. *Canadian Geotechnical Journal*, 34, 534-550.

**Chew SH, Kamruzzaman HM, Lee FH (2004).** Physicochemical and engineering behaviour of cement treated clays. *J Geotech Geoenviron Eng* 130(7):696–706

**Ding J, Fu Y. and Beaudoin J.J.. (1996)** “Study of Hydration Mechanisms in High-Alumina Cement—Sodium Silicate System,” *Cem. Concr. Res.*, 26 [5] 799–804.

**Directive 074 (2009).** Tailings performance criteria and requirements for oil sands mining schemes, Energy Resources Conservation Board (ERCB), Alberta

**Kaya A, Yukselen Y. 2005** Zeta potential of soils with surfactants and its relevance to electrokinetic remediation [J]. *Journal of Hazardous Materials*, B120: 119-126.

**Latifi, N., Eisazadeh, A., and Marto, A. (2014).** “Strength behavior and microstructural characteristics of tropical laterite soil treated with sodium silicate-based liquid stabilizer.” *Environ. Earth Sci.*, 72(1), 91–98.

**Ma, C., Qin, Z. H., Zhuang, Y. C., Chen, L. Z., and Chen, B. (2015).** “Influence of sodium silicate and promoters on unconfined compressive strength of Portland cement-stabilized clay.” *Soils and Foundations*, Vol. 55, No. 5, pp. 1222-1232.

**Maaitah Omer Nawaf, 2012.** Soil Stabilization by Chemical Agent, *Geotech Geol Eng* (2012) 30:1345–1356

**Mitchell J.K. and K. Soga,** *Fundamentals of soil behavior*. 3rd ed. (2005), NY: Wiley.

**Moayedi, H., Huat, B.B.K., Moayedi, F., Asadi A., and Parsaie, A. (2011)** Effect of Sodium Silicate on Unconfined Compressive Strength of Soft Clay, *Electronic Journal*

of Geotechnical Engineering, Vol. 16, p 289-295.

**Pangdaeng, S., Phoo-ngerksam, T., Sata, V., Chindaprasirt, P., 2014.** Influence of curing conditions on properties of high calcium fly ash geopolymer containing Portland cement as additive. *Mater. Des.* 53, 269–274.

**PQ Corporation, 2003.** Soluble silicate in geotechnical grouting applications. *Bulletin* 52–53, USA.

**Roshani, A., Fall, M., and Kennedy, K. (2017).** "Drying Behavior of Mature Fine Tailings Pre-Dewatered with Super-Absorbent Polymer (SAP): Column Experiments," *Geotechnical Testing Journal*, Vol. 40, No. 2, 2017, pp. 210-220.

**Sherwood, P. T. 1961.** Soil stabilization by the Use of Chemical Admixtures: A Review of the Present Position. *Roads and Road Construction*, Vol. 39, No. 460, pp. 102-110.

**Sridharan, A., Rao, S.M., Murthy, N.S., 1988.** Liquid limit of kaolinitic soils. *Geotechnique* 38 (2), 191–198.

**Sridharan, A., 1991.** Engineering behavior of fine grained soils — a fundamental approach. *Indian Geotechnical Journal* 21 (1), 1–136.

**Sunganya, K., Sivapullaiah, P. V., 2015.** Role of sodium silicate additive in cement treated Kuttanad soil. *Journal of Material in Civil Engineering* 28(6) 06016006-1– 6.

**Terzaghi, K. (1944).** "Ends and Means in Soil Mechanics", *Engineering Journal of Canada*, 27, pp.608.

**Tingle, J., Newman, J., Larson, S., Weiss, C., and Rushing, J. (2007).** "Stabilization mechanisms of nontraditional additives." *Transp. Res. Rec.*, 1989(1), 59–67.

**Yao, Y. (2016).** Dewatering behavior of fine oil sands tailings: an experimental study. Ph.D. Thesis, Delft University of Technology, Delft, Netherlands.

## **CHAPTER 6 CONCLUSION AND RECOMMENDATION**

### **6.1 Summary**

In this thesis, a study on stabilization of oil sands mature fine tailings (MFT) by chemical additives, i.e., Portland cement and liquid silicates, was conducted. The study was mainly focused on the solidification and strengthening effects of MFT after chemical treatment. The study was conducted in three phases:

- a) characterization of chemicals and MFT. The properties of chemical agents (Portland cement, NS and AAAS), as well as the geotechnical and mineralogical properties of MFT were determined prior to the treatment;
- b) determination of the macroscopic characteristics. After thorough mixing and a short curing period, the MFT paste was used to determine the final water (solid) content, undrained shear strength, Atterberg limits, pH at different time intervals (7, 14 and 28 days);
- c) determination of the microscopic characteristics. Scanning electron microscopy (SEM) and X-ray diffraction (XRD) tests were performed to characterize the microstructure and mineral composition of the treated MFT samples.

The results of this study show the potential use of chemicals in stabilization of MFT, i.e., it is possible to solidify and develop required undrained shear strength of MFT by adding appropriate amount of Portland cement and silicate grouts. However, compared to the silicate grouts, Portland cement is easier to store, transport and mix in the field.

### **6.2 Conclusion**

The main conclusions of this thesis can be made as following.

- The investigated MFT sample has the initial water content 185%, liquid limit 47.0%, plastic limit 23.9%, specific gravity 2.31, initial void ratio 4.27, silt fractions (81%), clay fractions (19%), pH 8.52 and zeta potential -38mV.

- The microstructure of investigated MFT sample is slightly flocculated ‘card-house’ structure, and the main minerals include Kaolinite, Illite and Quartz.
- The gelling product of AAAS is more consistent than NS gel, and does not show syneresis. Setting agent is not required for AAAS solution to trigger the gelling reaction when concentration of AAAS is lower than 40%.
- The undrained shear strength of chemically-treated MFT samples is increased by increasing the chemical dosages and curing time. After 28 days of curing, an undrained shear strength value (5 kPa) can be achieved by adding 10% PC (7.65 kPa), 15% NS (7.55 kPa) and 8% AAAS (5.5kPa), respectively. Addition of 1% PC and 3% NS does not cause any strength improvement of MFT. The sensitivity of NS-treated MFT samples is higher than that of AAAS-treated MFT samples.
- The solid content of MFT increases with the dosage of liquid silicates, and the effect is most significant in the first 7 days. The solid content of MFT increases immediately after mixing with PC, due to cement hydration. AAAS is more effective than NS in increasing the solid content of MFT at same curing period. 60%-AAAS-MFT sample achieved nearly 50% of solid content at the end of curing period (28 days), while 15%-PC-MFT sample achieved a solid content of 41.72%.
- Both Atterberg limits and plasticity index of MFT samples increase during chemical stabilization process. In general, the magnitude of the LL increase in AAAS-treated MFT samples is lower than that of NS-treated MFT samples. For PC stabilization, the most significant increase in LL is registered in 15%-PC-MFT sample, which also has a highest PL value among other cement-treated MFT samples.
- The addition of 10% and 15% Portland cement induce preconsolidation pressures in MFT samples after 14 days and 28 days, suggesting cementation effects. The consolidation results of the silicate-treated MFT samples are not presented.
- After adding PC and silicate grouts, the pH of MFT samples increases with curing time. After 28 days, the pH values of MFT samples varied within a narrow range from 10 to 11, with a low concentration of silicates; The MFT samples treated by 5%, 10%



and 15% PC have pH values greater than 10.5, less than 12.5.

- As evidenced by SEM, the needle-like C-S-H gels of PC bind the MFT particles; The amorphous NS gels create bonds and cross-linking network between MFT particles; The irregular AAAS gels encapsulate MFT particles and fill the voids between grains. Therefore, the microstructures of MFT become denser after chemical treatments.
- The peak intensities of clay minerals in XRD patterns are reduced after chemical treatment. The results clearly indicate the formation of C-S-H gel in cement-treated MFT samples, but no new crystalline phases related to the silicate grouts are detected.

### **6.3 Recommendations**

Recommendations for the future study include:

- An investigation of the effects of organic matter (e.g. residual bitumen) in oil sands tailings on cement hydration process.
- Further investigation towards the solidifying effects of cement and silicate grouts on MFT slurry at prolonged curing durations, i.e., beyond 28 days.
- Evaluation of the effects of the cement and silicate additions on the permeability and pore structure (e.g., pore size distribution) of MFT.
- Extend the silicate grouting formula for the oil sands tailings using supernatant water of MFT suspension.
- Further investigation on the interaction between silicate ions and clay particles in MFT.
- Further studies on thixotropic properties of the silicate-treated MFT samples after remolding, as well as the durability aspects of silicate-treated MFT like drying and wetting, freezing and thawing actions.
- Further investigation on the environmental impacts (e.g., leachability) of chemical treated MFT samples.

# APPENDIX A-1: GRAIN SIZE ANALYSIS (BT-9300S)

## PARTICLE SIZE ANALYSIS BY BT-9300S SYSTEM

SampleName: oil sand	SampleOwner: Civil Engr.
MediumName: Water	MeasureDept: CBE
Operator: Grace	AnalyDate: 2017-07-26
Remark: Laser Particle Size Analyser	AnalyTime: 11:03:26

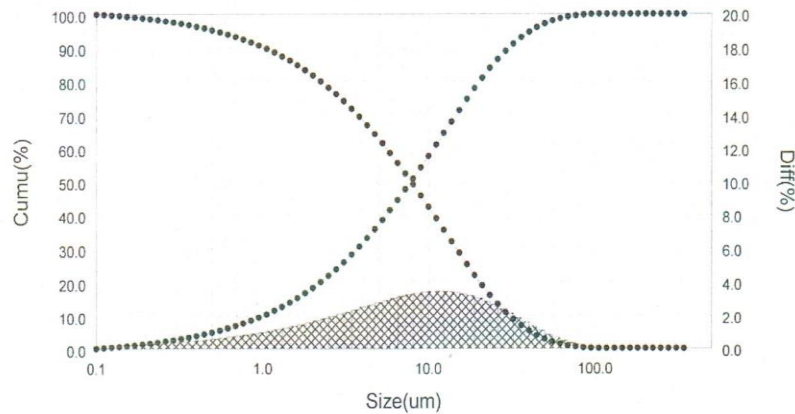
  

D(v,0.5)= 7.83 um	D[4.3]= 12.62 um	D[3.2]= 2.24 um	Obscuration: 25.29
SSA: 2226.37 m <sup>2</sup> /Kg	Sample Ref Re: 1.460	Sample Ref Im: 0.000	Medium Ref: 1.333

D(v,0.03)= 0.33 um	D(v,0.06)= 0.60 um	D(v,0.1)= 1.01 um	D(v,0.16)= 1.70 um	D(v,0.25)= 2.93 um
D(v,0.75)= 17.20 um	D(v,0.84)= 23.64 um	D(v,0.9)= 30.75 um	D(v,0.97)= 49.42 um	D(v,0.98)= 55.82 um

Diam um	Diff %	Cumu %	Diam um	Diff %	Cumu %	Diam um	Diff %	Cumu %	Diam um	Diff %	Cumu %
0.10 - 0.11	0.17	0.17	0.76 - 0.85	0.85	8.49	5.85 - 6.51	3.05	44.46	44.69 - 49.74	1.11	97.07
0.11 - 0.12	0.18	0.35	0.85 - 0.95	0.92	9.41	6.51 - 7.24	3.16	47.62	49.74 - 55.36	0.88	97.95
0.12 - 0.14	0.20	0.55	0.95 - 1.05	1.00	10.41	7.24 - 8.06	3.27	50.89	55.36 - 61.62	0.67	98.62
0.14 - 0.15	0.21	0.76	1.05 - 1.17	1.08	11.49	8.06 - 8.97	3.35	54.24	61.62 - 68.50	0.50	99.12
0.15 - 0.17	0.23	0.99	1.17 - 1.31	1.17	12.66	8.97 - 9.98	3.41	57.65	68.50 - 76.33	0.36	99.48
0.17 - 0.19	0.26	1.25	1.31 - 1.45	1.26	13.92	9.98 - 11.11	3.46	61.11	76.33 - 84.96	0.25	99.73
0.19 - 0.21	0.27	1.52	1.45 - 1.62	1.36	15.28	11.11 - 12.37	3.47	64.58	84.96 - 94.56	0.18	99.89
0.21 - 0.24	0.31	1.83	1.62 - 1.80	1.47	16.75	12.37 - 13.77	3.45	68.03	94.56 - 105.24	0.11	100.00
0.24 - 0.26	0.33	2.16	1.80 - 2.00	1.58	18.33	13.77 - 15.32	3.40	71.43	105.24 - 117.13	0.06	100.00
0.26 - 0.29	0.36	2.52	2.00 - 2.23	1.71	20.04	15.32 - 17.05	3.32	74.75	117.13 - 130.37	0.00	100.00
0.29 - 0.32	0.39	2.91	2.23 - 2.48	1.83	21.87	17.05 - 18.98	3.20	77.95	130.37 - 145.10	0.00	100.00
0.32 - 0.36	0.43	3.34	2.48 - 2.76	1.96	23.83	18.98 - 21.12	3.05	81.00	145.10 - 161.50	0.00	100.00
0.36 - 0.40	0.47	3.81	2.76 - 3.08	2.09	25.92	21.12 - 23.51	2.87	83.87	161.50 - 179.75	0.00	100.00
0.40 - 0.45	0.51	4.32	3.08 - 3.42	2.23	28.15	23.51 - 26.17	2.65	86.52	179.75 - 200.06	0.00	100.00
0.45 - 0.50	0.56	4.88	3.42 - 3.81	2.37	30.52	26.17 - 29.12	2.41	88.93	200.06 - 222.66	0.00	100.00
0.50 - 0.55	0.60	5.48	3.81 - 4.24	2.52	33.04	29.12 - 32.41	2.16	91.09	222.66 - 247.83	0.00	100.00
0.55 - 0.62	0.66	6.14	4.24 - 4.72	2.65	35.69	32.41 - 36.08	1.89	92.98	247.83 - 275.83	0.00	100.00
0.62 - 0.69	0.72	6.86	4.72 - 5.25	2.79	38.48	36.08 - 40.15	1.62	94.60	275.83 - 307.00	0.00	100.00
0.69 - 0.76	0.78	7.64	5.25 - 5.85	2.93	41.41	40.15 - 44.69	1.36	95.96	307.00 - 341.69	0.00	100.00

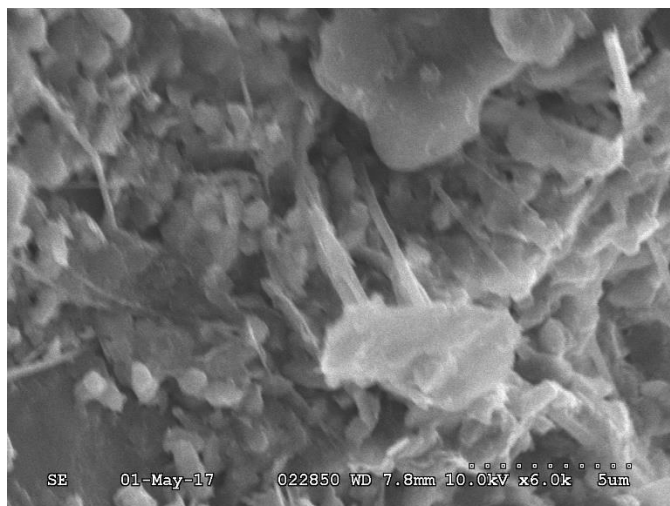


Company: DanDong BETTERSIZETEST INSTRUMENTS LTD. Address: No.141 Renmin Avenue, Dandong, Liaoning, China Postal Code: 118002

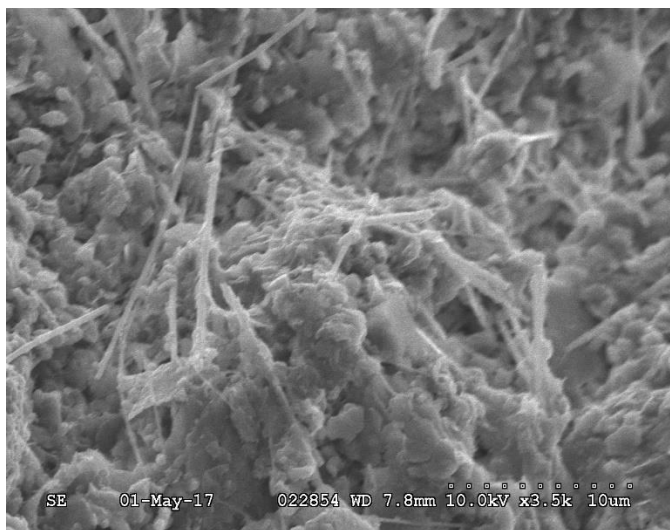
## APPENDIX B: SUPPLEMENTARY SEM PHOTOS



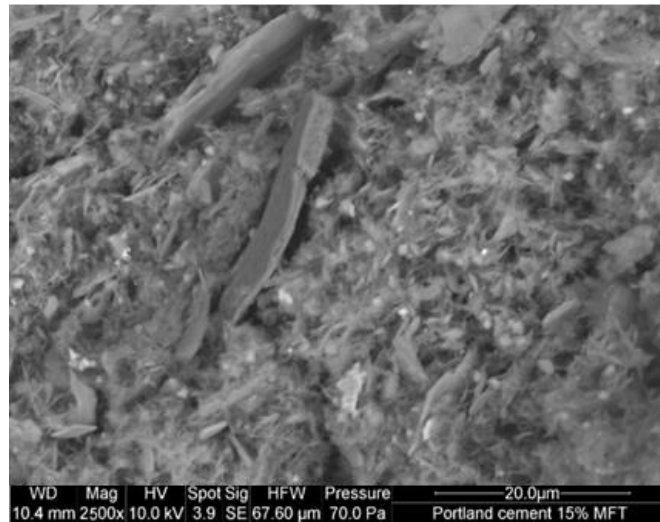
**Appendix B-1. SEM photo of 10%-PC-MFT at 28 days, 3500x**



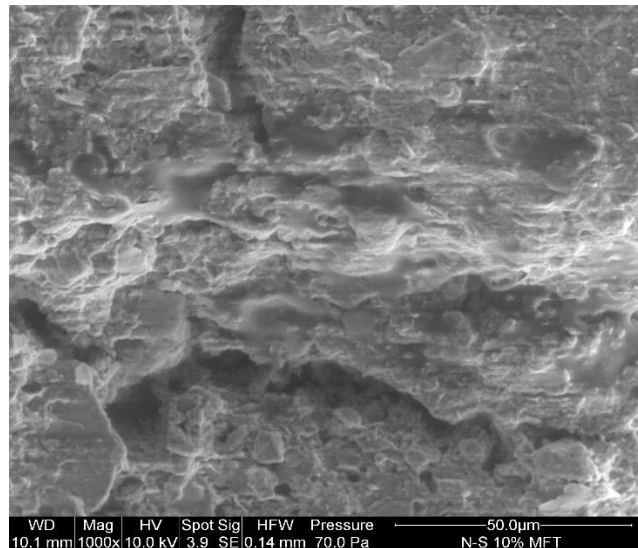
**Appendix B-2. SEM photo of 10%-PC-MFT at 28 days, 6000x**



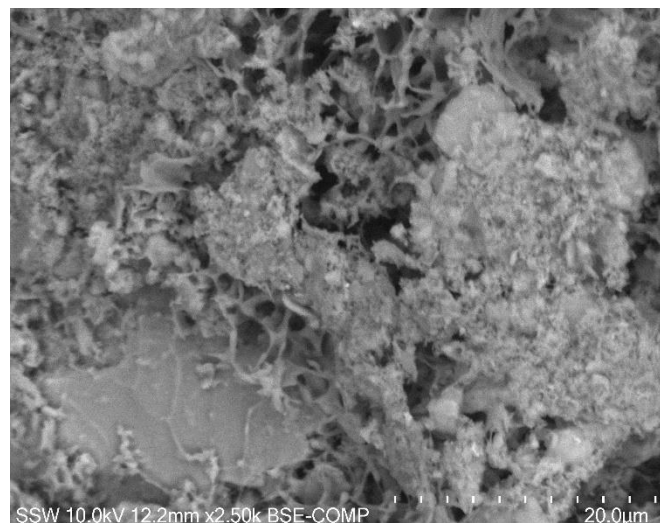
**Appendix B-3. SEM photo of 10%-PC-MFT at 28 days, 3500x**



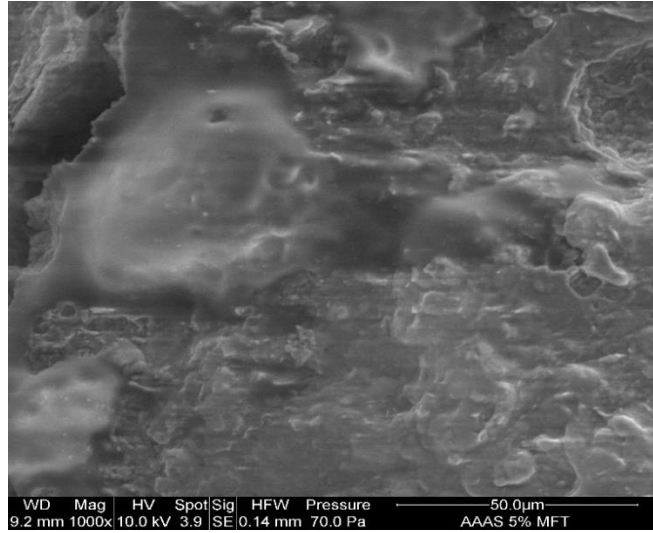
**Appendix B-4. SEM photo of 15%-PC-MFT at 28 days, 2500x**



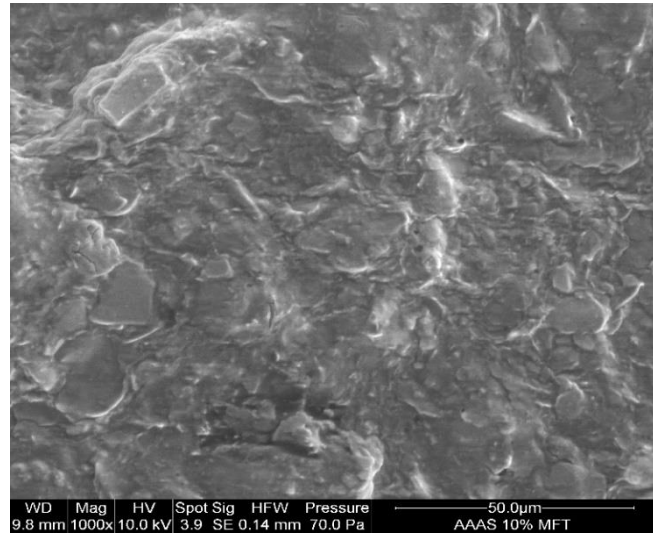
**Appendix B-5. SEM photo of 10%-NS-MFT at 28 days, 1000x**



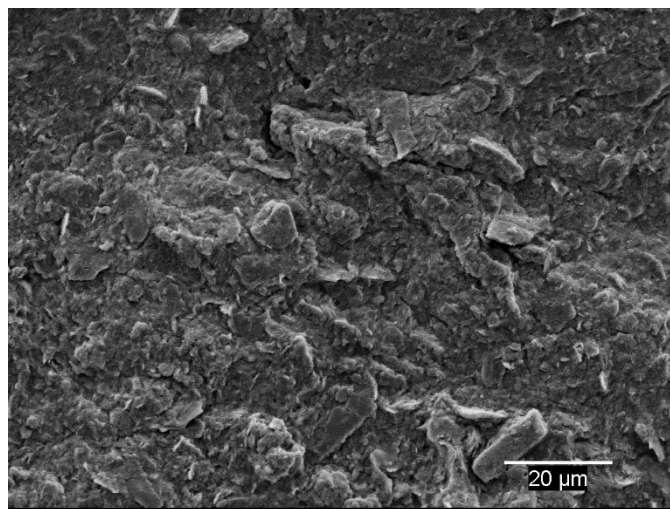
**Appendix B-6. SEM photo of 40%-NS-MFT at 28 days, 2500x**



**Appendix B-7. SEM photo of 5%-AAAS-MFT at 28 days**



**Appendix B-8. SEM photo of 10%-AAAS-MFT at 28 days**



**Appendix B-9. SEM photo of 40%-AAAS-MFT at 28 days**

## APPENDIX C: PHOTOS FROM THE STUDY



Appendix C-1. 3%-NS-MFT at 14 days



Appendix C-2. 5%-NS-MFT at 14 days

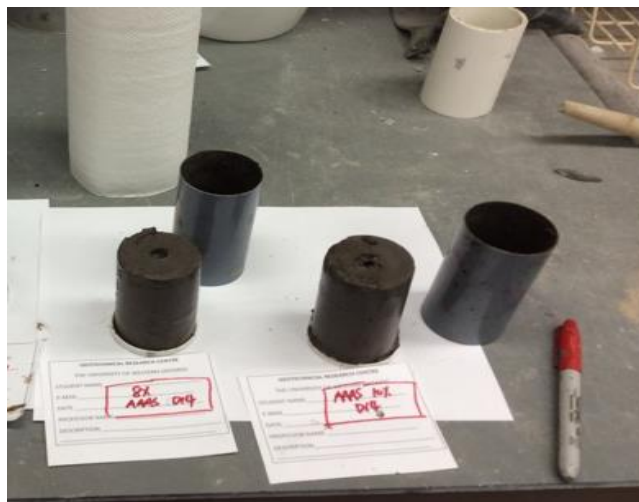


Appendix C-3. 8%-NS-MFT at 14 days (left); 10%-NS-MFT and 15%-NS-MFT (right) at 14 days





**Appendix C-4. 3%-AAAS-MFT at 14 days (left); 5%-AAAS-MFT at 14 days (Right)**



**Appendix C-5. 8%-AAAS-MFT at 14 days (left); 10%-AAAS-MFT at 14 days (Right)**



**Appendix C-6. 10%-AAAS-MFT at 28 days (left); 10%-NS-MFT at 28 days (Right)**



**Appendix C-7. 40%-AAAS-MFT and 40%-NS-MFT at 7 days (left); 50%-AAAS-MFT and 60%-AAAS-MFT at 14 days (right)**



**Appendix C-8. 40%-NS-MFT at 14 days**



**Appendix C-9. 40%-NS-MFT at 14 days (left); 50%-NS-MFT at 14 days (right)**

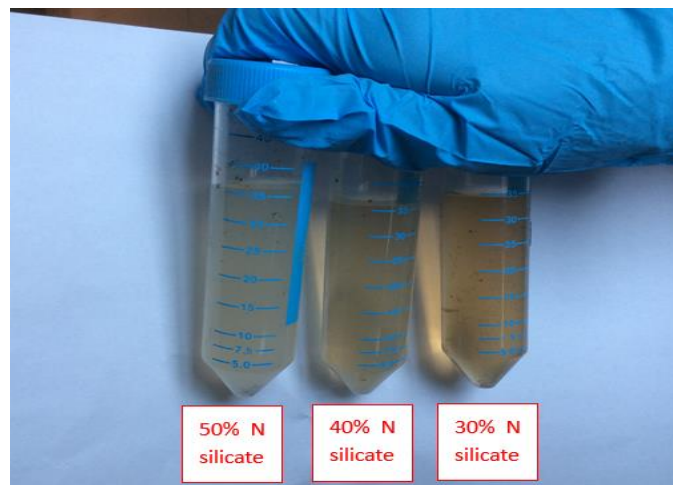




**Appendix C-10. 40%-NS-MFT (left) and 40%-AAAS-MFT (right) at 14 days;**



**Appendix C-11. 50%-NS-MFT (left) and 50%-AAAS-MFT (right) at 14 days;**



**Appendix C-12. Collected supernatant from NS-treated MFT after 28 days;**



**Appendix C-13. Sampling (Left); Centrifugation (Middle); Viscometer (Right)**



**Appendix C-14. Atterberg limits (Left); NS gel syneresis (Right)**



**Appendix C-15. Pycnometer (Left); Oedometer (Middle); Supernatant (Right)**



**Appendix C-16. Vane shear (Left); Falling cone (Middle); Falling cones (Right)**

## **CURRICULUM VITAE**

**NAME:** Yixuan Wang

**EDUCATION:** 2011– 2015 B.E.,  
Department of Civil Engineering, Shenzhen University, China

2015 – present M.E.Sc.,  
Department of Civil and Environmental Engineering, Faculty  
of Engineering, The University of Western Ontario, Canada

**EMPLOYMENT:** 2016.9-2017.4 Teaching Assistant,  
Department of Civil and Environmental Engineering, Faculty  
of Engineering, The University of Western Ontario, Canada

2016.9-2017.9 Research Assistant,  
Department of Civil and Environmental Engineering, Faculty  
of Engineering, The University of Western Ontario, Canada